



**Doctoral Thesis**

**THE ROLE OF MEIS  
TRANSCRIPTION FACTORS IN  
CARDIOMYOCYTES**

**Noelia Muñoz Martín**

Programa de Doctorado de Biociencias Moleculares  
Universidad Autónoma de Madrid

July 2019  
Madrid



DEPARTAMENTO DE BIOLOGÍA MOLECULAR  
FACULTAD DE CIENCIAS



NOELIA MUÑOZ MARTÍN

Licenciada en Biología

Director: Miguel Torres Sánchez

Centro Nacional de Investigaciones Cardiovasculares

Julio, 2019



This work was performed in Miguel Torres' laboratory in the Cell and Developmental Biology Area at the Centro Nacional de Investigaciones Cardiovasculares Carlos III (CNIC) in Madrid.

The CNIC is supported by the Ministerio de Ciencia, Innovación y Universidades (MCNU) and the Pro CNIC Foundation, and is a Severo Ochoa Center of Excellence (SEV-2015-0505).

This study was funded by grants RD12/0019/0005 and RD16/0011/0019 (TerCel, RETICS); S2010-BMD-2315 (Comunidad de Madrid); BFU2012-31086 (MINECO); BFU2015-71519 (MEIC) and ref. 17CVD04 (Leudcq Foundation Transatlantic Networks).

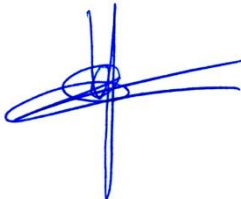
Noelia Muñoz Martín was recipient of a fellowship from “La Caixa-Severo Ochoa 2014” and EMBO-Short Term 2018.



Hereby I certify that Noelia Muñoz Martín has carried out the experimental work leading to her PhD thesis entitled “The role of Meis transcription factors in cardiomyocytes” under my supervision at the Centro Nacional de Investigaciones Cardiovasculares (CNIC) in Madrid.

I also declare that the work presented is novel and of great importance in the field, and of sufficient quality to merit to be presented in order to obtain a PhD degree by the Universidad Autónoma de Madrid.

Madrid, 12<sup>th</sup> June 2019



Miguel Torres Sánchez



*A mis padres, por darme los medios y la libertad para llegar hasta aquí.*

*“Todo el universo tiene ritmo, todo baila”*

Maya Angelou



# Table of Contents

<b>SUMMARY</b>	<a href="#">15</a>
<b>RESUMEN</b>	<a href="#">17</a>
<b>INTRODUCTION</b>	<a href="#">19</a>
<b>Heart development</b>	<a href="#">22</a>
<b>Postnatal heart maturation</b>	<a href="#">25</a>
<b>The cardiac conduction system</b>	<a href="#">26</a>
<b>Electrophysiology of the adult heart</b>	<a href="#">28</a>
<b>Molecular and cellular bases of cardiac conduction</b>	<a href="#">30</a>
<b>Cardiac Conduction System development</b>	<a href="#">32</a>
<b>Meis transcription factors</b>	<a href="#">34</a>
<b>OBJECTIVES</b>	<a href="#">37</a>
<b>MATERIALS &amp; METHODS</b>	<a href="#">41</a>
<b>Animal procedures</b>	<a href="#">43</a>
<i>Mouse lines</i>	<a href="#">43</a>
<i>Tamoxifen preparation</i>	<a href="#">44</a>
<i>Embryo harvest</i>	<a href="#">44</a>
<i>Adult mouse sacrifice</i>	<a href="#">45</a>
<i>BrdU treatment</i>	<a href="#">45</a>
<b>Tissue processing</b>	<a href="#">45</a>
<i>Cryo and paraffin-sectioning</i>	<a href="#">45</a>
<b><i>In situ</i> hybridization on sections</b>	<a href="#">46</a>
<b>Immunofluorescence</b>	<a href="#">46</a>
<i>In paraffin sections</i>	<a href="#">46</a>
<i>In gelatin sections</i>	<a href="#">47</a>
<i>Isolated CMs</i>	<a href="#">48</a>
<i>Whole mount atria from fetuses</i>	<a href="#">48</a>

<b>Hematoxilin &amp; Eosin and Sirius Red staining</b> .....	<a href="#">49</a>
<b>Image acquisition</b> .....	<a href="#">49</a>
<b>Echocardiography</b> .....	<a href="#">49</a>
<i>In pregnant females</i> .....	<a href="#">49</a>
<i>Adult mice</i> .....	<a href="#">50</a>
<b>Optical mapping</b> .....	<a href="#">50</a>
<b>Adult cardiomyocytes isolation</b> .....	<a href="#">52</a>
<b>Ploidy estimation in isolated cardiomyocytes</b> .....	<a href="#">54</a>
<b>Electrocardiogram</b> .....	<a href="#">54</a>
<b>RNA sequencing</b> .....	<a href="#">56</a>
<i>RNA isolation</i> .....	<a href="#">56</a>
<i>RNA-seq library production and sequencing</i> .....	<a href="#">57</a>
<i>RNA-seq data analysis</i> .....	<a href="#">57</a>
<b>Statistics</b> .....	<a href="#">58</a>
<b>RESULTS</b> .....	<a href="#">61</a>
<b>Meis expression pattern in the heart</b> .....	<a href="#">63</a>
<i>Meis1 And Meis2 Are Expressed In Cardiac Progenitors And The Three Layers Of The Developing And Adult Heart: Endocardium, Myocardium And Epicardium</i> .....	<a href="#">63</a>
<b>Meis function in cardiomyocytes during heart development</b> .....	<a href="#">67</a>
<i>Meis1 And Meis2 Double Deletion In CMs Causes Perinatal Death</i> .....	<a href="#">67</a>
<i>Meis1 And Meis2 dKO Hearts Present Morphological Alterations</i> .....	<a href="#">68</a>
<i>Constitutive Meis1 And Meis2 Deletion Leads To Smaller Hearts And Stress-induced Cardiac Rhythm Alterations</i> .....	<a href="#">71</a>
<i>Meis Deletion In CMs Leads To Slower Electrical Impulse Propagation Through The Ventricles</i> .....	<a href="#">77</a>
<b>Molecular mechanisms governing Meis1 and Meis2 dKO phenotype</b> .....	<a href="#">81</a>
<i>Meis Deletion In CMs Alters The Expression Of Genes Related To Cardiac Conduction</i> .....	<a href="#">81</a>
<b>Meis function in adult heart homeostasis</b> .....	<a href="#">83</a>
<i>Meis1 And Meis2 Double Deletion In Adult CMs Causes Cardiac Hypertrophy And Interstitial</i>	

<i>Fibrosis</i> .....	<a href="#">83</a>
<i>Loss Of Function Of Meis1 And Meis2 In Adult CMs Leads To Polyploidization Of Mononucleated CMs</i> .....	<a href="#">87</a>
<i>Double Inducible Deletion Of Meis1 And Meis2 In Adult CMs Causes Slower Ventricular Conduction</i> .....	<a href="#">89</a>
<i>Molecular mechanisms under the control of Meis1 and Meis2 in adult cardiomyocytes</i> .....	<a href="#">92</a>
<i>Meis1 And Meis2 Regulate Calcium Signaling And Conduction System Markers</i> .....	<a href="#">92</a>
<i>Cx43 Expression Is Significantly Reduced In idKO Ventricular Myocardium</i> .....	<a href="#">94</a>
<i>Acute Isoproterenol Treatment Does Not Preferentially Induce Arrhythmias in Meis1 and Meis2</i>	
<i>idKO</i> .....	<a href="#">95</a>
<b>Putative direct targets of Meis TFs in cardiomyocytes</b> .....	<a href="#">97</a>
 <b>DISCUSSION</b> .....	 <a href="#">101</a>
<b>Meis expression pattern in the heart</b> .....	<a href="#">103</a>
<b>Function of Meis in developing cardiomyocytes</b> .....	<a href="#">104</a>
<b>Function of Meis in adult cardiomyocytes</b> .....	<a href="#">105</a>
<b>Putative direct targets of Meis</b> .....	<a href="#">109</a>
 <b>CONCLUSIONS</b> .....	 <a href="#">113</a>
<b>BIBLIOGRAPHY</b> .....	<a href="#">119</a>
 <b>DIGITAL CONTENT</b> .....	 <a href="#">137</a>
 <b>ANEXO I</b> .....	 <a href="#">139</a>

# Index of figures

Figure 1. Anatomy of the mammalian adult heart. ....	<a href="#">21</a>
Figure 2. Mouse embryonic heart development.....	<a href="#">23</a>
Figure 3. Postnatal cardiomyocyte maturation. ....	<a href="#">26</a>
Figure 4. Cardiac conduction system and electrocardiogram interpretation.....	<a href="#">27</a>
Figure 5. Electrophysiology of human and murine ventricular cardiomyocytes. ....	<a href="#">29</a>
Figure 6. Calcium-Induced Calcium Release. ....	<a href="#">31</a>
Figure 7. Intercalated disc composition. ....	<a href="#">32</a>
Figure 8. Cardiac conduction system development. ....	<a href="#">33</a>
Figure 9. Meis1 and Meis2 mRNA in situ hybridization. ....	<a href="#">63</a>
Figure 10. Meis1 and Meis2 are expressed in developing cardiomyocytes. ....	<a href="#">64</a>
Figure 11. Meis1 and Meis2 are expressed in adult cardiomyocytes of the working and conducting myocardium. ....	<a href="#">66</a>
Figure 12. Meis1 and Meis2 double deletion in developing CMs causes perinatal death. <a href="#">67</a>	
Figure 13. Cardiac morphological alterations produced by CM-specific Meis1 and Meis2 deletion. ....	<a href="#">70</a>
Figure 14. External malformations in dKO hearts are visible at E14.5. ....	<a href="#">70</a>
Figure 15. Atrial malformations affect pectinate muscles. ....	<a href="#">71</a>
Figure 16. Echocardiography reveals smaller hearts in dKO fetuses.....	<a href="#">72</a>
Figure 17. Proliferation rate in the myocardium of control and mutant fetuses. ....	<a href="#">73</a>
Figure 18. dKO fetuses present normal cardiac function and higher heart rates. ....	<a href="#">73</a>
Figure 19. dKO hearts manifest arrhythmias during trans-uterine echo acquisition.....	<a href="#">75</a>
Figure 20. Normal beating heart rate and cardiac rhythm in fetuses during trans-abdominal echocardiography. ....	<a href="#">76</a>
Figure 21. Heart beat rate and Atrio-Ventricular delay measured by Optical Mapping.....	<a href="#">78</a>
Figure 22. dKO hearts present slower ventricular activation curves.....	<a href="#">79</a>

Figure 23. Optical mapping at E16.5 did not show any significant difference between Control and dKO hearts. ....	<a href="#">80</a>
Figure 24. Arrhythmic dKO hearts detected by optical mapping.....	<a href="#">81</a>
Figure 25. RNA-seq analysis of E15.5 Control vs dKO atria and ventricles. ....	<a href="#">82</a>
Figure 26. dKO hearts present reduced Cx43 expression. ....	<a href="#">83</a>
Figure 27. Meis1 and Meis2 inducible deletion in adult hearts leads to mild-hypertrophy. ....	<a href="#">85</a>
Figure 28. Meis1 and Meis2 loss of function in adult CMs induces interstitial fibrosis.....	<a href="#">86</a>
Figure 29. $\alpha$ -MHC-MerCreMer carrier mice develop mild interstitial fibrosis .....	<a href="#">86</a>
Figure 30. idKOs show normal CM size and increased BrdU incorporation in mononucleated CMs.....	<a href="#">88</a>
Figure 31. The majority of BrdU <sup>+</sup> mononucleated CMs undergo DNA endoreplication and not proliferation. ....	<a href="#">89</a>
Figure 32. QRS complex is elongated upon Meis1 and Meis2 double deletion in adult CMs. ....	<a href="#">91</a>
Figure 33. Measurement of ECG intervals in MerCreMer carriers.....	<a href="#">91</a>
Figure 34. The $\alpha$ -MHC-MerCreMer allele does not recombine efficiently in the atria of adults.....	<a href="#">93</a>
Figure 35. ARVC and calcium signaling related genes appeared differentially expressed in idKO ventricles.....	<a href="#">93</a>
Figure 36. Cx43 expression is reduced in idKO ventricular myocardium.....	<a href="#">95</a>
Figure 37. idKO mice respond similar to Controls after acute isoproterenol treatment. ....	<a href="#">96</a>
Table 1. Arrhythmic episodes after isoproterenol injection where not related to genotype. ....	<a href="#">96</a>
Figure 38. Analysis of coincident DEGs in the 3 RNA-seq experiments performed reveals putative direct targets of Meis TFs.....	<a href="#">97</a>
Figure 39. Putative binding sites of Meis found by CHIP-seq analysis.....	<a href="#">99</a>
Figure 40. Summary of defects and gene expression changes found in CMs lacking Meis1 and Meis2.....	<a href="#">111</a>

# List of abbreviations

<b>AP</b>	Action Potential
<b>ARVC</b>	Arrhythmogenic Right Ventricular Cardiomyopathy
<b>AVC</b>	Atrio-Ventricular Canal
<b>AVN</b>	Atrio-Ventricular Node
<b>BB</b>	Bundle Branch
<b>BPM</b>	Beats per minute
<b>CC</b>	Cardiac Crescent
<b>CCS</b>	Cardiac Conduction System
<b>CHD</b>	Congenital Heart Defect
<b>CICR</b>	Calcium Induced Calcium Release
<b>CM</b>	Cardiomyocyte
<b>CNC</b>	Cardiac Neural Crest
<b>dKO</b>	double Knockout
<b>ECG</b>	Electrocardiogram
<b>EF</b>	Ejection Fraction
<b>FHF</b>	First Heart Field
<b>HB</b>	Hiss Bundle
<b>HT</b>	Heart Tube
<b>ID</b>	Intercalated Disc
<b>idKO</b>	inducible double Knockout
<b>IVS</b>	Interventricular septum
<b>LA</b>	Left atrium
<b>LAX</b>	Long axis
<b>LV</b>	Left Ventricle
<b>LVPW</b>	Left ventricular posterior wall
<b>OFT</b>	Outflow Tract
<b>PF</b>	Purkinje Fiber
<b>RA</b>	Right atrium
<b>RV</b>	Right ventricle
<b>SAN</b>	Sinoatrial Node
<b>SAX</b>	Short axis
<b>SHF</b>	Second Heart Field
<b>SR</b>	Sarcoplasmic Reticulum
<b>TF</b>	Transcription Factor
<b>Tx</b>	Tamoxifen
<b>VCS</b>	Ventricular Conduction System
<b>VOCC</b>	L-type Voltage-operated Calcium Channel
<b>WGA</b>	Wheat germ agglutinin
<b>WT</b>	Wild type





# SUMMARY

The heart is the pump that irrigates the body to satisfy the nutrient and oxygen demands essential for keeping the organism alive. Understanding how the heart is formed and how its homeostasis is maintained in adulthood, is of great interest and can provide new insights on the etiology of cardiovascular diseases. In this doctoral thesis we studied the role of *Meis1* and *Meis2* transcription factors as possible regulators of cardiac development and homeostasis.

We developed two mouse models for the conditional simultaneous deletion of *Meis1* and *Meis2* in cardiomyocytes either during development or during adulthood. Analysis of *Meis1* and *Meis2* double deletion in the developing heart revealed cardiac malformations and perinatal death, together with impaired electrical impulse propagation through the ventricles. Adult mice with *Meis1* and *Meis2* loss of function in cardiomyocytes presented mild cardiac hypertrophy, polyploidization of mononucleated cardiomyocytes and impaired electrical impulse conduction through ventricular myocardium.

The transcriptomic analysis of the mutants suggests that *Meis1* and *Meis2* transcription factors regulate calcium and sodium currents and GAP junction communication in developing and adult cardiomyocytes, which is in accordance with the electrical phenotypes observed. Moreover, the set of genes sensitive to *Meis1* and *Meis2* deletion shows significant coincidence with those altered in mouse models of arrhythmogenic right ventricular cardiomyopathy, suggesting a role for these transcription factors in the pathogenesis of this disease.



# RESUMEN

El corazón es la bomba que alimenta el sistema circulatorio para satisfacer las necesidades de nutrientes y oxígeno del cuerpo. Entender cómo se regula el desarrollo del corazón y su homeostasis durante la vida adulta es de vital importancia para comprender la etiología de muchas enfermedades cardiovasculares. En esta tesis doctoral, estudiamos el papel de los factores de transcripción *Meis1* y *Meis2* como posibles reguladores de estos procesos.

Hemos generado dos modelos de ratón para el estudio de la función de *Meis1* y *Meis2* en cardiomiocitos bien durante el desarrollo o durante la edad adulta. Tras la pérdida de función de *Meis1* y *Meis2* en cardiomiocitos durante el desarrollo, encontramos que los fetos mueren al nacer, presentando alteraciones morfológicas y defectos en la propagación del impulso eléctrico, necesario para el mantenimiento del ritmo de latido. Por otro lado, la delección de estos factores en los cardiomiocitos del corazón adulto no es letal, pero conlleva la aparición de fibrosis, poliploidización de los cardiomiocitos mononucleados y cierta respuesta hipertrófica. Además, de forma similar a lo observado en la delección embrionaria, encontramos un empeoramiento de la conducción eléctrica con alargamiento del segmento QRS en el electrocardiograma.

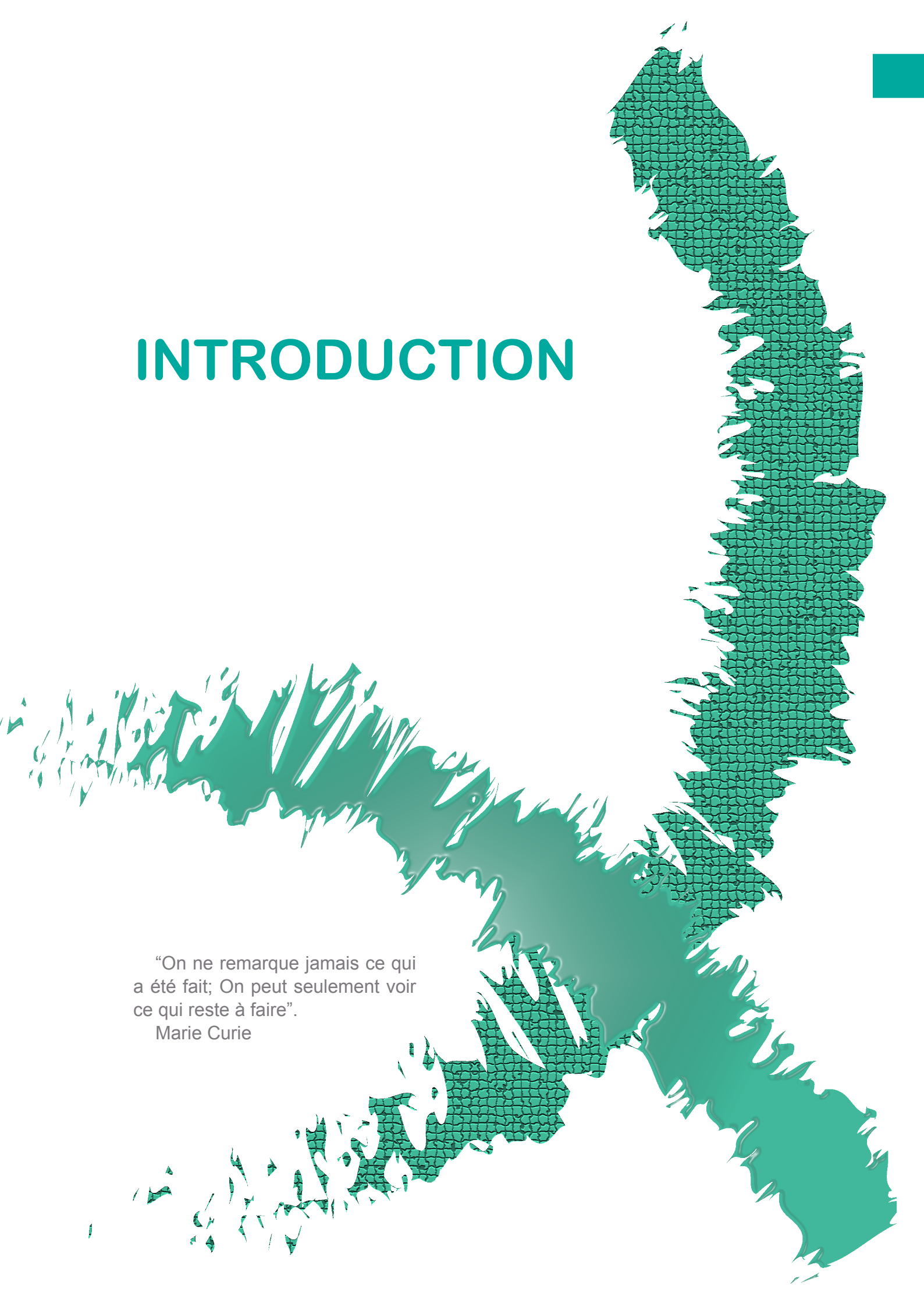
El análisis del transcriptoma de los mutantes indica que *Meis1* y *Meis2* podrían estar regulando las corrientes de sodio y calcio y la formación de uniones GAP, lo que correlaciona con las alteraciones encontradas en la propagación del impulso eléctrico del corazón en ambos modelos. Además, el conjunto de genes alterados por la falta de función de *Meis* presenta coincidencias significativas con el grupo de genes que se altera en un modelo de ratón de la enfermedad ARVC (“*Arrhythmogenic Right Ventricular Cardiomyopathy*”), sugiriendo que *Meis1* y *Meis2* podrían estar implicados en la patogénesis de esta cardiomiopatía.



# INTRODUCTION

“On ne remarque jamais ce qui a été fait; On peut seulement voir ce qui reste à faire”.

Marie Curie





The heart is a powerful pump that impulses the blood to irrigate all body organs. The mechanical action of the heart is provided by the cardiac muscle, which contracts during systole to pump the blood. After contraction, the muscle is dilated during diastole, creating negative pressure to get the blood back into the heart and pump it again. The adult mammalian heart is composed by two atria and two ventricles feeding two parallel circuits: the systemic circulation and the pulmonary circulation (Fig. 1). Atria and ventricles communicate through the atrioventricular valves. When the deoxygenated blood (blue in Fig. 1) from the systemic circulation enters the right atrium, there is an increase in pressure that leads to the opening of the tricuspid valve and the subsequent filling of the right ventricle. Then, the blood goes through the pulmonary valve to the lungs, gets oxygenated and comes back to the heart through the left atrium, where the same process is repeated (pink in Fig. 1). In this case, the atrioventricular valve is called mitral or bicuspid and the oxygenated blood leaves the ventricle through the aortic valve.

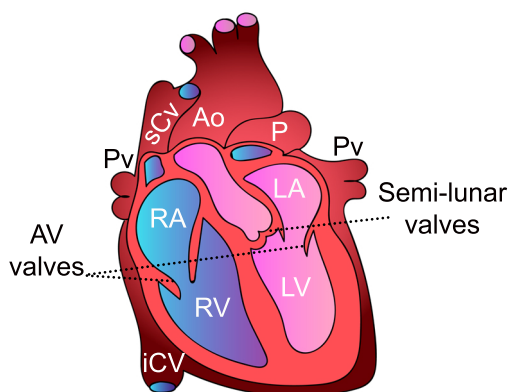


**Figure 1. Anatomy of the mammalian adult heart.**

Blue and pink colors represent deoxygenated and oxygenated blood respectively.

RA, right atrium, RV, right ventricle, LA, left atrium, LV, left ventricle, Ao, aorta, P, pulmonary artery, sCv and iCv, superior and inferior cava vein, Pv, pulmonary veins.

This process is essential for life, because it supplies a constant flow of nutrients and oxygen to all cells in the body. Thus, the heart is the first functional organ during embryonic development and any alteration of cardiac formation can lead to embryonic lethality or congenital heart defects (CHD). Currently, 30% of human pregnancies that do not come to term present cardiac malformations (Bruneau, 2008) and 3% of born humans present some kind of CHD (Fahed *et al.*, 2013; Parker *et al.*, 2010). These percentages reflect how important the proper regulation of heart development is, in order to produce a functional organ throughout lifespan.

## Heart development

Mouse gestation spans 19 days, which implies that developmental processes occur very rapidly. The mammalian heart starts to be formed very early in development as the first cardiac progenitors arise at E6.5 from the pluripotent cells of the epiblast. These epiblast-derived cells migrate anteriorly from the primitive streak and form the cardiac mesoderm at both sides of the ventral midline (Lawson *et al.*, 1991; Tam & Behringer, 1997). This pool of cells expresses *Mesp1* (Mesoderm Posterior 1) which is a key regulator for cardiac specification (Saga *et al.*, 1999; Saga *et al.*, 2000). One day later, *Mesp1*<sup>+</sup> cells migrate anteriorly and fuse medially, forming the cardiac crescent (CC) (Fig. 2). At this stage, many transcription factors necessary for cardiogenesis are activated: *Gata4*, *Nkx2.5*, *Mef2c*, *Hand1/2* and *Tbx5* (Martin-Puig *et al.*, 2008; Bondue & Blanpain, 2010). The CC is a peristaltic pump located under the growing head folds (Ivanovitch *et al.*, 2017). It is composed of an inner layer of endocardium and an outer layer of myocardium (Vincent & Buckingham, 2010). The progenitors that give rise to the CC are known as First Heart Field (FHF) (Kelly, 2012; Später *et al.*, 2013).

As the CC grows, cells move to form a transversal hemi-tube which later adopts a more spherical shape and is dorsally open (Ivanovitch *et al.*, 2017). The endoderm serves as a transient dorsal wall and the hemi-tube is progressively closed giving rise to the primitive heart tube (Kelly *et al.*, 2014; Evans *et al.*, 2010). The primitive HT has the same two layers as the CC, but venous and arterial poles are now present. The future left ventricle and part of the atria arise from the primitive HT (Zaffran *et al.*, 2004). There is another pool of cardiac progenitors which remains undifferentiated and starts differentiation after the linear HT is formed. This pool is called Second Heart Field (SHF). *Fgf10* and *Isl1* are some of the factors characteristic of this region. The SHF is located dorso-medially to the CC in the region of the splanchnic mesoderm and progenitors are incorporated into the HT through the venous and arterial poles, contributing to HT elongation (Kelly *et al.*, 2001; Mjaatvedt *et al.*, 2001; Waldo *et al.*, 2001; Cai *et al.*, 2003). SHF progenitors will form the right ventricle, the outflow tract and part of the atria (Zaffran *et al.*, 2004). As the HT elongates, it undergoes rightward looping and chambers start to be specified (E8.5) (Fig. 2). Outflow tract (OFT) and

forming right and left ventricles can be already identified at this point. The connection between atria and ventricles is made by the atrioventricular canal. At E10.5 outflow and inflow tracts align with the ventricles reaching their definitive location (Watanabe & Buckingham, 2010).

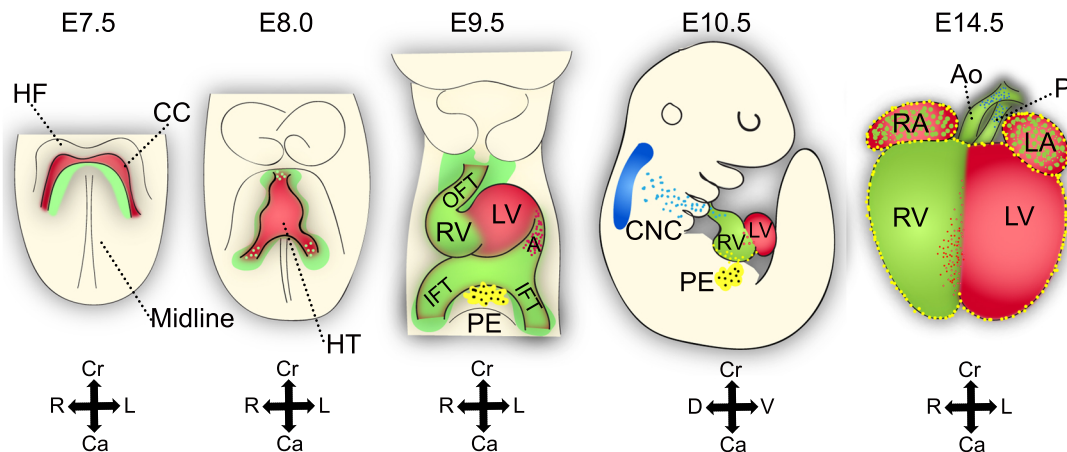


**Figure 2. Mouse embryonic heart development.** Schematic representation of key phases in murine cardiac development. From left to right, cardiac crescent (CC) at E7.5, located under the head folds (HF), with first heart field (FHF, in red) and second heart field progenitors (SHF, in green). The heart tube (HT) is formed (E8.0) and elongates as SHF progenitors incorporate to the tube through the arterial and venous poles (E9.5). Between E8.0 and E9.5, the heart loops and chambers are specified. The right ventricle (RV), outflow tract (OFT) and inflow tract (IFT) are represented in green as SHF derivatives, while left ventricle (LV) and part of the atria (A) are in red, as FHF derivatives. The proepicardium (PE) is represented in yellow. Cardiac neural crest cells (CNC, blue) are incorporated into the OFT region. The last draw represent an E14.5 embryonic heart with the 4 chambers and great vessels, aorta and pulmonary arteries (Ao;P) differentiated. Cartoon adapted from Stéphane D. Vincent and Margaret E. Buckingham, 2010.

Later on, the developing heart initiates an expansion process by proliferation at specific regions of the outer curvature of the heart tube, which generates the chambers, according to the ballooning model (Christoffels *et al*, 2000). Between E9.5 and E14.5 there is not only growth but also complete chamber specification and morphogenesis. After looping, CMs continue dividing and some of the newly formed CMs will protrude towards the endocardium. This protruding CMs slow their proliferative rate and form the trabeculae, which are transient ridge-like structures that protrude towards the lumen of the chambers. The initial layer of myocardium is now called compact layer and will continue proliferating and increasing in thickness (Blausen *et al*, 1990; Sedmera *et*

*al*, 2000, 2003; Staudt *et al*, 2014). At E14.5 all chambers are established and further proliferation and maturation will occur until the first postnatal days (Fig. 2). The increase in compact layer thickness is accompanied by the development of the coronary system that serves to irrigate the myocardium, which satisfies the high metabolic rate of cardiomyocytes. Ventricular chamber maturation involves trabecular remodeling and compaction. During compaction, the trabecules become thicker and coalesce until the spaces between them form capillaries (Wessels & Sedmera, 2003). By the end of gestation, right and left ventricles are completely separated by the septum. However, the atrial septum does not close until around postnatal day 7 (P7) (Cole-Jeffrey *et al*, 2012).

The FHF and SHF are the main sources of progenitors during cardiogenesis, but there are other pools of progenitor which are essential for heart formation (Vincent & Buckingham, 2010). **The epicardium** is the outer-most layer of the heart and it derives from the proepicardium. The proepicardium is a pool of cells that derive from the coelomic epithelium located in the dorsal pericardial wall. PE cells expressed different markers, among which, *Tbx18* and *Wt1* are the best established. From E9.5 to approximately E14.5, cells detach from the PE and cover the heart progressively by migration and proliferation, (Fig. 2) (Viragh & Challice, 1981) (Wu *et al*, 2010).

Moreover, epicardial cells undergo epithelial-mesenchymal transition to invade the myocardium and there differentiate into fibroblasts, vascular smooth muscle cells and part of the vascular endothelial cells (Wessels & Pérez-Pomares, 2004). It has been proposed they might also contribute to CMs but this is still a debate and remains to be elucidated (Krainock *et al*, 2016).

Another source of progenitors is the **cardiac neural crest** (CNC). This progenitor population arises from the dorsal neural tube and migrates towards the heart around mid-gestation (Fig. 2) (Lee *et al*, 1995; Jiang *et al*, 2000; Brown & Baldwin, 2006). It has been shown that CNC cells contribute to the smooth muscle cells from the arterial pole of the heart and their incorporation to this structure is important for OFT remodeling and division into aorta and pulmonary arteries (Keyte *et al*, 2014).

## Postnatal heart maturation

During the first week of life, the heart still undergoes important genetic and metabolic changes. In the last decades, many studies have focused on the description of those changes and their regulation.

After birth, the CMs proliferative rate is dramatically decreased in mice and humans (Fig. 3) (Soonpaa *et al*, 1996; Mollova *et al*, 2013). However, in a few days, the size of the heart is duplicated due to a hypertrophic process of the CMs (Li *et al*, 1996). This hypertrophy is linked to an increase in CM ploidy that results predominantly in binucleation of CMs in mice and nuclear polyploidization in humans (Fig. 3) (Bergmann *et al*, 2015). Whereas developing CMs are mononucleated, around P21 85-90% of CMs are binucleated in mice (Soonpaa *et al*, 1996; Walsh *et al*, 2010). In general, genes promoting CM proliferation are strongly downregulated while genes inhibiting the cell cycle are upregulated during this process (Engel *et al*, 2005; Quaiife-Ryan *et al*, 2017). The reasons for these changes are still under study. It has been proposed, that the increase in oxygen levels after birth might lead to the activation of the oxidative stress damage response and the subsequent cell cycle arrest (Puente *et al*, 2014; Kimura *et al*, 2014).

In addition, it has been recently discovered that the neonatal mouse heart presents the capability to regenerate after injury during the 3-4 first postnatal days, although at P7 this ability is lost (Porrello *et al*, 2011). This was a very encouraging finding because it opened the possibility of activating adult CM proliferation to stimulate cardiac injury repair. Many efforts have been concentrated on understanding the molecular mechanisms underlying CMs cell cycle arrest (Tzahor & Poss, 2017). Activation of Hippo signaling is one of the mechanisms shown to inhibit postnatal CMs proliferation (Heallen *et al*, 2011; von Gise *et al*, 2012) and administration or upregulation of extracellular matrix proteins has been shown to modify the regenerative capacity of the heart (D'Uva *et al*, 2015; Bassat *et al*, 2017). Recently, *Meis1* was identified as negative regulator of postnatal CMs cell cycle (Mahmoud *et al*, 2013). More studies in this field are still needed to achieve adult CM regeneration, although recent advances in the pig

model are encouraging (Gabisonia *et al*, 2019).

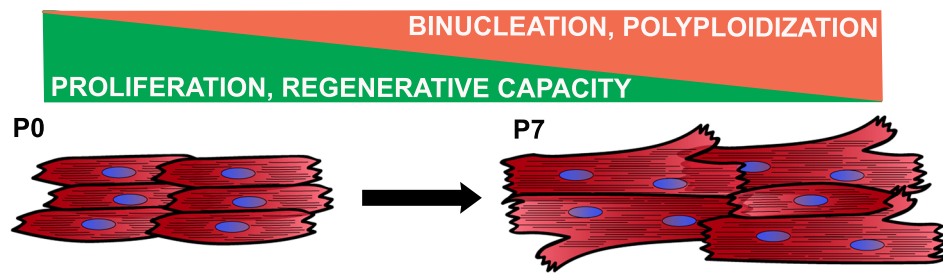


**Figure 3. Postnatal cardiomyocyte maturation.** Changes between P0 and P7 in mammalian cardiomyocytes. Cell cycle is arrested and the regenerative capacity is lost, while the binucleation and polyploidization become predominant in cardiomyocytes at P7.

## The cardiac conduction system

The formation of a proper functional heart requires not only the accomplishment of complex and varied morphogenetic processes, but also the establishment of the adequate cardiac rhythm. In mammals, the nervous system and hormones regulate the cardiac rate to adapt it to the needs of body's cells for oxygen and nutrients. However, there are specialized CMs with the capability of automaticity in electrical pacing, known as the pace-maker cells, which, in the absence of extrinsic influences, can maintain constant basal heart rhythm (Gordan *et al*, 2015). These CMs present few sarcomeres, less mitochondria and T tubules and enriched glycogen content (Virágh S, 1977; Myers & Fishman, 2003).

Heartbeats originate as a spreadable rapid rise and fall of voltage across the cellular membrane which is called action potential (AP). The AP is generated in the sinoatrial node (SAN) and spreads through a system of specialized CMs known as the Cardiac Conduction System (CCS). All CCS CMs can generate action potentials, although the SAN has the fastest rate of spontaneous depolarization and, therefore, acquires the role of pacemaker. The SAN is located at the dorsal part of the right atrium, close to the superior cava vein entrance (Fig. 4A). From the SAN, the impulse spreads throughout the atria inducing their contraction. Then, the AP reaches the atrio-ventricular node (AVN), where it suffers a delay before entering the His Bundle (HB) at the base of the

ventricles (Fig. 4A). The delay created by the AVN is essential to allow blood flow from atria to fill the ventricles during atrial systole and before ventricular systole. The atrial and ventricular myocardium are electrically isolated from each other by the annulus fibrosus and central fibrous body. The HB is the only CCS element that crosses this insulation, running through the crest of the ventricular septum and transmitting the electrical impulse from atria to ventricles.

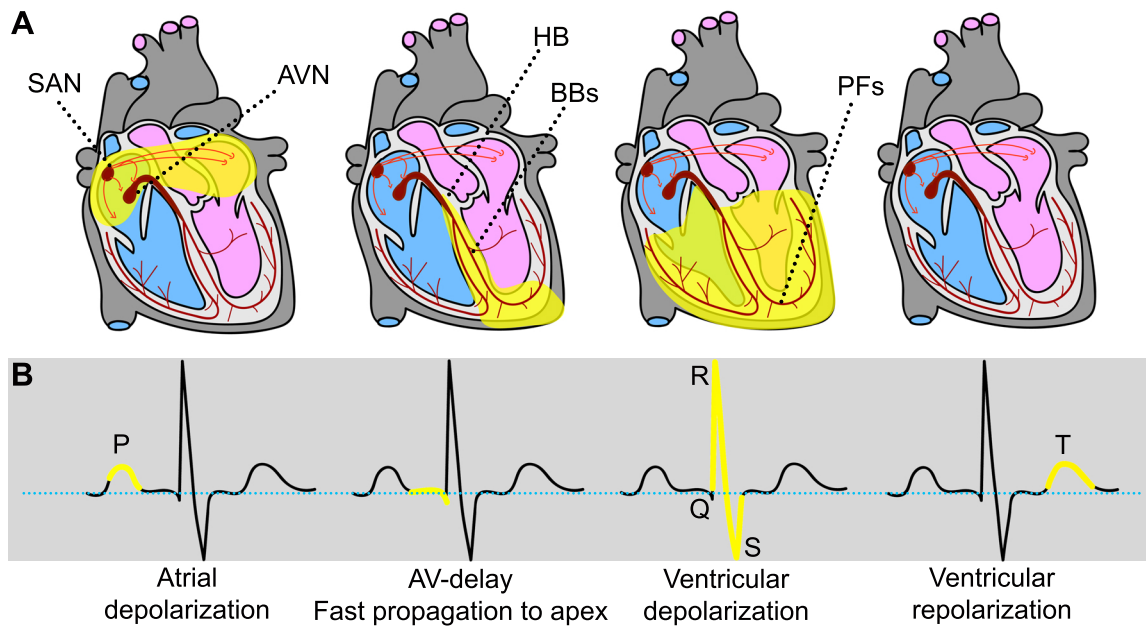


**Figure 4. Cardiac conduction system and electrocardiogram interpretation.** (A). Adult heart representation with cardiac conduction system anatomy in red. From left to right, yellow areas represent the sequence of activated regions upon electrical impulse generation in the sinoatrial node (SAN). Atrioventricular node (AVN), Hiss Bundle (HB), right and left Bundle Branches (BBs) and Purkinje Fibers (PFs). (B). Example of human electrocardiogram with highlighted areas in yellow that correspond to the phases represented in (A).

Two branches arise from the HB, right and left bundle branches (RBB; LBB) located at either side of the interventricular septum. BBs prolong from the top of the septum towards the apex and connect to the Purkinje Fiber network (PF) at the tips (Fig. 4A). Then, the AP is rapidly transmitted to the whole ventricles, from apex to base, leading to subsequent ventricular contraction and ejection of blood through the great arteries. PFs are distributed throughout the ventricular walls and they are mainly located in a sub-endocardial position (Van Weerd & Christoffels, 2016). The ventricular conduction system (VCS), composed of the HB, the BBs and the PFs is electrically isolated from

the working myocardium by connective tissue, so that the electrical impulse only reaches the working myocardium through the Purkinje-Myocyte junctions. This ensures the proper timing and the apex-to-base contraction of the ventricles for efficient blood pumping (Munshi, 2012).

## Electrophysiology of the adult heart

The adequate function of the CCS is essential for life. Perturbations of heart rhythm lead to an important proportion of morbidity and mortality in the human population. Nowadays, the overall prevalence of arrhythmias is approximately 3.4% (Andersson *et al*, 2013; Zoni-Berisso *et al*, 2014; Clauss *et al*, 2019), however, the pathophysiology of arrhythmias is complex and not completely understood.

The electrocardiogram (ECG) is a diagnostic tool that allows the study in detail of CCS function. It is widely used in humans and also in animal experiments. It consists on the measurement of voltage versus time, which generates a pattern with several waves and isoelectric segments, each one reporting the activity of a particular part of CCS and working myocardium electrical activity (Fig. 4B). A proper interpretation of the electrocardiogram is essential for a good description of CCS function. The human ECG was described for the first time in 1895 by Einthoven and eighty-three years later, in 1968, the first description of the mouse ECG was published (Fye, 1994; Goldberg *et al*, 1968). Comprehension of both ECGs is of crucial importance for the extrapolation of the results in mouse models to human health.

Before ECG interpretation, it is necessary to explain the molecular basis of the action potential. The AP is produced by the interchange of ions between the cell and the intercellular space (Fig. 5A). AP shape varies between species and also between different regions of the heart. In general, the resting voltage potential across the CM plasma membrane (sarcolemma) is usually -90mV with higher concentrations of Na<sup>+</sup> outside the cell and of K<sup>+</sup> inside. When the action potential is generated, fast sodium channels are opened creating an inward Na<sup>+</sup> current that rapidly increases voltage across the sarcolemma to values of +10mV (Fig. 5A, B). This phenomenon is known as depolarization. The returning to the resting membrane voltage is called repolarization

and is achieved by outward  $K^+$  current to the intercellular space (Fig. 5A, B). In human CMs, there is an intermediate phase, after the beginning of repolarization, called plateau phase. In this phase, calcium channels are opened, so that  $Ca^{2+}$  enters the cell while  $K^+$  outward current occurs, keeping voltage on values of about 0mV before complete repolarization (Fig. 5A, B) (Nerbonne & Kass, 2005). Transient hyperpolarization is normally observed in human CMs due to the potassium outward current that brings the voltage to more negative values than in the resting phase. These differences in AP between mice and humans creates different ECG patterns.

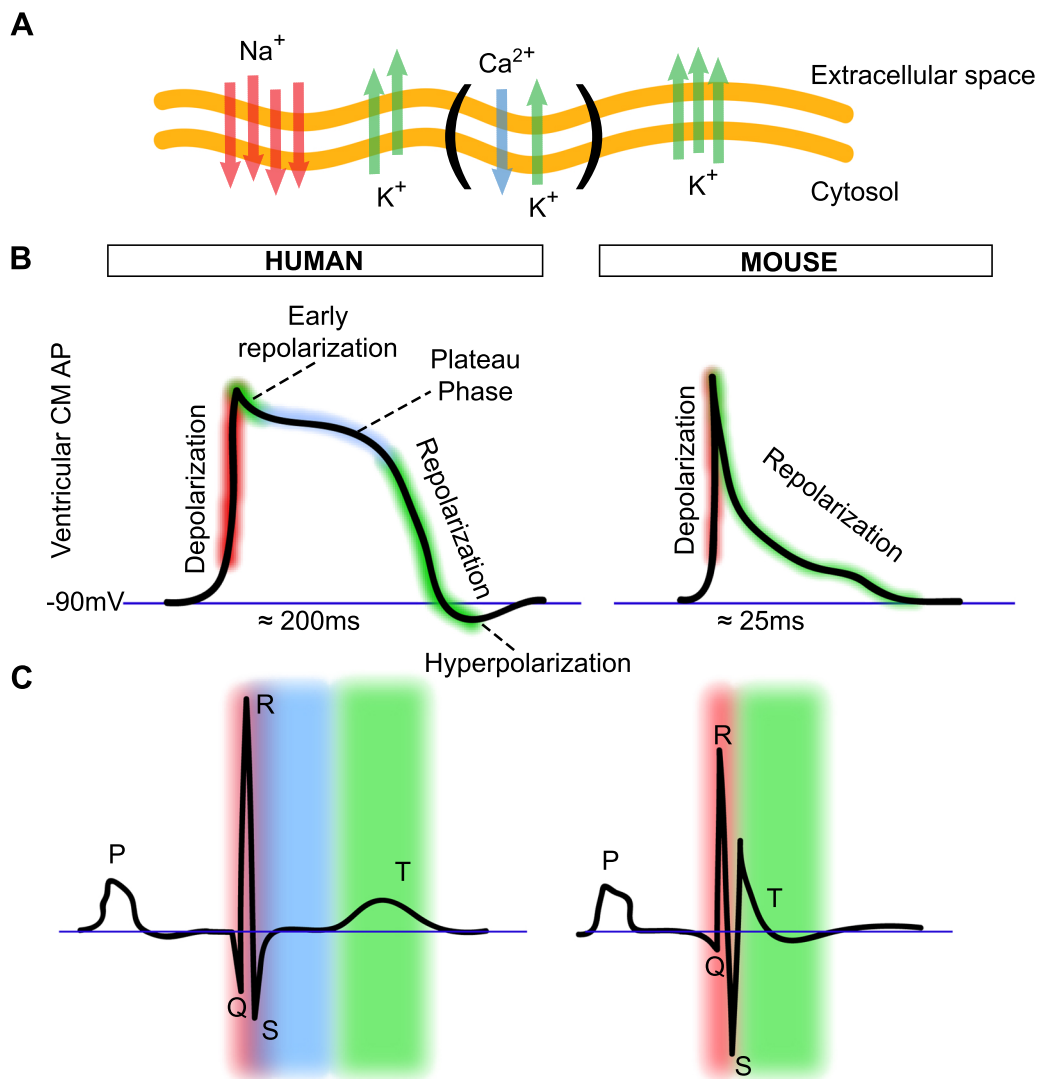


**Figure 5. Electrophysiology of human and murine ventricular cardiomyocytes.** (A). Schematic representation of ion exchange during AP phases through CMs sarcolemma. Brackets indicate the plateau phase that is exclusive of human CMs. (B). Action potential shapes in human and mouse ventricular CMs. (C). The ECG profile in human and murine hearts with indication of each wave. Colors indicate the phases of AP: red, depolarization; green, repolarization; blue, plateau phase.

The time between the end of P wave and the initiation of Q wave corresponds to the delay between atrial and ventricular conduction (Fig. 4B, 5C). Prolongation of this segment might indicate an atrio-ventricular conduction delay or block. Then, the QRS complex appears, reflecting ventricular depolarization, with a morphology that differs between mice and humans (Fig. 4B, 5C).

In mice, ventricular repolarization occurs immediately after the QRS, however, in humans, ventricular repolarization takes a longer time and generates the T wave after and isoelectric segment (Fig. 4B, 5C) (Boukens *et al*, 2014). In mice, the T wave voltage is negative and ends when it reaches the isoelectric line (Fig. 5C) (Boukens *et al*, 2014). The atrial repolarization wave is not seen probably because is hidden by the QRS complex.

## Molecular and cellular bases of cardiac conduction

Synchronous impulse propagation and contraction requires proper excitation-contraction coupling. Calcium signaling is a key regulator of this process allowing to pair depolarization with mechanical contraction. When electrical impulse reaches working CMs and depolarization starts, L-type Voltage-operated  $\text{Ca}^{2+}$  channels (VOCC) (Cav1.2) are opened (Fearnley *et al*, 2011).  $\text{Ca}^{2+}$  flows into a restricted space between sarcolemma and sarcoplasmic reticulum (SR) known as “dyadic cleft”.  $\text{Ca}^{2+}$  accumulation in this micro domain induces opening of RyR2 (Type 2 Ryanodine Receptor) located in the SR and produces a  $\text{Ca}^{2+}$  release signal known as “ $\text{Ca}^{2+}$  spark” in a process called “calcium-induced calcium release” (CICR) (Fig. 6).  $\text{Ca}^{2+}$  ions diffuse to engage the Troponin C, which is the  $\text{Ca}^{2+}$  binding component of the contractile machinery, and contraction occurs. After activation of contractile units,  $\text{Ca}^{2+}$  is rapidly removed from the cytosol causing relaxation and preparing the cell for the next action potential (Shannon and Bers, 2004). The main mechanisms for calcium efflux from the cytosol is the  $\text{Ca}^{2+}$  ATPase2 (SERCA2) pump located at the SR (Fig. 6). There are also sodium/calcium exchanger channels (NCX) in the sarcolemma that contribute to this process in a smaller percentage (Fig. 6) (Fearnley *et al*, 2011). It has been shown this system has high adaptability robustness, since SERCA2 cardiac-specific knockout mice showed

minimal cardiac dysfunction due to a compensatory increase in NCX activity (Andersson *et al*, 2009).

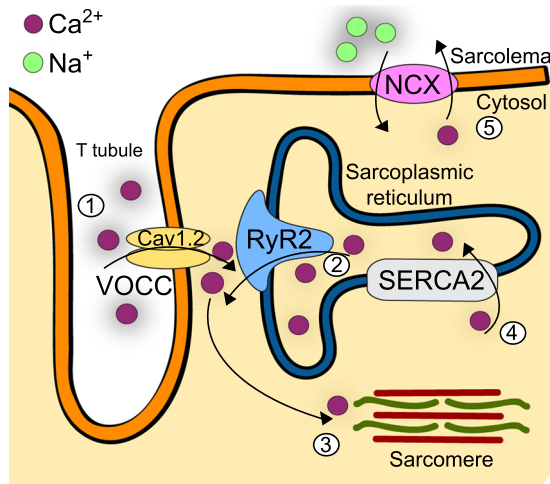


**Figure 6. Calcium-Induced Calcium Release.** (1) Extracellular calcium enters cytosol through L-type Voltage open Calcium Channels (VOCC) inducing RyR2 calcium release from the sarcoplasmic reticulum (2). Increased cytosolic calcium concentration allows contraction of the sarcomeres (3). Initial calcium levels are recovered via SERCA2 which recruit calcium in the SR (4) and NCX that interchanges cytosolic calcium with extracellular sodium (5).

The contractile and electrical forces spread readily between adjacent CMs thank to the intercalated disc (ID). IDs are located at the ends of the rod shaped CMs and are composed of desmosomes (intercellular adhesion), fascia adherens (transmission of contractile forces) and Gap junctions (AP propagation) (Fig. 7) (Estigoy *et al*, 2009). It has recently been observed that these elements are in close interaction, so defects in the structural part of IDs can affect excitability of the cells and vice versa (Moncayo-Arlandi & Brugada, 2017).

In vertebrates, gap junctions are formed by connexins, which are trans-membrane proteins that enable the direct cytoplasmic exchange of ions and low molecular weight metabolites between adjacent cells (Nielsen *et al*, 2012). In the adult murine heart, there are different connexin isoforms and Cx43, Cx40, Cx45 and Cx30.2 are the predominant ones (Davis *et al*, 1994; Jansen *et al*, 2010). Cx43 is the major isoform, expressed in both atrial and ventricular myocardium. Cx40 is present in the atria, AVN and VCS (Beyer *et al.*, 1987; Davis *et al.*, 1994). Cx45 and Cx30.2 are less studied and their expression is more restricted to the CCS (Coppin *et al*, 1999; Kreuzberg *et al*, 2009, 2005). Furthermore, sodium channels, like Nav1.5, essential for electrical impulse conduction, concentrate at the intercalated disc too (Fig. 7) (Dhar Malhotra *et al*, 2001).

Disorganized intercalated discs can lead to several cardiac diseases. One example is the arrhythmogenic right ventricular cardiomyopathy (ARVC), that arises from mutations in structural proteins of the desmosomes and leads to fibrosis, reduced and mislocalized Cx43 and arrhythmias, that can lead to sudden cardiac death (Gard *et al*, 2005; Cerrone *et al*, 2012a). Brugada Syndrome, is considered a channelopathy, mainly related with mutations in *Scn5a* (Nav1.5), however, mutations in proteins of the desmosomes can also affect *Scn5a* expression and reproduce several Brugada Syndrome features (Moncayo-Arlandi & Brugada, 2017). These data indicate that the structural and the excitability components of the IDs do interact with each other.

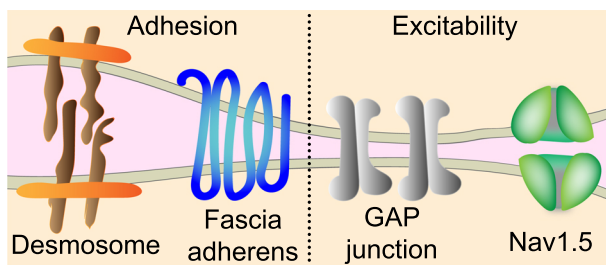


**Figure 7. Intercalated disc composition.** Draw of the different structures that can be found in intercalated discs of CMs classified by function: adhesion and excitability. Orange is cytosol and pink extracellular space between two couple CMs.

## Cardiac Conduction System development

Genetic and environmental factors are both contributing to the development of arrhythmias. The comprehension of CCS embryonic development can help to elucidate the genetic origin of some types of arrhythmias.

In the mouse, as mentioned above, the CC is already a beating structure. Those beats are automatically generated by the newly formed CMs derived from the FHF. At this stage, CMs are poorly differentiated, presenting underdeveloped sarcomeres and SR, which resembles adult conducting CMs. Markers that are later exclusive for CCS, such as *Hcn4* and *Cx40* are expressed in the myocardial layer of the HT (Mommersteeg *et al*; Später *et al*, 2013). At E8.0, when the HT is formed, the dominant automaticity is located in the venous pole and all cells conduct similarly, so that blood is pumped towards the arterial pole or OFT in a peristaltic mode (Fig. 8). The transcription factor *Nxk2.5* is initially expressed in the CC and SHF precursors, although later on, when the heart elongates and starts looping, *Tbx18* becomes the predominant marker in the

venous pole, where pacemaker CMs are formed (Christoffels *et al*, 2006; Mommersteeg *et al*; Wiese *et al*, 2009). The SAN can be anatomically distinguished for first time at E11.5 (Challice & Virágh, 1980).

The atrioventricular canal (AVC) is the structure of the primitive tube that separates atria and ventricles and gives rise to the atrio-ventricular ring and AVN (Fig. 8). The AVC comes from Tbx2<sup>+</sup> cells at the IFT of the HT. Around E9, the AVC expresses Bmp2, Tbx2 and Tbx3 (Singh *et al*, 2012). This combination of TFs represses the expression of markers for chamber myocardium and keeps Cx30.2, which is important for the slow conduction phenotype of the AVN. From E12.5 onwards the annulus fibrosus insulates atria from ventricles and Tbx3<sup>+</sup> cells form the AVN. It has been described that Tbx5 and Gata4 also contribute to the slow conduction velocity found in the AVN (Munshi *et al*, 2009). In contrast, the ventricular conduction system is fast conducting due to expression of Cx40 and Nav1.5. The HB forms from the arterial pole of the HT and the timing is similar to that of the AVN (Mohan *et al*, 2017) (Fig. 8). However, the BBs and the PFs are specified later in development, around E15.5. BBs come from sub-endocardial CMs located in the trabecules of the septum and PFs from the trabecules of the ventricular chambers, being SHF-derived in the RV and FHF-derived in the LV (Christoffels & Moorman, 2009; van Eif *et al*, 2018).

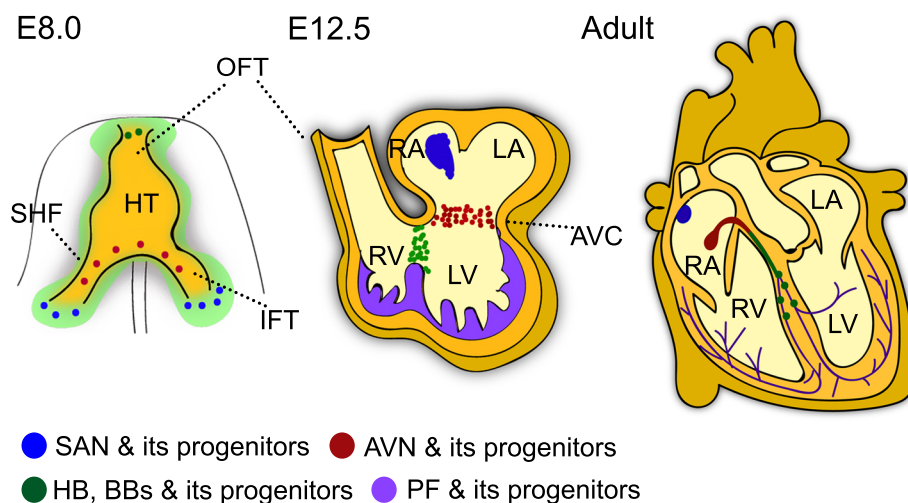


**Figure 8. Cardiac conduction system development.** From left to right, E8.0 heart tube (HT), E12.5 and adult heart representation with CCS elements. Each color indicates a different part of the adult CCS and correspond to the location of their progenitor cells at E8.0 and E12.5.

The origin of the VCS has been long debated and still some aspects of it remained obscure. Clonal analysis has shown that VCS share a common progenitor with surrounding working CMs and after specification there are limited rounds of proliferation (biphasic model) (Miquerol *et al*, 2010). However, it has been suggested that CNC and epicardial derived cells can contribute to the VCS, although there are not yet definitive conclusions about this possibility (Nakamura *et al*, 2006; Aanhaanen *et al*, 2010). Nevertheless, it is clear that different elements of the CCS derive from different progenitor pools of the FHF and SHF, although in the adult heart, they are integrated in a single conduction system (Miquerol *et al*, 2011).

### Meis transcription factors

As described, cardiogenesis is a complex process that requires to be tightly regulated. Transcription factors (TF) play an important role in the regulation of embryonic development, since they possess the capability to bind DNA and control the expression of a subset of genes. There are TFs whose function in heart development has been studied for decades, but many others have been recently discovered.

Meis TFs belong to the TALE family (Three Aminoacid Loop Extension) and are highly conserved among species at the molecular and functional level (Longobardi *et al*, 2014a). *Meis1* (myeloid ecotropic viral integration site 1 ) was the first gene of the family to be identified (Moskow *et al*, 1995). In mammals, two more genes with high homology were identified; *Meis2* and *Meis3* (Nakamura *et al*, 1996; Oulad-Abdelghani *et al*, 1997). Except in the head, the expression patterns of *Meis1* and *Meis2* in embryos are highly similar and both genes encode very similar proteins, which suggests they might have redundant functions. In contrast, *Meis3* expression is mainly restricted to the hindbrain, although it can be also detected in the heart, spleen and lung at later stages (Nakamura *et al*, 1996). A *Meis3* knockout mouse has not been generated so very little is known about *Meis3* functions in mammalian development.

*Meis1* is expressed in the neural tube, the eye, the ear primordium, gut, cardiac chambers, lung, paraxial mesoderm (Hisa *et al*, 2004; González-Lázaro *et al*, 2014) and proximal domain of the forming limb (Mercader *et al*, 1999). *Meis2* expression

pattern overlaps with that of *Meis1* in many of the areas described above. However, *Meis2* is not expressed in the eye, while it does so in midbrain, forebrain and kidneys, where *Meis1* has not been detected (Oulad-Abdelghani *et al*, 1997; Cecconi *et al*, 1997; Mercader *et al*, 1999).

In addition, Meis TFs function as cofactors of other TFs, such as Pbx, Prep or Hox factors (Mann & Affolter, 1998; Ryoo *et al*, 1999). They can form dimers or trimers, modifying the cofactors' affinity and selectivity for DNA-binding sites. Thus, there is increased difficulty in understanding Meis TFs function, because it varies depending on the context.

*Meis1* knockout mice die around E14.5 due to failing hematopoiesis (Hisa *et al*, 2004; Azcoitia *et al*, 2005). Defects in these mutant embryos also present eye and fetal liver hypoplasia and interventricular septal defects in the heart (Hisa *et al*, 2004; Azcoitia *et al*, 2005; Stankunas *et al*, 2008; González-Lázaro *et al*, 2014). It has been reported that *Meis2* knockout mice also die around E14.5, presenting hemorrhages and *Persistent Truncus Arteriosus* (PTA) (Machon *et al*, 2015). This defect derives from the failure in separating the aortic and pulmonary trunks, and is a relatively common CHD in humans.

*Meis1* functions have been also studied in adult organisms, where it is important for the maintenance of hematopoietic stem cell quiescence in the hematopoietic niche (Simsek *et al*, 2014; Unnisa *et al*, 2012). It plays a key role in the development of leukemia and other cancer diseases (Wong *et al*, 2007; Zha *et al*, 2014) and it is associated with the Restless Legs Syndrome in humans (Spieler *et al*, 2014). Moreover, regarding the heart, it has been shown that *Meis1* is important for the cell cycle arrest of postnatal CMs in mice (Mahmoud *et al*, 2013) while *Meis1* genetic variants are associated with PR elongation in humans, suggesting a role in the CCS function (Pfeufer *et al*, 2010; Smith *et al*, 2011a). In addition, sporadic germline heterozygous *Meis2* mutations in humans lead to palatal defects, intellectual disability and congenital heart defects, mainly affecting the interventricular septum and OFT positioning (Louw *et al*, 2015; Verheije *et al*, 2019; Giliberti *et al*, 2019).





# OBJECTIVES

*“Al investigador no hay que decirle lo que tiene que investigar. Hay que dejarle libertad para que investigue lo que le interesa”.*

Margarita Salas



We consider there are enough evidences suggesting *Meis1* and *Meis2* play a role in cardiomyocytes of the developing and adult heart but they have not been explored in detail yet. Moreover, understanding *Meis1* and *Meis2* function in the heart will generate new knowledge in the cardiovascular field that might be relevant for the comprehension of certain human diseases.

Thus, the main goal of this thesis is to study the role of *Meis1* and *Meis2* transcription factors in the context of cardiac development and adult heart homeostasis.

To achieve this goal, we propose the following concrete objectives:

1. Describe the expression pattern of *Meis1* and *Meis2* in the developing and adult heart.
2. Generate mouse models for the cardiomyocyte-specific constitutive and inducible double deletion of *Meis1* and *Meis2*.
3. Characterize the phenotype generated upon *Meis1* and *Meis2* constitutive and inducible loss of function in cardiomyocytes.
4. Describe molecular determinants of *Meis* function in cardiomyocytes.
5. Identify potential direct targets of *Meis1* and *Meis2* in cardiomyocytes.





# MATERIALS & METHODS

*"If you want something you've  
never had, you must be willing to  
do something you've never done".*  
Thomas Jefferson



## Animal procedures

### Mouse lines

All animals in this project were handled following CNIC Ethics Committee, Spanish laws and the EU Directive 2010/63/EU. All the experiments were approved by CNIC and Universidad Autónoma de Madrid Committees for “Ética y Bienestar Animal” and the area of “Protección Animal” of Comunidad de Madrid with reference PROEX 220/15. In this study mice were maintained on a mixed genetic background.

To study the expression of *Meis1* we took advantage of two knock-in mouse lines previously generated in the laboratory: *Meis1-ECFP* and *Meis1-CreER* (González-Lázaro *et al.*, 2014). *Meis1-CreER* was crossed with *R26RTdTomato* line (Madisen *et al.*, 2010) containing a STOP cassette flanked with LoxP sites, followed by Tomato fluorescence protein, in the R26 locus. Upon Cre recombination STOP cassette is removed and Tomato fluorescence protein is expressed in the recombined cell and its offspring. *Meis1-CreER* is only active for recombination in the presence of tamoxifen. Tamoxifen was administered orally to adult mice (1mg/day for 5 consecutive days). Hearts were harvested two days after tamoxifen injection.

To understand the function of *Meis1* and *Meis2* in developing and adult CMs, we generated two models that allowed us to simultaneously delete both genes specifically in CMs. To generate a *Meis1<sup>flox/flox</sup>; Meis2<sup>flox/flox</sup>* mouse line, we combined a *Meis1-flox* (Unnisa *et al.*, 2012) gently given by Dr. Sadek and a *Meis2-flox* allele generated in the laboratory of Miguel Torres (Roselló and Giovinazzo, unpublished). Loxp sites flank exon 8 in *Meis1* and exon 3 in *Meis2*. Upon recombination, *Meis1* loses the homeodomain coding region, essential for *Meis1* activity and *Meis2* does not produce any protein. For the induction of LoxP recombination, we used two transgenic Cre lines specific for CMs,  *$\alpha$ -MHC-Cre* (Agah *et al.*, 1997) and  *$\alpha$ -MHC-MerCreMer*, inducible by tamoxifen (Sohal *et al.*, 2001).

We crossed *Meis1<sup>flox/flox</sup>; Meis2<sup>flox/flox</sup>* females with *Meis1<sup>flox/wt</sup>; Meis2<sup>flox/flox</sup>;  $\alpha$ -MHC-Cre<sup>tg</sup>/wt* males in order to obtain 25% of embryos with *Meis1* and *Meis2* double homozygous

deletion, *Meis1*<sup>flox/flox</sup>; *Meis2*<sup>flox/flox</sup>;  $\alpha$ -MHC-Cre<sup>tg/wt</sup> (dKO), 25% *Meis1*<sup>flox/flox</sup>; *Meis2*<sup>flox/flox</sup>;  $\alpha$ -MHC-Cre<sup>wt/wt</sup> and 25% *Meis1*<sup>flox/wt</sup>; *Meis2*<sup>flox/flox</sup>;  $\alpha$ -MHC-Cre<sup>wt/wt</sup> (both used as control) and 25% of *Meis1*<sup>flox/wt</sup>; *Meis2*<sup>flox/flox</sup>;  $\alpha$ -MHC-Cre<sup>tg/wt</sup> (M1Het;M2KO).

In the case of *Meis1* and *Meis2* deletion in adult CMs, we continued using the same *Meis1*<sup>flox/flox</sup>; *Meis2*<sup>flox/flox</sup> mice but crossing them with *Meis1*<sup>flox/flox</sup>; *Meis2*<sup>flox/flox</sup>;  $\alpha$ -MHC-MerCreMer<sup>tg/wt</sup> to obtain 50% of *Meis1*<sup>flox/flox</sup>; *Meis2*<sup>flox/flox</sup>;  $\alpha$ -MHC-MerCreMer<sup>tg/wt</sup> (inducible-dKO or idKO) and 50% of *Meis1*<sup>flox/flox</sup>; *Meis2*<sup>flox/flox</sup>;  $\alpha$ -MHC-MerCreMer<sup>wt/wt</sup> (Control). As an extra control for possible Cre toxicity we used  $\alpha$ -MHC-MerCreMer<sup>tg/wt</sup> (CRE) compared to their wild type (WT) littermates. Tamoxifen was administered through oral-gavage (1mg/day for 5 consecutive days) to mice around 10 weeks of age. All experimental groups of this model were given tamoxifen.

Animals were genotyped by PCR following protocols detailed in the publication of each line. In the case of *Meis2*<sup>flox/flox</sup>, here are explained the primers and program used:

Fw: CAA GGA CGC AAT CTA TGG GTA

Rv: TGC AGA AAA CTT TCC TCT TAA TCA

PCR program: (3'95°, 35x (30''95°, 30''51°, 1'30''72°) 7'72° and 4°)

### *Tamoxifen preparation*

200mg of tamoxifen (Sigma-T5648-1G) were dissolved in 20ml of corn oil (Sigma-C8267) for a final concentration of 10mg/ml. The solution was sonicated for 1 hour in ice with ultrasonic homogenizer (Bandelin) and then aliquoted to store at 4°C. When the stock solution preparation was older than 1 week, the aliquots were re-sonicated for 15 min before use. 100ul were given by oral-gavage to the mice per day, during 5 days.

### *Embryo harvest*

Mice were mated in the afternoon and females were checked in the morning for the presence of vaginal plug. The stage of the embryos was defined by the day when the plug was observed, considering at noon of that day embryonic day 0.5 (E0.5).

Pregnancy was always checked again before sacrifice, to avoid false positives. Pregnant females were euthanized by CO<sub>2</sub> inhalation and the uterus was extracted through an incision of the abdominal cavity and transferred to PBS. Then, in a petri dish containing PBS, the muscular layer of the uterus was removed with forceps. For embryos at E13.5 or younger, a piece of the yolk sac was collected for genotyping and from E14.5 onwards the tip of the tail was used instead. After removing the yolk sac and amnion, embryos were decapitated and the thorax was opened to collect the heart. Hearts were quickly wash in PBS and fixed in paraformaldehyde (PFA) (Merck) 2% in PBS overnight at 4°C.

### *Adult mouse sacrifice*

Heparin (ROVI 1000UL/mL) was injected intraperitoneal in mice (200µL), 30 minutes before sacrifice to improve blood removal. Adult mice were sacrificed at different experimental points by CO<sub>2</sub> inhalation and hearts were harvested by opening the thorax with scissors and forceps. Hearts were place in a petri dish with a KCl 30mM solution to stop beating in the phase of diastole. After removing lungs and thymus, hearts were weighted and placed in another petri dish with PBS for cannulation. A 5ml syringe (Beckton Dickinson) with a blunt needle was introduced in the left ventricle through the aorta and PBS was infused slowly until blood was removed. Then, hearts were fixed in PFA 2% in PBS 24 hours at 4°C. The left posterior leg of every mice was cut, and skin and muscle removed, to measure tibia length with a caliber.

### *BrdU treatment*

Adult mice were treated with BrdU (5-Bromo-2'-desoxyuridine; Merck B5002) dissolved at 0.5mg/mL in drinking water for 3 weeks. The treatment started one week after tamoxifen administration.

### **Tissue processing**

#### *Cryo and paraffin-sectioning*

After fixation, tissues were washed several times in PBS and cryopreserved with 15% sucrose overnight at 4°C. Then, tissues were incubated in a solution with 15% sucrose and 7.5% gelatin in PBS at 37°C for at least 4 hours, changing the solution and

agitating occasionally. Gelatin blocks were prepared in a P6 dish at room temperature for gelatin solidification. Blocks were cooled down at 4°C and frozen in isopentane at -80°C for 1 minute and kept stored at -80°C until cryo-sectioning. 8 µm-thick sections were obtained using a Leica CM1950 automated Cryostat and stored at -20°C.

If the objective was to do paraffin sections, tissues were directly washed with 70% ethanol after fixation. Then, samples were incubated in different solutions at room temperature with increasing percentage of ethanol, until incubation with xilol. Samples were embedded in paraffin at 65°C and after orientation, left at 4°C to solidify. The dehydration process was usually done in a Thermo Excelsior SA processor at the Histopathology Unit at CNIC. Paraffin blocks were cut at 4 µm (10 µm for in situ hybridization) using a Leica RM2245 semi-automatic microtome. Sections were stored at 4°C.

In both cases sections were collected on Superfrost+ slides (Fisherbrand).

### ***In situ* hybridization on sections**

Paraffin sections were rehydrated from xilol to PBS passing through sterile solutions with decreasing concentrations of ethanol. Sections were digested with proteinase K (10µg/ml) at 37°C for 10 minutes. Riboprobe hybridization was performed at 65°C overnight. The next day, sections were washed and incubated with anti-DIG antibody at 4°C overnight. Then, sections were developed with BM-purple (Roche, ref 11442074001) at room temperature or 37°C. Time of development was about 5 days.

## **Immunofluorescence**

### ***In paraffin sections***

Slides were incubated in xilol and solutions with decreasing concentrations of ethanol, washed in distilled water and PBS. Antigen retrieval was performed to break methylene bridges formed with fixation that cross-link proteins and mask the antigen sites. We used the heat-induced method with two different buffers. The most common

was the sodium citrate but Meis antibodies worked better with Tris-EDTA buffer.

**Here are the recipes for each buffer:**

<b>Citrate Buffer</b>		
Citric Acid Monohydrate	Sigma-33114	10mM
Distilled water		1L
Adjust pH to 6.0 with NaOH		
Tween 20		0.05%
Store at room temperature for 1 month		

<b>Tris-EDTA Buffer</b>		
Trizma Base	Sigma-93350	10mM
EDTA solution	Sigma-E6758	1mM
Distilled water		1L
Adjust pH to 9.0		
Tween 20		0.05%
Store at room temperature for 1 month		

For antigen retrieval, the buffer was pre-heated in the microwave for 5 minutes. Samples were immersed in the buffer and heated for 20 minutes. Then, buffer with samples were let to temper for 20 minutes. Permeabilization was done with Triton X-100 0.5% in PBS for 30 minutes. In the case of Cx43, Triton concentration was reduced to 0.25%. Peroxidase block was done, if needed, after permeabilization, using H<sub>2</sub>O<sub>2</sub> 3% in methanol for 1 hour in darkness. To avoid unspecific binding of the antibody, sections were incubated with the universal TNB blocking reagent FP1012-Perkin Elmer, 1 hour at room temperature. Primary antibodies were incubated in the same TNB solution overnight at 4°C. Secondary antibodies were incubated in PBS 1 hour at room temperature. Slides were washed several times between every step with Tween 0.1% in PBS. Finally, slides were mounted with Dako fluorescence mounting medium (s3023).

*In gelatin sections*

Slides were incubated in Tween 0.1% in PBS at 37°C for 15 minutes and washed several times at room temperature until gelatin was removed. Then continued with the steps explained before without performing antigen retrieval.

### Isolated CMs

After fixation, PFA was carefully washed several times with PBS. Then we followed the same steps explained before, starting with permeabilization. For BrdU staining a step of DNase digestion was needed. It was performed after permeabilization, with DNase I 1:20 (Roche) for 1 hour at 37°C. After secondary antibody, Vectashield mounting medium (Vector Laboratories) was added to the dishes.

### Whole mount atria from fetuses

Atria were washed with PBS after fixation and incubated with Triton X-100 0.5% in PBS for 24 hours at 4°C. Blocking reagent was incubated for 8 hours and solution with Wheat Germ Agglutinin (WGA-Thermo Scientific-W21404) and DAPI for three days. Before confocal acquisition atria were transparent with CUBIC 1 for 1 day at 4°C (Susaki *et al*, 2015).

#### Primary antibodies used:

TARGET	HOST	CONCENTRATION	REFERENCE
Meis a *	Rabbit	1:500	Torres' Lab
Meis 2 *	Rabbit	1:500	Torres' Lab
Hcn4	Mouse	1:100	Abcam ab85023
c-TnT	Mouse	1:200	MS-295 Thermo Scientific
Cx43	Rabbit	1:200	Sigma C6219
CFP	Goat	1:200	Acris R1091P
BrdU	Mouse	1:50	Invitrogen 347580
PH3	Rabbit	1:100	Millipore 06-570

\*Anti-Meis-a antibody and anti-Meis2 were generated in rabbits with a synthetic peptide corresponding to the conserved C-terminal domain of Meis1 and Meis2 (GMNMGMDGQWHYM) and to a Meis2-specific N-terminal domain of Meis2 (HAPRPIPPVHHLNHGPP), respectively (Mercader, 2005).

#### Secondary antibodies used:

REACTIVITY	CONJUGATED	CONCENTRATION	REFERENCE
Rabbit	A633	1:500	Life technologies A21071
Rabbit	A594	1:500	Life technologies A11012
Rabbit	HRP	1:500	Dako P0448
Mouse	A488	1:500	Life technologies A11029
Mouse	A568	1:500	Life technologies A11004
Mouse	A647	1:500	Life technologies A21052
Goat	Biotin	1:500	Jackson 705-065-003

## Hematoxilin & Eosin and Sirius Red staining

H&E and Sirius Red staining were performed at the CNIC Histopathology Unit. H&E staining was carried out using the Leica Automated Slide Stainer ST5020. For Sirius Red staining, the sections were brought to water and the nuclei were stained with Wiegerts hematoxylin. The tissue was then stained with Sirius red solution for one hour followed by differentiation in acetic acid and finally dehydrated and mounted in DPX.

## Image acquisition

Images of the *in situ* hybridization were acquired with a Nikon Eclipse 90i microscope. H&E and Siruis Red stained sections were scanned with Hamamatsu Nanozoomer 2.0 RS and NDP.Scan 2.5 software. Analysis and quantifications were performed with NDP.Analyzer software. Immunofluorescence sections were acquired with a Zeiss LSM 700 confocal microscope and a Leica TCS SP8 coupled to a DMI8 inverted confocal microscope Navigator module equipped with white light laser. Whole-mount images of hearts were acquired with Nikon DXM1200F coupled to a Leica MZFLIII scope with a Plan Apo 1x objective.

## Echocardiography

### *In pregnant females*

In a first approach, pregnant females, with the belly shaved were anesthetized with 2% isoflurane in oxygen. Abdominal surgery was then performed for uterus exposure. After surgery, isoflurane was adjusted to maintain a heart rate at  $450\pm 50$  bpm and fetuses were exposed one at a time to keep them as warm as possible. An infrared heat lamp was used for the same purpose during acquisition. Echocardiography was performed by an expert operator using a high-frequency ultrasound system (Vevo 2100, Visualsonics, Canada) with a 50-MHz probe on a heating platform. Bidimensional (2D), M-Mode and Doppler echocardiography were used to visualize the hearts in long and short axis view (LAX and SAX, respectively). Left and right ventricular ejection fraction (EF), wall thickness and diastolic and systolic chamber dimensions were assessed from the M-Mode SAX view. Color flow Doppler was placed at the base of the left or right ventricle to visualize simultaneously the inflow and outflow blood pattern. Heart

rate was calculated using three consecutive outflow waves. The position of the fetuses was recorded, so that fetal identity could be tracked for genotyping. This procedure was therefore blinded to the genotype of the fetuses.

In the second approach, pregnant females were lightly anesthetized with 0.5-2% isoflurane in oxygen, adjusting the isoflurane to maintain heart rate at  $450\pm 50$  bpm. Abdominal palpation was done to identify number of fetuses and position before image acquisition. Transabdominal echocardiography was performed by an expert operator using the same ultrasound system and acquiring the same images as explain above. Afterwards, a small incision was done in the abdominal cavity to confirm embryo number and position and track fetal identity for genotyping.

### *Adult mice*

Transthoracic echocardiography was performed blinded by an expert operator using a high-frequency ultrasound system (Vevo 2100, Visualsonics, Canada) with a 40-MHz linear probe on a heating platform. Mice were lightly anesthetized with 0.5-2% isoflurane in oxygen, adjusting the isoflurane to maintain heart rate at  $450\pm 50$  bpm. A base-apex electrocardiogram was continuously monitored. Images were analyzed using Vevo 2100Workstation software. Parasternal standard, 2D and MM, long and short axis views at the level of the papillary muscles (LAX and SAX view, respectively) were acquired.

### **Optical mapping**

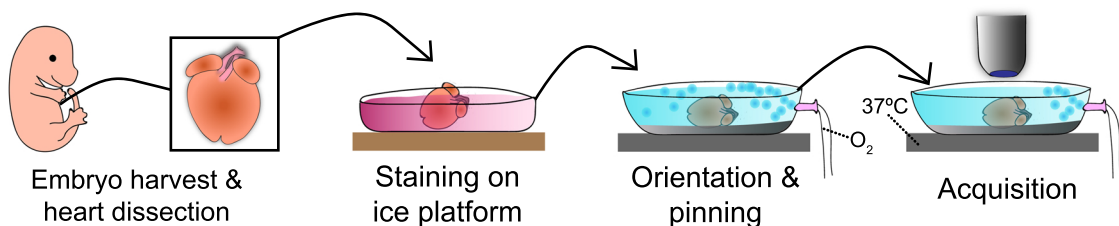
The optical mapping technique provides action potential recordings at the tissue level with a high temporal and spatial resolution, and can be used from the subcellular level to the whole heart in vivo. We performed the technique in hearts from E14.5 and E16.5 fetuses following similar protocol to previous publications by Dr. Sedmera's group (Benes *et al*, 2014).

Pregnant females were sacrificed by cervical dislocation and embryos were harvested as explained above. While hearts were dissected, embryos were placed on a petri dish with ice-cold Tyrode's Buffer to prevent ischemic damage. Harvested hearts

were placed in wells of a P12 dish on ice and incubated for 15 minutes in 500mL of cold Tyrode's Buffer with 2 $\mu$ L of di-4-ANEPPS (Invitrogen) (dye with fluorescence voltage dependent) and 15 $\mu$ L of blebbistatin (it stops heart beat and avoids movements during recording) in darkness. After staining, hearts were placed on a special warm dish (37°C) with Tyrode's Buffer and constant oxygen flow. Hearts were pinned and oriented for the desired acquisition view. Data was recorded using Ultima L high-speed camera and bundled software.

Tyrode's Buffer	
NaCl	145mM
KCl	5.9mM
HEPES	5mM
CaCl <sub>2</sub>	1.1mM
MgCl <sub>2</sub>	1.2mM
Glucose	11mM
Adjust pH to 7.4 at 37°C	

#### Schematic representation of optical mapping procedure:



Data analysis and maps were done with BrainVision Analysis software. AP recordings were processed with Medium (3x3) and High Pass (0.5) filter to reduced noise and derivatives were calculated. Usually, the first beat was selected for mapping and a spatial filter of 3x3 was applied to improve map resolution. For activation curves calculations, the area of each color band in each ventricle was measured and expressed as percentage of whole ventricular area. Limit between left and right ventricles was defined by hand from apex aperture to base following the septum shadow in bright field pictures. Heart rates were calculated from the distance between one AP maximum peak and the next one. A-V delay time was determine by the time between the beginning of atrial AP and the beginning of ventricular AP.

## Adult cardiomyocytes isolation

Adult mice were sacrificed by CO<sub>2</sub> inhalation and the thoracic cavity was opened to expose the heart. Hearts were dissected and cannulated in a petri dish with Perfusion Buffer. The cannula was secured to the aorta with surgical thread and then placed in the Langendorff system (Obame *et al*, 2008), where Perfusion Buffer was infused for approximately 5 minutes until blood was removed.

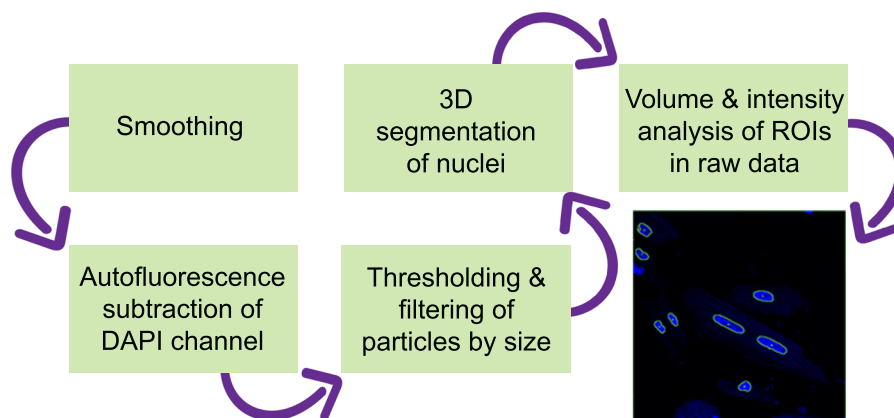
The Langendorff system enables the buffer to enter the heart through the aorta with a constant flux achieved by a peristaltic pump and constant temperature at 37°C. After cleaning the blood, the Digestion Buffer was infused to digest the extracellular matrix and isolate cardiac cells. Digestion was performed for about 20 minutes. Once the heart was completely digested, the cannula was removed and the cardiac tissue placed in a petri dish for complete disaggregation with a Pasteur pipette. From this point onwards, steps were carried out at room temperature. Cardiac cells were filtered through a 100µm strain net for extracellular matrix removing and transferred to a 50mL Falcon tube with Stopping Buffer I. After 15 minutes of decantation, the supernatant was discarded and cells newly resuspended in Stopping Buffer II in a 15mL Falcon tube for 10 minutes. CMs are the largest cells in the adult heart, so they are the first to reach the bottom. Thus, short steps of decantation allow an enrichment in CMs of the final pool of cells. Then, cells were transferred to a new 15mL Falcon tube containing T2 buffer for calcium reintroduction for 10 minutes and the step was repeated to incubate cells in T5 buffer. CMs were then plated on laminin-coated MatTeK glass-bottom dishes with plating medium and incubated at 37°C for about 2-4 hours. When CMs were attached to laminin, the medium was washed with PBS and 2% PFA was added overnight at 4°C for fixation before immunostaining.

Here are the recipes for each buffer:

	<b>REAGENT</b>	<b>COMPANY</b>	<b>CONCENTRATION</b>
<b>PERFUSION BUFFER</b>	Sodium chloride	Sigma - Aldrich	113mM
	Potassium choride	Sigma - Aldrich	4,7mM
	Potassium phosphate monobasic	Sigma - Aldrich	0,6mM
	Sodium phosohate dibasic	Sigma - Aldrich	0,6mM
	Magnesium sulphate heptahydrate	Sigma - Aldrich	1,2mM
	Sodium bicarbonate	Sigma - Aldrich	12mM
	Potassium bicarbonate	Sigma - Aldrich	10mM
	Phenol Red	Sigma - Aldrich	0,032mM
	HEPES salt	Sigma - Aldrich	10mM
	Taurine	Sigma - Aldrich	30mM
	Butanodione monoxime (BDM)	Sigma - Aldrich	10mM
	Glucose	Sigma - Aldrich	5,5mM
	H <sub>2</sub> O		
<b>DIGESTION BUFFER</b>	Perfussion buffer		1X
	Liberase TM 100mg	Roche Appl. Biosc	0,2mg/ml
	Trypsin 2,5%	Gibco	0,14mg/ml
	Calcium Chloride 100mM	Sigma - Aldrich	12,5µM
	H <sub>2</sub> O		
<b>STOPPING BUFFER I</b>	Perfussion buffer		1X
	Fetal Bovine Serum	Gibco	5%
	Calcium Choride 10mM	Sigma - Aldrich	12,5µM
<b>STOPPING BUFFER II</b>	Perfussion buffer		1X
	Fetal Bovine Serum	Gibco	10%
	Calcium Choride 10mM	Sigma - Aldrich	12,5µM
<b>T2</b>	Stopping Buffer II		1X
	Calcium Choride	Sigma - Aldrich	100µM
<b>T5</b>	Stopping Buffer II		1X
	Calcium Choride	Sigma - Aldrich	1mM
<b>PLATING MEDIUM</b>	Medium 199	Invitrogen	
	PEN-STREPT	Lonza	100U/ml
	L-Glutamine	Lonza	1%
	BSA	Sigma-Aldrich	0,2%
	NaHCO <sub>3</sub>	Sigma-Aldrich	22mM
	FBS	GIBCO	5%
	BDM (2,3-Butanedione monoxime		10mM
	Blebbistatin		25uM

## Ploidy estimation in isolated cardiomyocytes

To measure nuclear volumes and DAPI intensity in isolated CMs we acquired confocal z-stacks at high magnification (63X) with steps of 2 $\mu$ m using Zeiss LSM 700 confocal microscope. Image J (<https://imagej.nih.gov/ij/>) was used for image analysis. The first step was to segment the DAPI channel, for which images were filtered with Gaussian Blur to improve automatic recognition of nuclei. The green channel (autofluorescence) was used to subtract background signal in the DAPI channel and the threshold tool was used to create a 3D binary file. If necessary, the “fill holes” tool was applied and “analyzed particles” tool was used to eliminate small dots from background. The next step was to use 3D ROI manager to create a 3D selection around the nuclei (Ollion *et al*, 2013). Objects touching the border of the pictures were not consider for analysis. Finally, objects created were placed on the original DAPI channel to measure their volume and intensity. The same objects were used to measure BrdU intensity in the red channel.



## Electrocardiogram

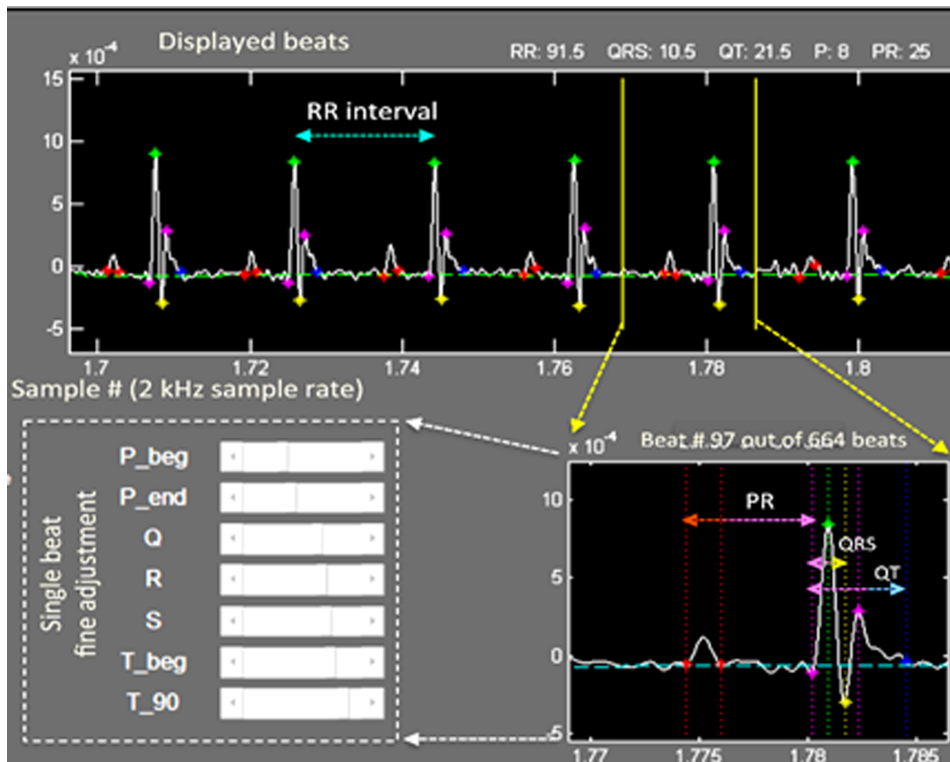
Adult mice were lightly anesthetized with 1.5% isoflurane in oxygen and placed facing up on a metallic platform. Electrodes were introduced subcutaneously in each limb and ECG was recorded for about 2 minutes.

When mice were challenged with isoproterenol, 5 minutes were recorded before treatment. Then, isoproterenol (3mg/kg) was injected intraperitoneal and heart beats were recorded for additional 20 minutes. During the last minute the isoflurane was turned off to observe heart conduction during the recovery phase. Experiments always

finished before animals were completely awake, to avoid stress. Moreover, an infrared heat lamp was used to keep normal body temperature in mice and protective cream was apply in the eyes before starting the experiment.

Analysis were performed on manually selected 40-second-fragments containing about 300-400 beats of stable ECG. Measurements were calculated with custom MatLab scripts design by the group of Dr. David Filgueiras at CNIC. To detect the R-peak of the QRS complex we used parabolic fitting of the coiflet wavelet transformation and further detection of the maximum magnitude point. All R-peak detections were supervised to ensure accuracy of ECG segmentations (see picture bellow-green dots). After detection of QRS complex, P and T waves, ECG intervals were extracted using adaptive windowing depending upon beat-to-beat R-R changes. Specifically: PR intervals were measured from the beginning of the P wave to the beginning of the R wave; QRS intervals were measured from the beginning of the Q wave until the lowest amplitude point of S wave; QT intervals were measured from the beginning of the Q wave until the point where the T-wave declines to 90% (T90) from the peak; QTt intervals were measured from the beginning of the Q wave to the point where the tangential line from the beginning of T wave crosses the baseline. Adaptive heart-rate-corrected QT and QTt values (QTc; QTtc) were derived using a modification of Bazzet's formula for murine electrocardiography (Mitchell *et al*, 1998).

Here is an example of how the ECG is visualized and automatically analyzed with this software:



## RNA sequencing

RNA-seq was performed in four different conditions, atria and ventricles from fetal hearts at E15.5 and from adult hearts to compare Meis1 and Meis2 double deletion (constitutive or inducible) with control littermates. In all cases, 4 replicates were used for each condition.

## RNA isolation

Fetuses were harvested at E15.5 from four independent litters and a Control and a dKO were selected from each litter. Hearts were dissected in ice-cold sterile PBS. Atria and ventricles were separated and OFT removed, to be immediately frozen with liquid nitrogen and stored at  $-80^{\circ}\text{C}$  until all the samples were collected. Tissue lysis was performed with TissueLyser LT (Quiagen) and RNA isolation with RNeasy Mini Kit (Quiagen).

Adult hearts from 8 male littermates were harvested two weeks after tamoxifen induction, as explained in previous chapters, and cannulated to clean the blood with

ice-cold sterile PBS. Atria and ventricles were separated and OFT removed before being frozen at  $-80^{\circ}\text{C}$ . Tissue lysis was done with TriReagent (Trizol; Sigma-T9424) using TissueLyser LT (Quiagen). Total RNA isolation was completed following RNeasy Midi Kit (Quiagen) protocol for RNA cleanup.

### *RNA-seq library production and sequencing*

It was performed at CNIC Genomic Unit. 20ng of total RNA were used to generate barcoded RNA-seq libraries using the NEBNext Ultra RNA Library preparation kit (New England Biolabs). Briefly, poly A+ RNA was purified using poly-T oligo-attached magnetic beads followed by fragmentation and then first and second cDNA strand synthesis. Next, cDNA ends were repaired and adenylated. The NEBNext adaptor was then ligated, followed by uracil excision from the adaptor and PCR amplification. Finally, the size and the concentration of the libraries was checked using the TapeStation 2200 DNA 1000 chip.

Libraries were sequenced on a HiSeq2500 (Illumina) to generate 60-base single reads. FastQ files for each sample were obtained using bcltofastQ software 2.20.

### *RNA-seq data analysis*

Read quality was assessed with FastQC (<http://www.bioinformatics.babraham.ac.uk/projects/fastqc/>). Over-represented sequences were trimmed with Cutadapt 1.7.1 (Martin, 2012), which also discarded reads that were shorter than 30 bp. The resulting reads were mapped against the mouse transcriptome (GRCm38, release 91; aug2017 archive) and quantified using RSEM v1.2.20 (Ritchie *et al.*, 2015). Data were then processed with a differential expression analysis pipeline that used Bioconductor package LIMMA (Ritchie *et al.*, 2015) for normalization and differential expression testing, using a paired strategy.

Genes with at least 1 count per million in at least 4 samples were considered for statistical analysis. We considered as differentially expressed those genes with Benjamin-Hochberg adjusted  $p$ -value $<0.05$ . Fold change and log (ratio) values were calculated to represent gene expression differences between conditions.

Gene Set Enrichment Analysis was performed with genes differentially expressed using the Broad Institute GSEA “Molecular Signatures Database” (<http://software.broadinstitute.org/gsea/msigdb/index.jsp>) computing overlaps with KEGG and Gene Ontology gene sets.

## Statistics

Parametrical T student test was performed to compare two groups of data. For comparisons with more than two groups of data, Two-way ANOVA was used. In this analysis the influence of two factors, time and genotype, in the distribution of the sample, were studied. Chi square test was used for comparisons between observed and expected frequencies. Data is indicated as mean  $\pm$  SEM except for ECG data which are expressed as median  $\pm$  SEM.

All comparisons and graphs were made using Prism 7.0 statistical analysis software. In all cases adjusted values of  $P < 0.05$  were considered statistically significant.







# RESULTS

*“La science est faite d’erreurs,  
mais ce sont des erreurs qu’il est  
utile de faire, parce qu’elles condui-  
sent peu à peu à la vérité”.*

Jules Verne



## Meis expression pattern in the heart

### *Meis1 And Meis2 Are Expressed In Cardiac Progenitors And The Three Layers Of The Developing And Adult Heart: Endocardium, Myocardium And Epicardium*

Determining the expression pattern of a gene is crucial to be able to understand its function. Thus, we performed *in situ* hybridization for *Meis1* and *Meis2* mRNAs at different embryonic days in the mouse heart (Fig. 9). Similar expression patterns were found for *Meis1* and *Meis2* in the developing heart. At early stages, both genes were expressed in second heart field progenitors, epicardium and endocardium (Fig. 9). However, at E14.5 we detected strong signal of *Meis2* RNA in the valves while *Meis1* was almost absent in this area.

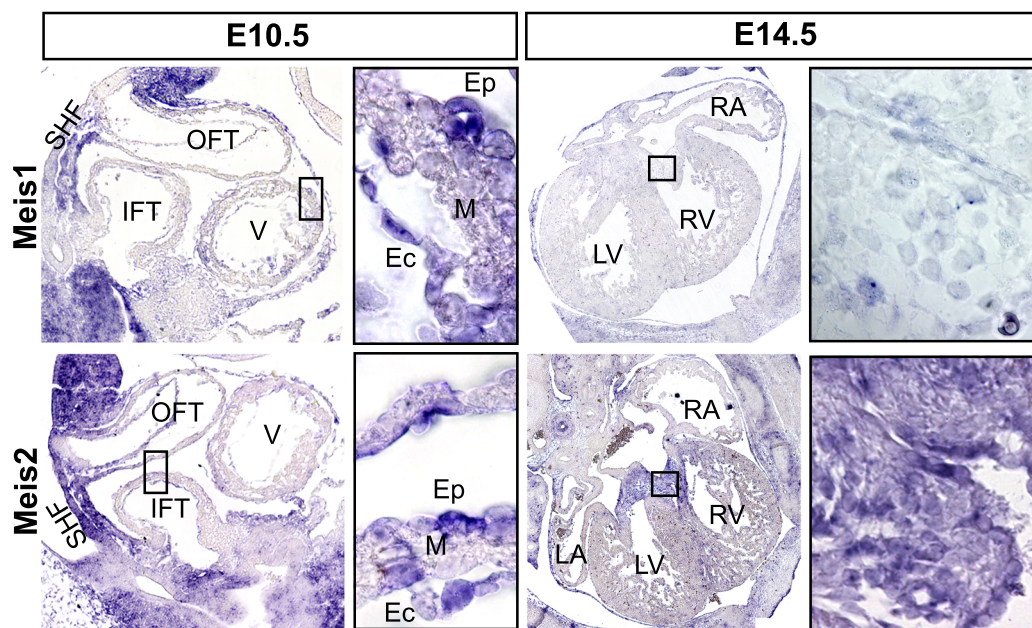


**Figure 9. *Meis1* and *Meis2* mRNA in situ hybridization.** *Meis1* and *Meis2* mRNA was detected in the second heart field (SHF), pericardium, endocardium (Ec) and epicardium (Ep) in E10.5 wild type embryos. Boxed regions indicate magnifications shown to the right. Panels on the right show *Meis1* and *Meis2* expression at E14.5. Magnified boxes show expression pattern in the atrio-ventricular valves. Inflow tract (IFT), Outflow tract (OFT), Ventricle (V), Myocardium (M), Right Atrium (RA), Left Atrium (LA), Left Ventricle (LV), Right Ventricle (RV).

We were not able to observe a clear signal in the myocardium area with this technique so we tried with immunofluorescence (IF) using an antibody that recognizes *Meis1* and *Meis2* proteins. A nuclear signal for *Meis* was found in compact and trabecular

myocardium throughout development (Fig. 10A).

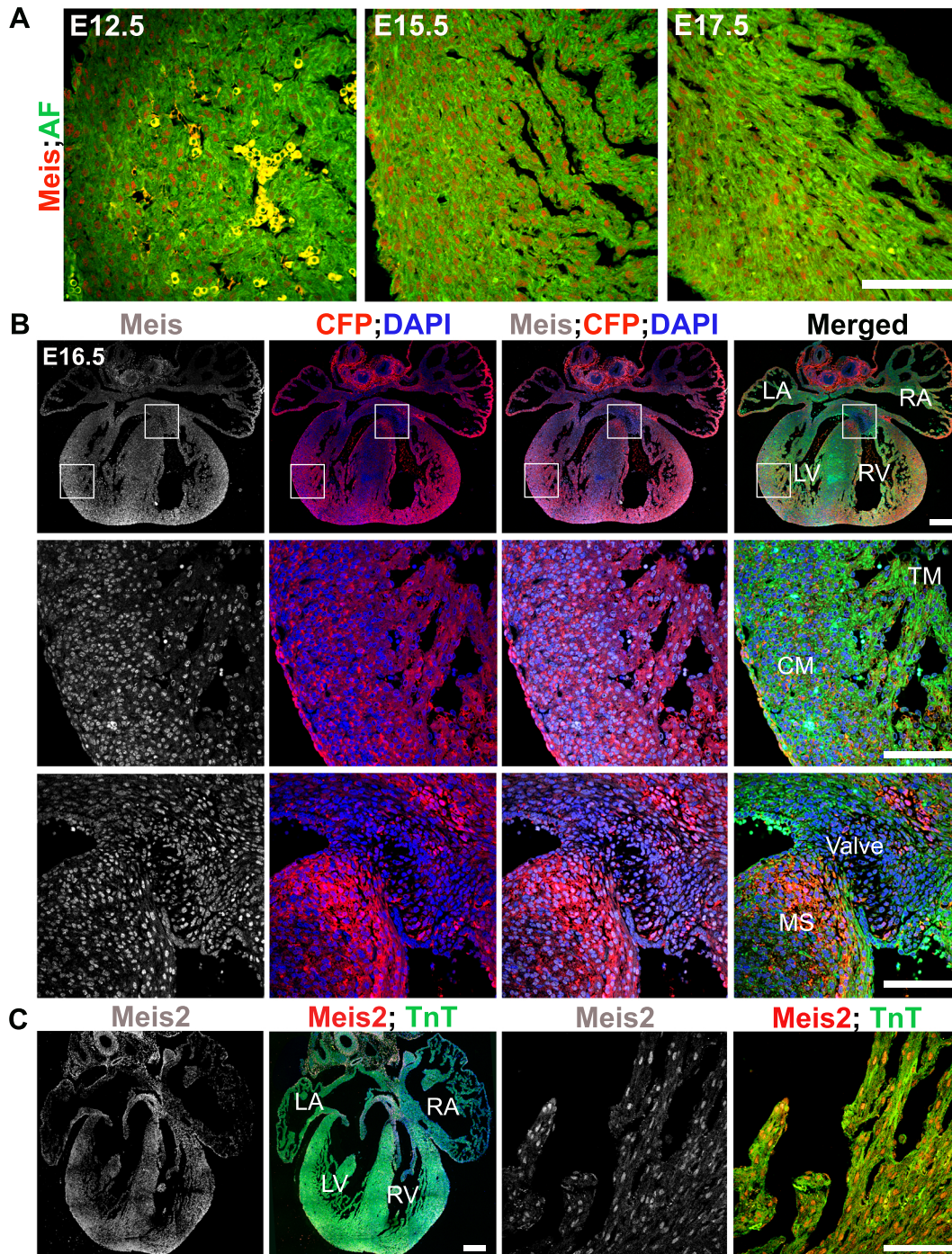


**Figure 10. Meis1 and Meis2 are expressed in developing cardiomyocytes.** (A). Confocal images of ventricles at different embryonic days. Anti-Meis-a immunofluorescence is shown in red. (B). Confocal sections of E16.5 hearts of the *Meis1-ECFP* line combined with Meis-a immunofluorescence. Boxes indicate magnified regions shown below corresponding to ventricular compact (CM) and trabecular (TM) myocardium (middle panel) and sub-membranous area of the septum (lower panel). (C). Immunofluorescence with anti-Meis2 specific antibody. Right panels show a high magnification of a ventricular myocardium region. Scale bars: 100µm in all pictures.

In order to better understand the expression dynamics of Meis in the myocardium, we took advantage of a *Meis1-ECFP* knock-in line and compared the ECFP fluorescence with a Meis antibody IF at E16.5 (Fig. 10B). The ECFP signal was detected in myocardium of the atria and ventricles. The pattern was quite homogeneous, except in the septum, where a strong ECFP signal was present in the sub-membranous and sub-endocardial layers (Fig. 10B). The central part of the septum showed weak ECFP signal, while the Meis antibody stains this region. This suggests that Meis2 could be the prevalent factor in the central septum area as well as in the valves. Moreover, we confirmed these results using an antibody specific for Meis2 protein, which detected a nuclear signal in the valves, the septum and also the compact and trabecular myocardium (Fig. 10C).

We next addressed the same question in the adult heart. We continued using the *Meis1-ECFP* tool and observed a strong signal in the sinoatrial and atrio-ventricular nodes and the His Bundle (Fig. 11A). The atria were also labeled, but this was not clear in the case of ventricular myocardium (Fig. 11A). IF for Meis and Hcn4 confirmed the preferential expression of these transcription factors in the CCS and in atrial and ventricular cardiomyocytes (Fig. 11B). To further confirm our results, we used *Meis1-CreER; R26-TdTomato* as a reporter of Meis1 lineage upon adult tamoxifen administration. Hearts were harvested right after the tamoxifen induction (1mg/day for 5 days). TdTomato reporter expression was found in the CCS, including the VCS and the atrial CCS with its nodes. The strongest recombination was found in the SAN (Fig. 11C). In addition, many CMs from the atria were labeled and several in the ventricles (Fig. 11C). We consider that not all CMs were labeled due to low Cre recombination efficiency, and the usual variability associated to the use of tamoxifen.

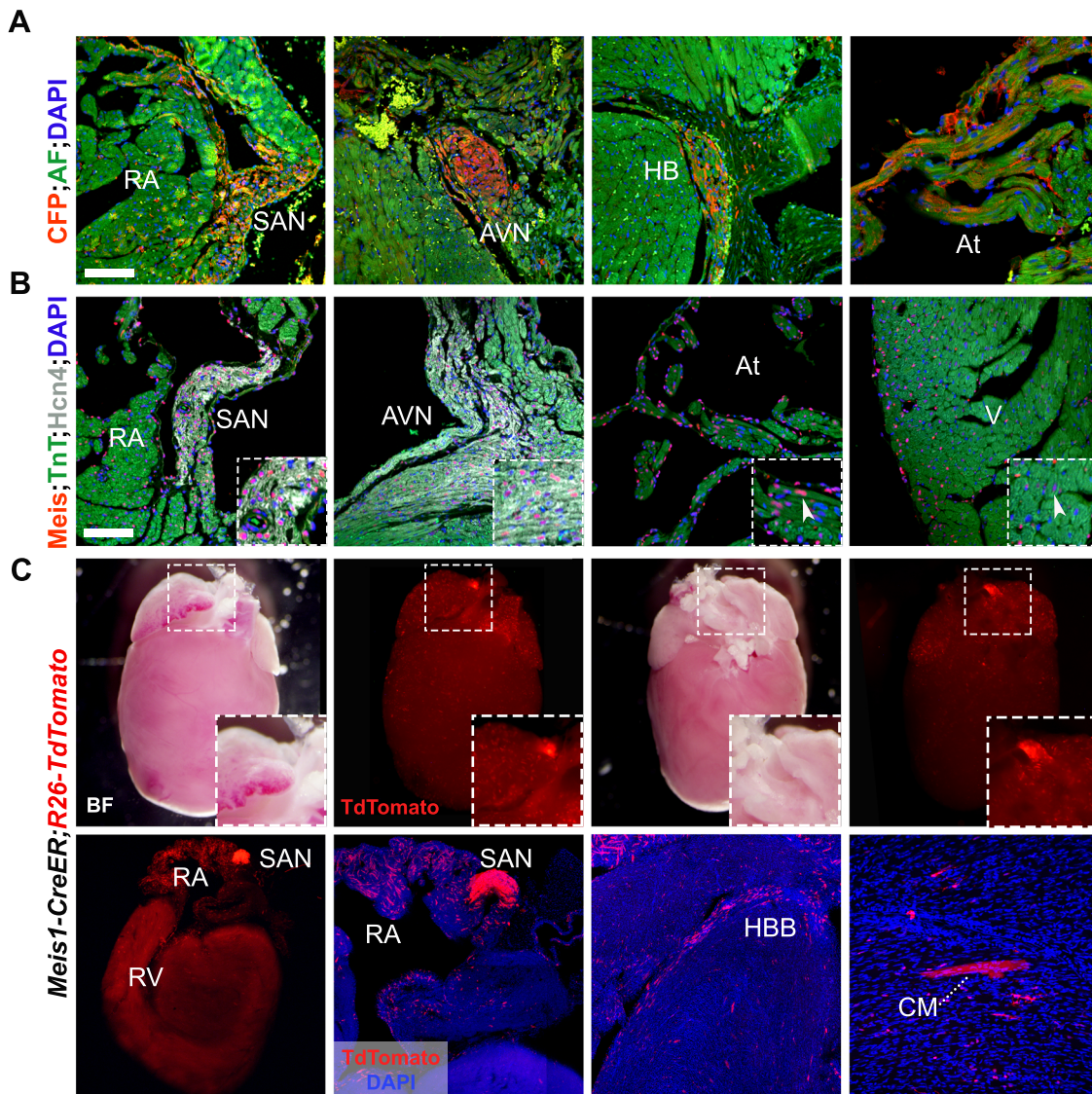


**Figure 11. Meis1 and Meis2 are expressed in adult cardiomyocytes of the working and conducting myocardium.** (A). Confocal images showing expression of *Meis1-ECFP* in CCS and atrium myocardium (At). Sinoatrial node (SAN), Atrio-Ventricular node (AVN), His Bundle (HB) (B). Left panels show co-immunofluorescence of Meis-a and Hcn4 in the SAN and AVN, respectively. Right panels show Meis-a signal in atrial (At) and ventricular (V) CMs. Arrowheads in boxes point to CMs positive for Meis-a. Scale bar in A and B is 100 $\mu$ m. (C). Upper panels show whole-mount *R26TdTomato;Meis1-CreER* hearts. Boxes show a magnification of the SAN area. Bottom panels show thick sections (200 $\mu$ m), acquired with a confocal, of a *R26TdTomato;Meis1-CreER* heart co-stained with DAPI in blue.

## Meis function in cardiomyocytes during heart development

### *Meis1 And Meis2 Double Deletion In CMs Causes Perinatal Death*

In order to study the function of Meis TFs in cardiomyocytes, we generated a new mouse model, in which *Meis1* and *Meis2* were simultaneously deleted by recombination with  $\alpha$ -MHC-Cre (Fig. 12A).

The recombination pattern of  $\alpha$ -MHC-Cre is very specific for CMs (Agah *et al*, 1997) and it starts to recombine at E8.5 with some patches. We studied the recombination using the *R26R-LacZ* reporter line and observed at E10.5 the whole left ventricle is already recombined, while atria and right ventricle take one or two days longer for full recombination (Fig. 12B).

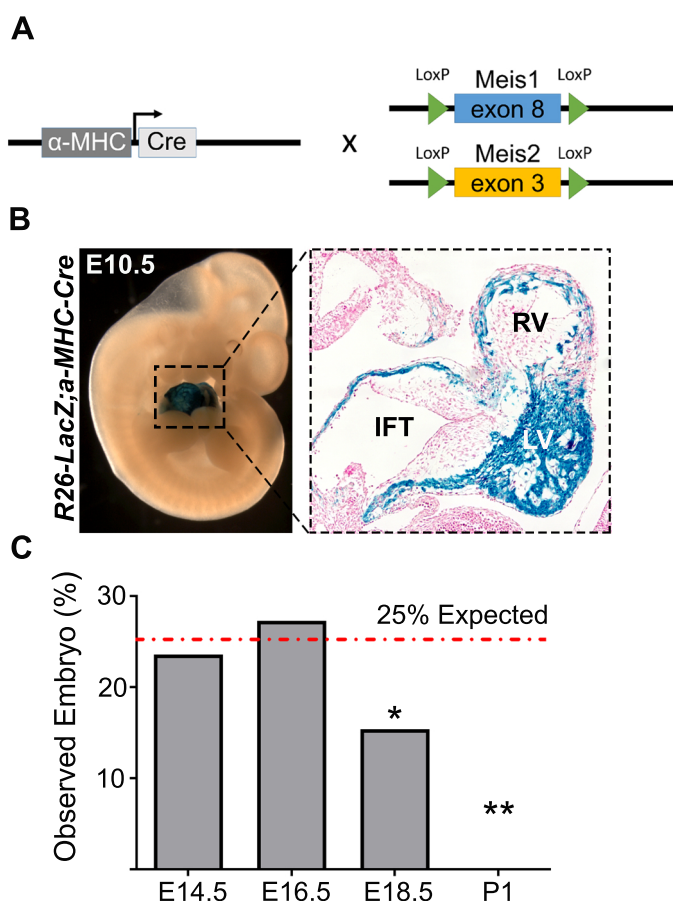


**Figure 12. *Meis1* and *Meis2* double deletion in developing CMs causes perinatal death.** (A). Model for simultaneous constitutive deletion of *Meis1* and *Meis2* in CMs. (B). Recombination pattern of  $\alpha$ -MHC-Cre shown by LacZ staining in E10.5 whole-mount embryo. Black box in the right shows recombination in the heart after sectioning. (C). Graph showing expected and observed frequencies of *Meis1* and *Meis2* dKO fetuses at different embryonic days.

We analyzed the frequencies of the different genotypes at several time points. We noticed that at the latest stages of development, the frequency of dKO embryos was below the expected value (Fig. 12C). At postnatal day one we were not able to recover any dKO (Fig. 12C). These results indicate that Meis1 and Meis2 TFs are essential in CMs for survival at birth.

### *Meis1 And Meis2 dKO Hearts Present Morphological Alterations*

The next step was to analyze in detail the phenotype of dKO hearts to elucidate what are the alterations derived from *Meis* loss of function in cardiomyocytes.

We harvested hearts at E18.5 and described external morphological alterations in the atria of dKOs compared to controls (Fig. 13A). The left atrium is the most affected presenting finger-like protrusions and a reduced size (Fig. 13B). The right atrium also showed finger-like structures but they were less prominent than those in the left (Fig. 13B). The junction between right and left ventricle, at the apex, was not properly closed. We performed histological analysis to study internal structures and observed ventricular septal defects and a tendency to present thinner compact myocardium (Fig. 13C). VSD was present in 40% of the dKO fetuses at E18.5 and about 80% of them were accompanied by overriding aorta (Fig. 13D). Wall-thickness was measured on sections and dKO hearts showed a non-significant tendency to present thinner ventricular compact myocardium (Fig. 13E).

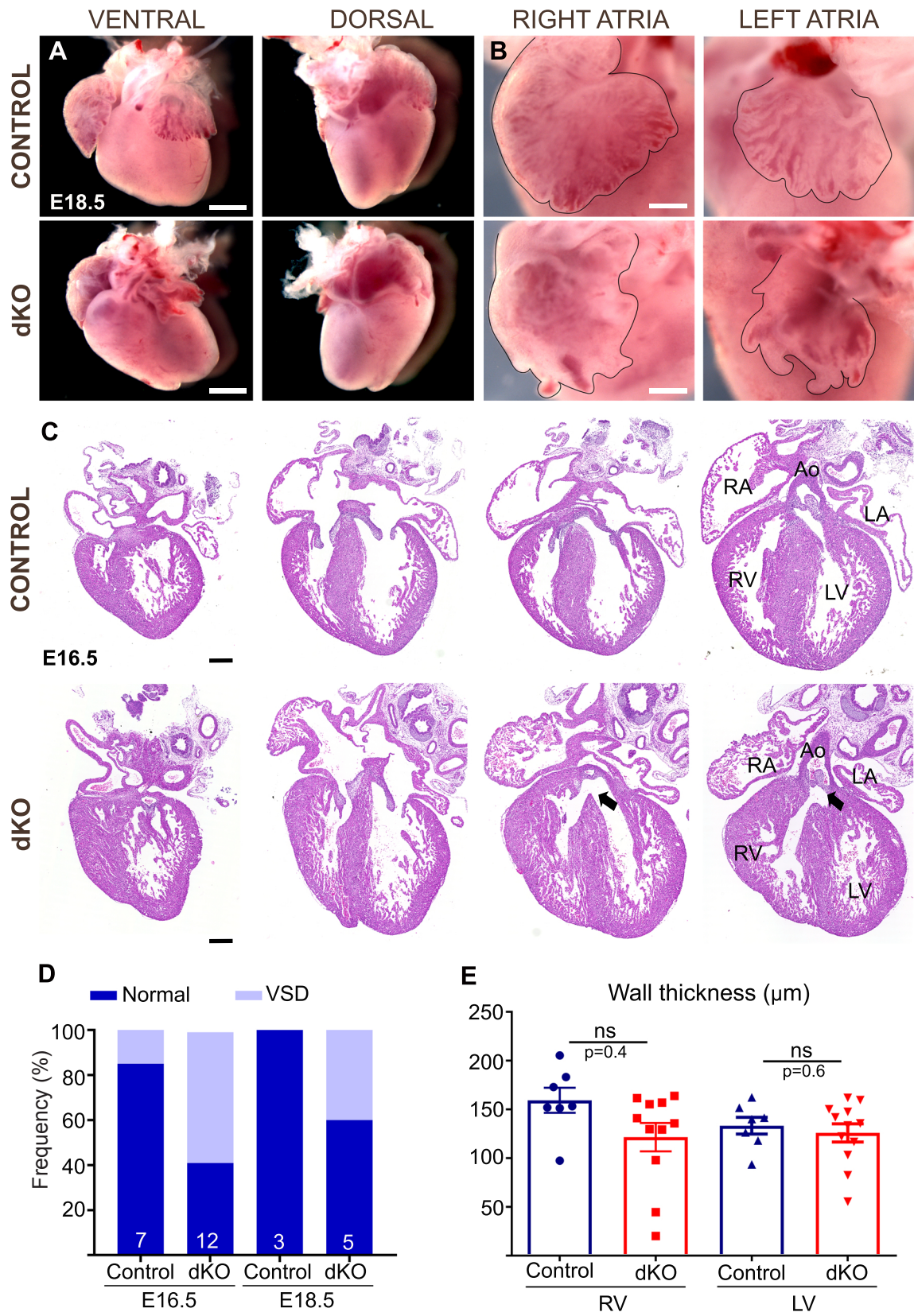


**Figure 13. Cardiac morphological alterations produced by CM-specific *Meis1* and *Meis2* deletion.** (A). Dorsal and ventral view of representative whole-mount E18.5 hearts from control and dKO littermates. Scale bar 500um. (B). Left and right atrium from control and dKO hearts. Scale bar 200um. (C). H&E staining on sections from control and dKO E18.5 hearts. From left to right the sectioning plane progresses from dorsal to ventral. Arrow point to VSD and overriding aorta. Scale bar 200um. (D). Percentage of fetuses with VSD at E16.5 and E18.5. (E). Graph showing compact myocardium thickness of control and dKO hearts at E16.5 measured in sections. Datapoints are the mean of three central sections per heart.

Harvesting hearts at earlier stages we found that dKO hearts can be clearly identified at E14.5 by atrial malformations, while at E12.5 it was more difficult to differentiate by eye (Fig. 14).

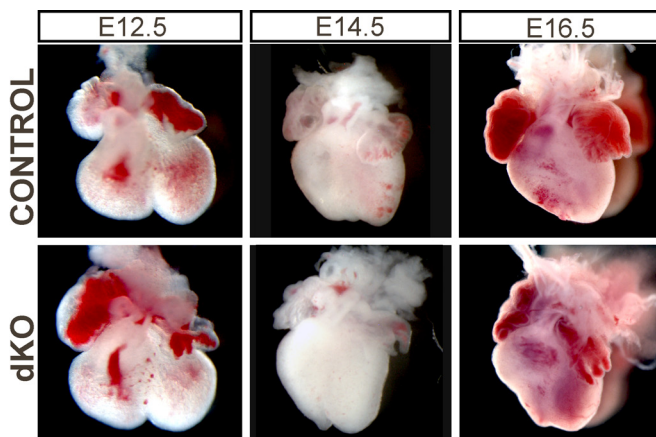


**Figure 14. External malformations in dKO hearts are visible at E14.5.** Whole-mount images of Control and dKO hearts at three different embryonic days. Atrial finger-like protrusions are already present at E14.5.

In order to better understand atrial malformations we dissected atria from E18.5 hearts and stained them in whole mount for tissue visualization in confocal. 3D reconstruction highlighted the different morphology in dKO atria compared to control littermates (Fig. 15A). Studying confocal sections in detail, we observed thinner and disorganized pectinate muscles in dKO when compare to control (Fig. 15B). Altogether, these data suggest Meis TFs play a role in cardiac morphogenesis.

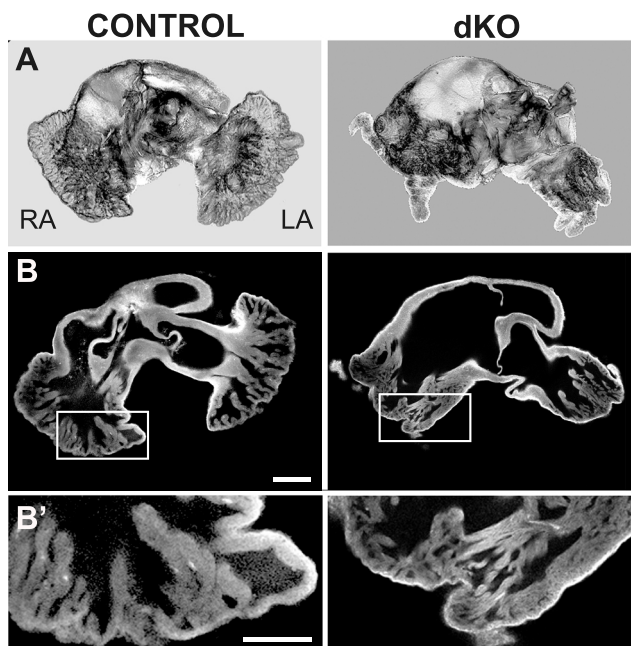


**Figure 15. Atrial malformations affect pectinate muscles.** (A). 3D reconstruction of whole-mount confocal images from Control and dKO atria stained with WGA at E18.5. (B). Confocal section of atria in panel A. Box regions indicate magnifications shown in B'. Scale bar: 400µm. (B'). Magnifications of right atria in B showing pectinate muscles in Control and dKO. Scale bar: 200µm.

### *Constitutive Meis1 And Meis2 Deletion Leads To Smaller Hearts And Stress-induced Cardiac Rhythm Alterations.*

The morphological defects found do not necessarily explain the lethality of dKOs embryos at birth. Thus, we decided to explore by echocardiography the morphology and function of mutant fetal hearts in utero. For these experiments, pregnant females were anesthetized and the uterus was directly exposed for trans-uterine echocardiography (Fig. 16A). First, we measured the size of the interventricular septum and found a reduction in dKO hearts at E18.5, although it was not detected at earlier stages (Fig. 16B). Moreover, left and right ventricular masses were also reduced by the end of gestation but not before (Fig. 16B). These data, together with our previous result on wall thickness, determine *Meis* loss of function in CMs leads to smaller hearts. Thus, we decided to explore whether the small cardiac size was due to defective proliferation in dKOs. Surprisingly, dKO hearts presented a non-significant tendency to proliferate more than control hearts at E16.5 (Fig. 17).

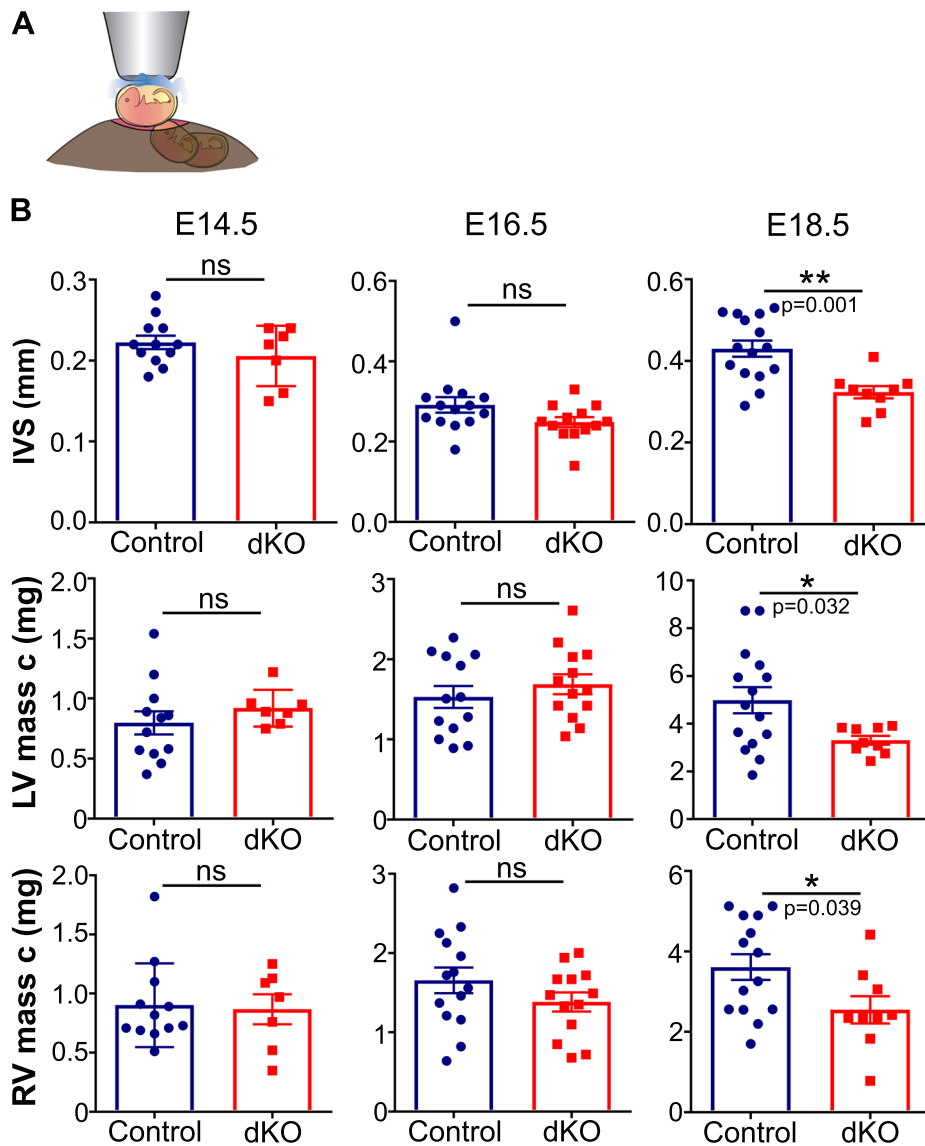


**Figure 16. Echocardiography reveals smaller hearts in dKO fetuses.** (A). Schematic representation of trans-uterine Echo-Doppler procedure in pregnant females. (B). Graphs summarizing results obtain from interventricular septum (IVS) thickness, left and right ventricular masses at three different embryonic days in Control and dKO fetuses.

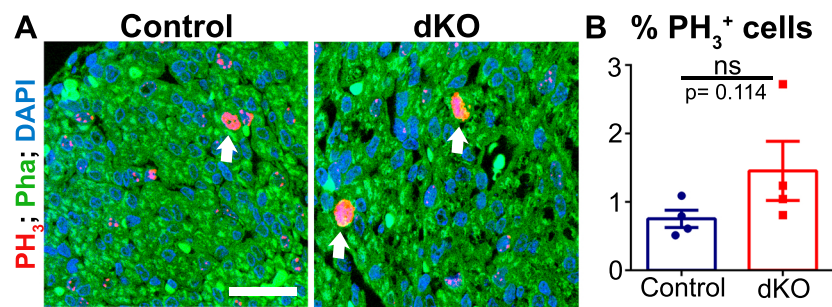


**Figure 17. Proliferation rate in the myocardium of control and mutant fetuses.** (A). Confocal section of control and dKO ventricle stained with PH<sub>3</sub> in red and Phalloidin in green. White arrows indicate mitotic cells. Scale bar: 25µm. (B). Graph showing quantification of cells PH3 + per total number of nuclei in terms of percentage. Datapoint is the mean of 6 sections per embryo.

Regarding cardiac function, we were not able to detect any difference in left ventricular ejection fraction, at any of the developmental points analyzed (Fig. 18A). This observation, together with the moderated reduction in heart size suggest insufficient cardiac output is not the cause of lethality. Nevertheless, heart rate was found significantly higher in dKO embryos at the end of gestation, suggesting alterations in cardiac rhythm (Fig. 18B).

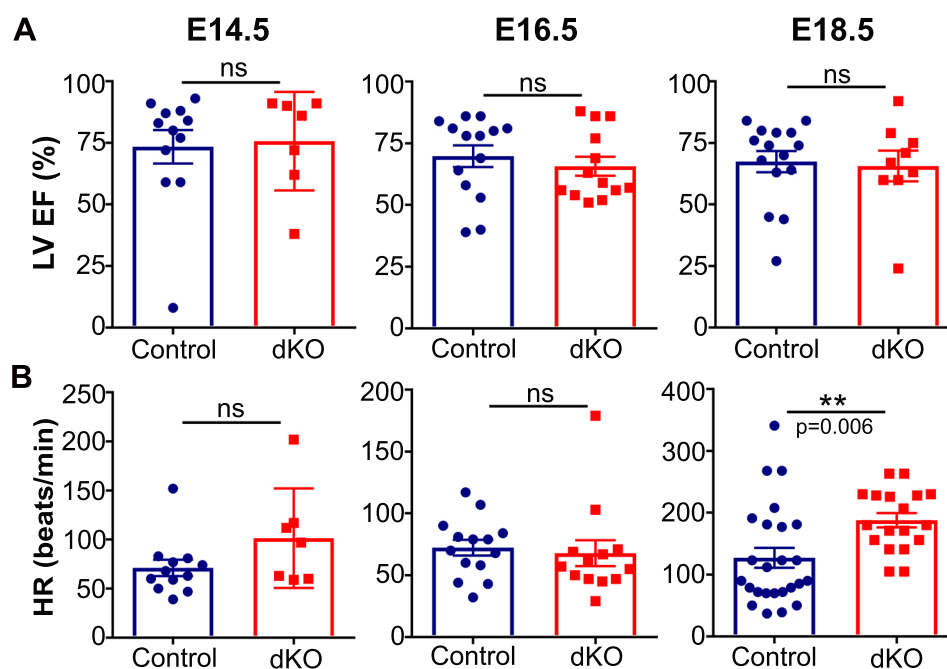


**Figure 18. dKO fetuses present normal cardiac function and higher heart rates.** (A-B). Left ventricular ejection fraction and heart rate measurements during trans-uterine echocardiography, in Control and dKO hearts at the indicated embryonic days.

We then decided to focus on flow pulse records through which we can detect passive filling of the ventricle when it is relax (E wave), the atrial contraction by the flow of blood coming into the ventricle (A wave) and ventricular contraction by blood flow going out through great vessels (Ejection wave) (Fig. 19B). Using this methodology we found higher frequency of arrhythmias in dKOs at different developmental stages (Fig. 19B, C). Looking in detail at flow pulse records from dKO fetuses, we observed changes in atrial contraction rhythmicity, although it is difficult to determine whether atrial contraction is delay or absent in some beats (Fig. 19B). These results suggest dKO fetuses present a tendency to tachycardia (Fig. 18B, 19B) and point to the SAN as a possible origin of the arrhythmia but further studies are needed.

We next studied the influence of uterine exposure on the alterations in cardiac rhythm. For this, we implemented methodology that enabled us to record blood flows in embryonic hearts without surgical procedures and without losing track of fetus identity (Fig. 20A, B). This technique allowed us to longitudinally analyze the same litter from E16.5 to E18.5, keeping track of individual fetuses. In this case no differences were found on heart rate (Fig. 20B, C), and arrhythmias did not appear in any genotype (Fig. 20B; 20D). These results indicate that Meis loss of function in CMs renders hearts more sensitive to certain stress conditions associated to surgery. We hypothesize that the stress of delivery and adaptation to extra-uterine life leads to cardiac rhythm alterations in Meis mutants that can lead to death.

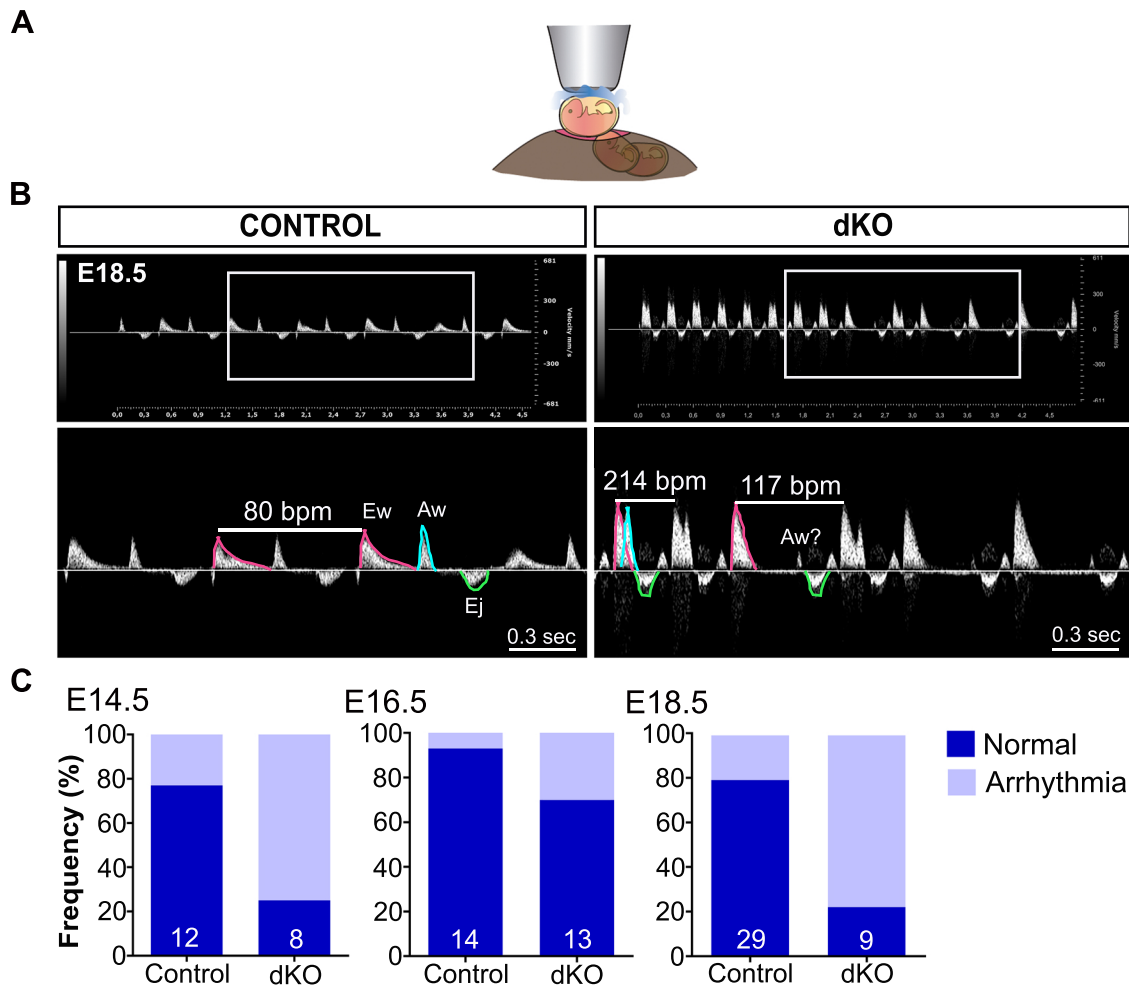


**Figure 19. dKO hearts manifest arrhythmias during trans-uterine echo acquisition.** (A). Schematic representation of trans-uterine echocardiography. (B). Five seconds of blood flow recording in Control and dKO hearts upon uterus exposure. Low panels are magnification of areas in white boxes. E-wave (Ew) corresponds to the passive filling of the ventricle, A-wave (Aw) corresponds to the active filling of the ventricles upon atrial contraction. Ejection (Ej) corresponds to the blood exiting from the ventricles through great arteries after ventricular systole. Beats per minute (bpm). dKO heart show beats with no clear A wave (Aw?). (C). Percentage of fetuses for each genotype that present some arrhythmic episode during Echo-Doppler acquisition after uterus exposure at the indicated embryonic days.

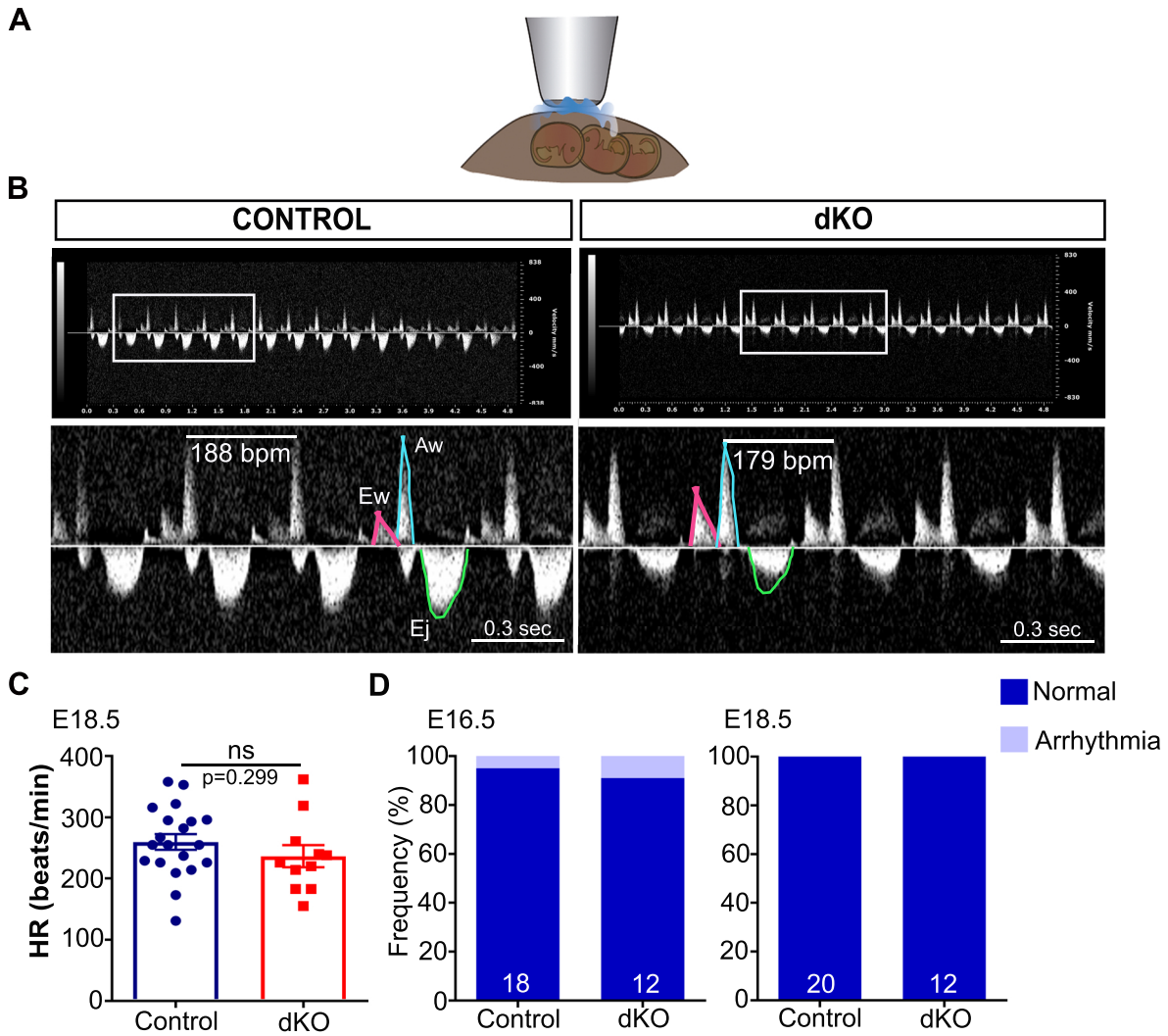


**Figure 20. Normal beating heart rate and cardiac rhythm in fetuses during trans-abdominal echocardiography.** (A). Schematic representation of trans-abdominal echocardiography. (B). Five seconds blood flows of Control and dKO fetuses acquired in pregnant females without uterus exposure. Low panels are magnification of areas in white rectangles. Pink line indicates E wave, blue, A wave and green, ventricular ejection (Ej). (C). Control and dKO heart beating rates during trans-abdominal echocardiography. (D). Percentage of normal and arrhythmic hearts found during trans-abdominal echocardiography at E16.5 and E18.5.

### *Meis Deletion In CMs Leads To Slower Electrical Impulse Propagation Through The Ventricles*

In light of these results, we wanted to further explore cardiac conduction physiology in dKO hearts. Thus, we decided to characterize the electrical activity of the fetal hearts using optical mapping technique (In collaboration with Dr. David Sedmera, Prague). Optical mapping allowed us to study the changes in voltage membrane that occur during the transmission of the electrical impulse through the heart.

We first started with E14.5 hearts when technically optical mapping is more likely to succeed and *Meis* should already be completely deleted but no overt morphological alterations are found in ventricles. We recorded approximately 16 seconds per heart and measured different parameters. Heart rates were similar between controls and mutants (Fig. 21A, B). We observed a non-significant tendency to a shorter delay between atrial and ventricular depolarization in mutants (Fig. 21C, D).

Analysis of voltage maps revealed a slower activation curve in the left and right ventricle of hearts lacking *Meis* compared to controls, mostly due to a delay during the first two milliseconds of ventricular depolarization (Fig. 22A,B). This parameter reflects the conduction velocity and therefore suggests an impairment of electrical propagation in mutants. We studied the atrial activation curve but we did not detect significant differences in this case (Fig. 22C). However, we cannot discard conduction anomalies in atria because of a very high variability among maps of the same experimental group due to the irregular atrial surface.

Moreover, we calculated total area of ventricles and atria to ensure the changes in activation curve reflect changes in depolarization velocity and not in heart size (Fig. 22D). These results suggest that constitutive double deletion of *Meis1* and *Meis2* in cardiomyocytes impairs electrical impulse transmission through the ventricles.

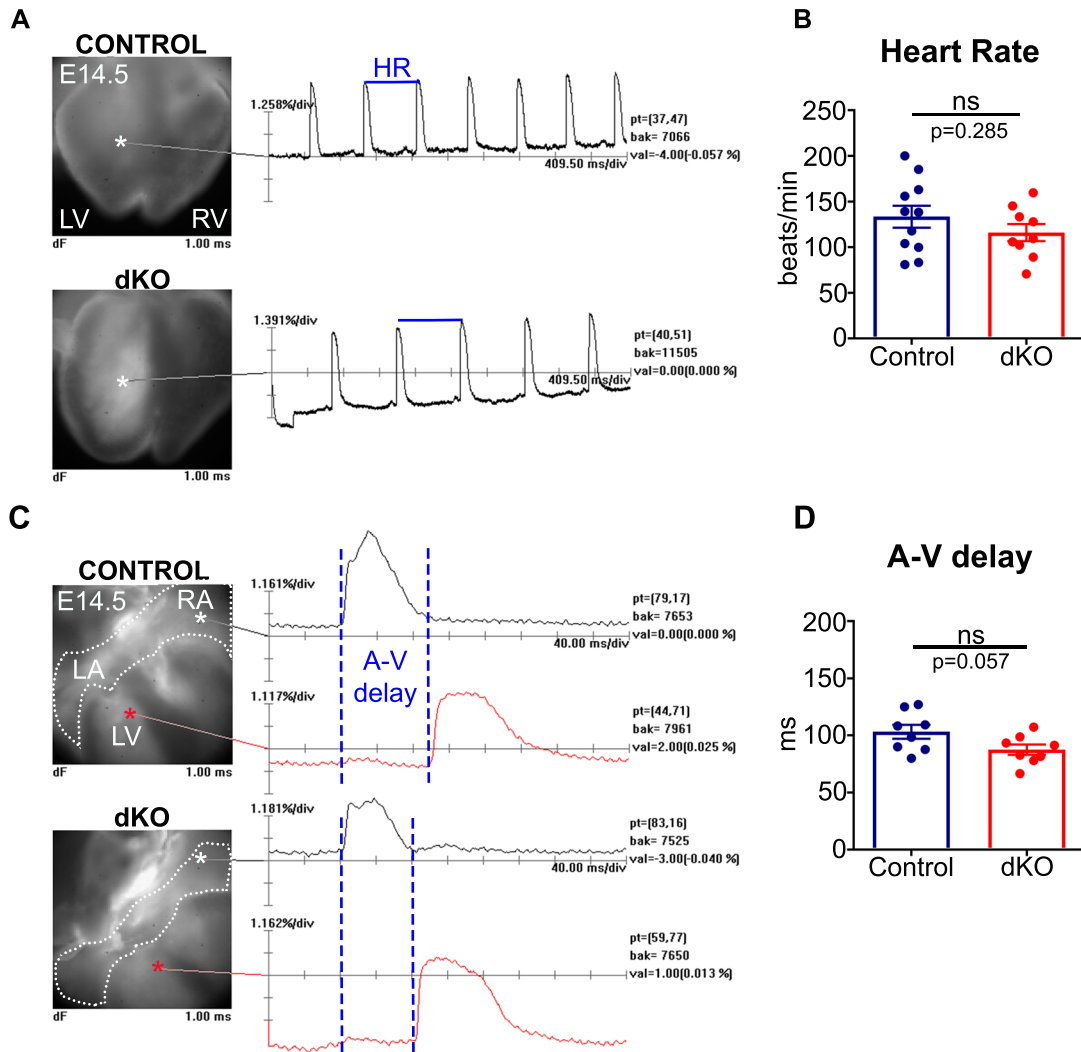


**Figure 21. Heart beat rate and Atrio-Ventricular delay measured by Optical Mapping.** (A). Bright field image of Control and dKO ventricles (dorsal view) during optical mapping. Peaks on the right show action potentials of a particular spot in the ventricles (\*) along 400 ms. (B). Quantification of heart beat rate (HR) in Controls and dKOs during optical mapping at E14.5. Datapoint is the mean of 5 consecutive beats per heart. (C). Bright field image of Control and dKO hearts (angled dorsal view to visualize the atria) during optical mapping. Peaks on the right show one action potential from atrium (white \*) and ventricle (red \*) of a selected spot along 40 ms. (D). Quantification of time between atrial and ventricular activation in Control and dKO hearts during optical mapping. Individual datapoints are the mean of 3 consecutive beats per heart.

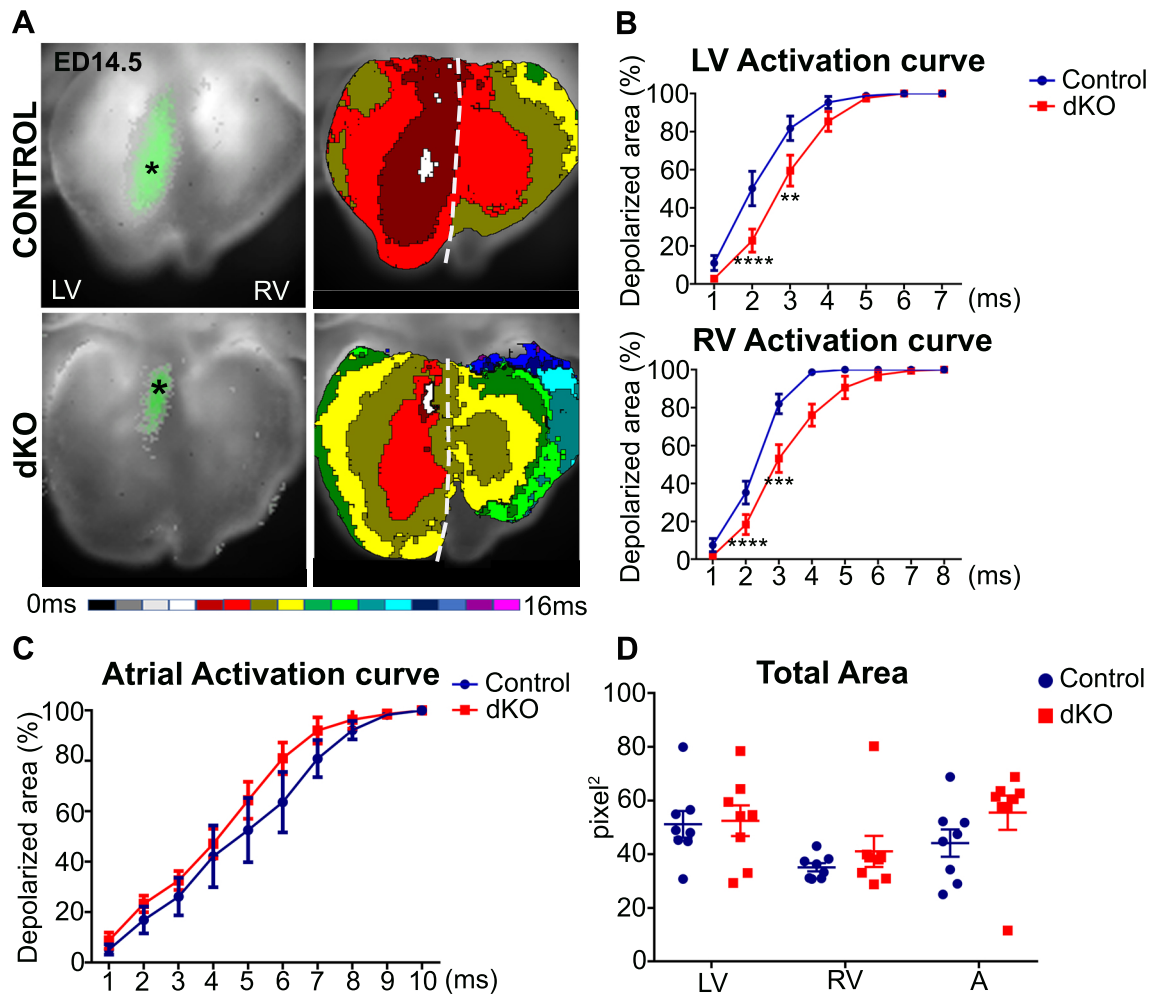


**Figure 22. dKO hearts present slower ventricular activation curves.** (A). Representative Control and dKO optical maps of ventricular depolarization. \* indicates the area where the first AP appears. White line shows manual division of left and right ventricle for analysis. Color bar shows temporal scale in the maps (1 color = 1ms). (B). Left and right ventricular activation curves showing depolarized area (%) per millisecond obtain from the maps (n=8/group). (C). Atrial activation curve from atria (n=8/group). (D). Total area of left and right ventricles and atria in Control and dKO groups. Data obtained from more than three independent litters.

We next studied the same parameters two days later in development, at E16.5. We noticed dKO hearts were frequently not beating by the time of recording (Fig. 23A), suggesting dKO hearts were extremely sensitive to the technique. Measurements of heart rate, A-V delay (Fig. 23B, C) and activation curves were similar in both groups (Fig. 23D, E). We speculate that we were not able to find significant differences because, likely, the non-beating hearts were the ones presenting a more severe phenotype. It is important to mention that, even though the time of recording was very

short, we detected three dKO hearts that were temporally arrhythmic, two at E14.5 and one at E16.5 (Fig. 24). None of the control hearts showed changes in rhythm.

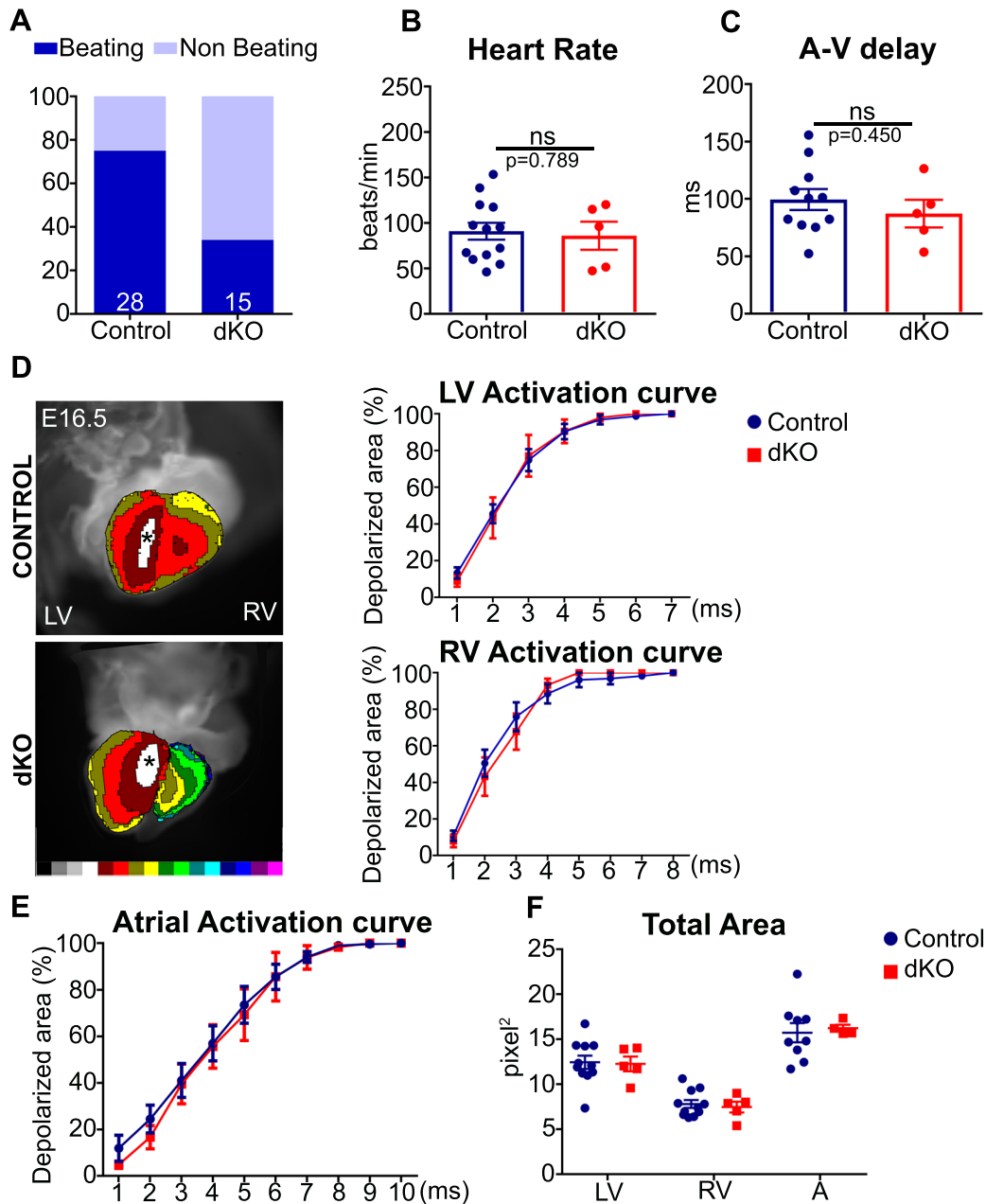


**Figure 23. Optical mapping at E16.5 did not show any significant difference between Control and dKO hearts.** (A). Beating proportion of hearts at E16.5 during optical mapping recording. (B-C). Heart rates and A-V delay times of Control and dKO beating hearts. (D). Maps and curves of left and right ventricular activation times in Control (n=11) and dKO (n=5) at E16.5. \* indicates the area where the first AP appears. Color bar shows temporal scale from 0 to 16ms. (E). Atrial activation curve. (F). Total area measured in each heart from every region analyzed.

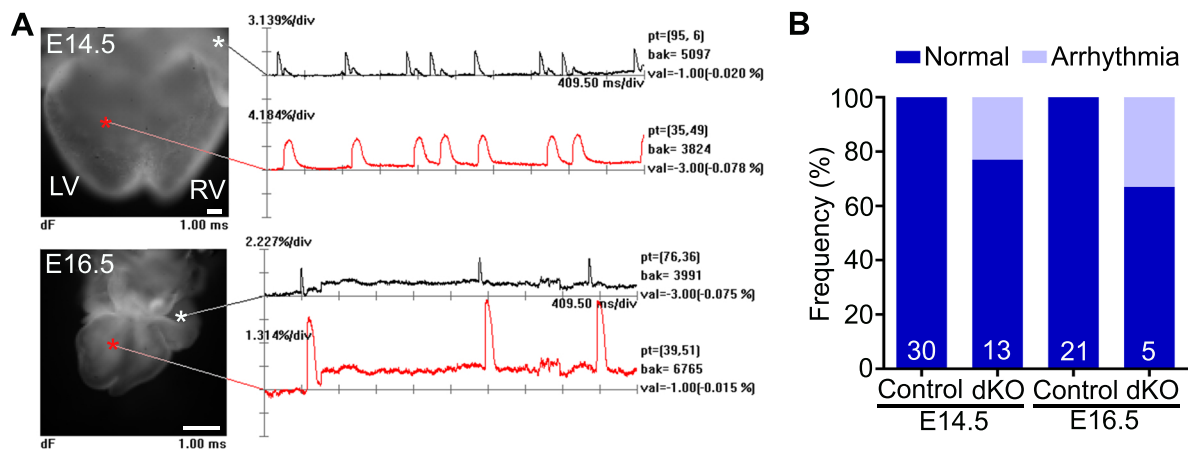


**Figure 24. Arrhythmic dKO hearts detected by optical mapping.** (A). Bright field pictures and signals recorded by optical mapping in two E14.5 (10x) and E16.5 (4x) dKO hearts. Scale bar: 200µm. (B). Percentage of normal and arrhythmic dKO hearts found at each time point.

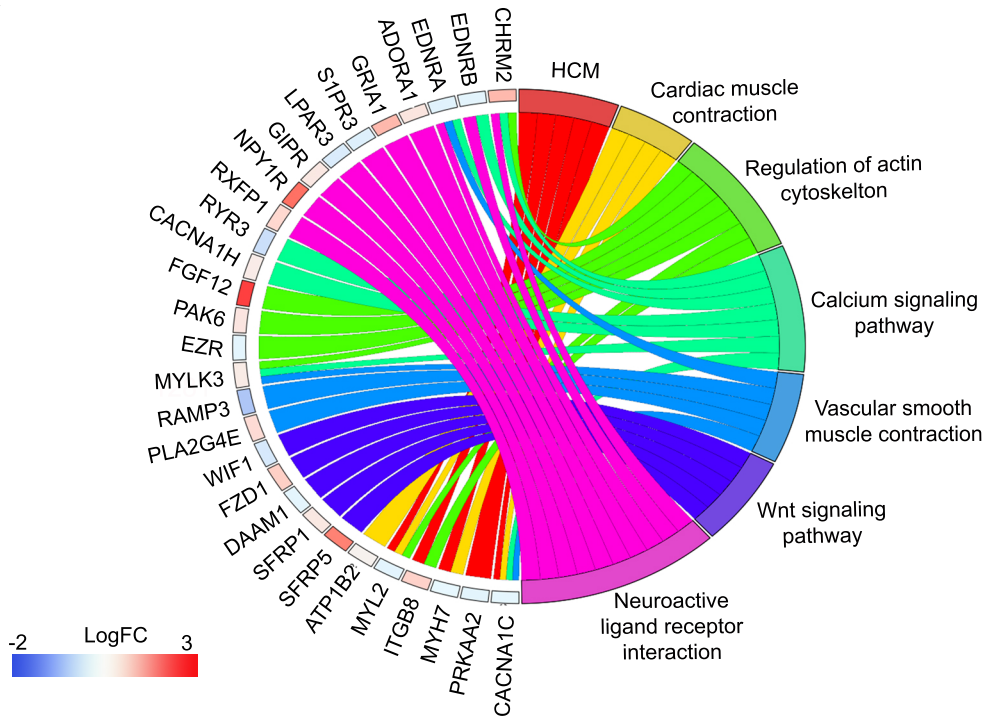
## Molecular mechanisms governing *Meis1* and *Meis2* dKO phenotype

### *Meis* Deletion In CMs Alters The Expression Of Genes Related To Cardiac Conduction

In order to unravel the molecular mechanisms responsible for the mutant phenotype, we performed RNA-seq analysis in atria and ventricles separately, at E15.5. We found more differentially expressed genes (DEGs) in atria (1281) than in ventricles (268) (Supp. table 1, 2), which might explain the morphological alterations affecting atria. Gene Set Enrichment Analysis (GSEA) of DEGs in the KEGG database showed downregulation of important genes for calcium signaling (*RyR3*, *Cacna1h*, *Cacna1c*) and cardiac muscle contraction (*Myh7*, *Myh2*) in the ventricles (Fig. 25A). The changes detected in the atria were more pronounced, including not only calcium and contraction alterations but also genes involved in focal adhesion, Wnt signaling pathway and genes associated with various cardiac pathologies (Fig. 25B).

Furthermore, we found that *Gja1*, the gene encoding Cx43, was significantly downregulated in atria and ventricles of dKO hearts at E15.5. IF of Cx43 supported the RNA-seq finding (Fig. 26A, B) and is consistent with the slower ventricular depolarization observed by optical mapping.

A



B

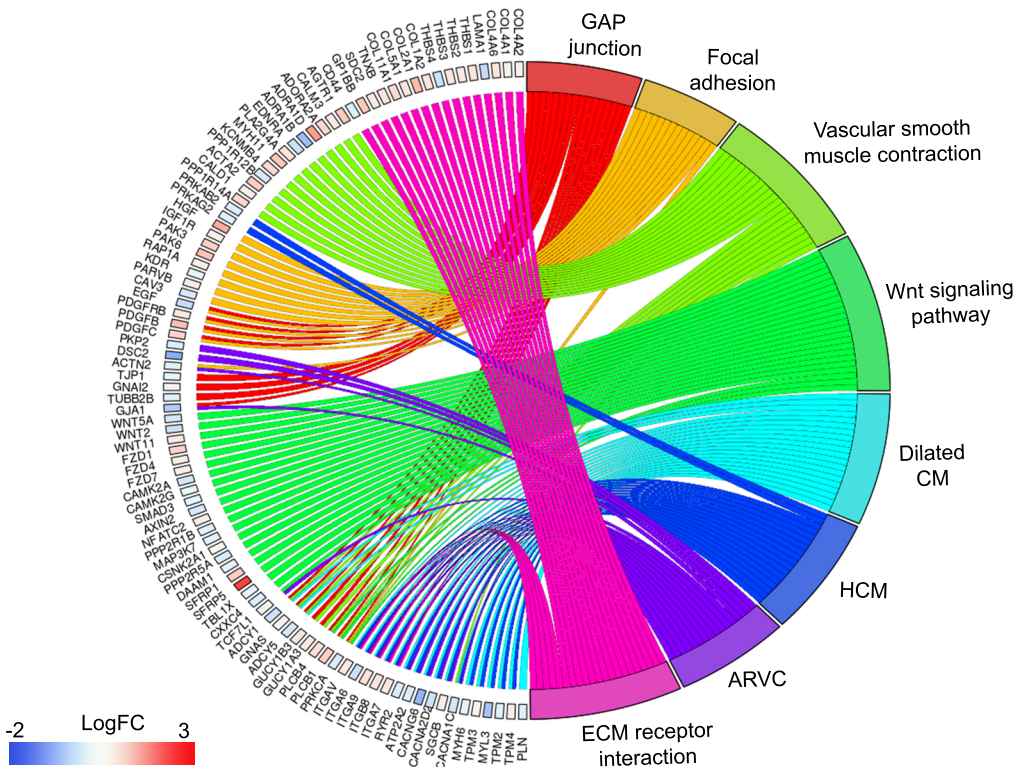


**Figure 25. RNA-seq analysis of E15.5 Control vs dKO atria and ventricles. (A-B).** GO plots showing DEGs in dKO ventricle (A) and atria (B) that belong to significantly enriched KEGG database categories, as indicated. Colorcode rectangles next to gene names indicate fold change values.

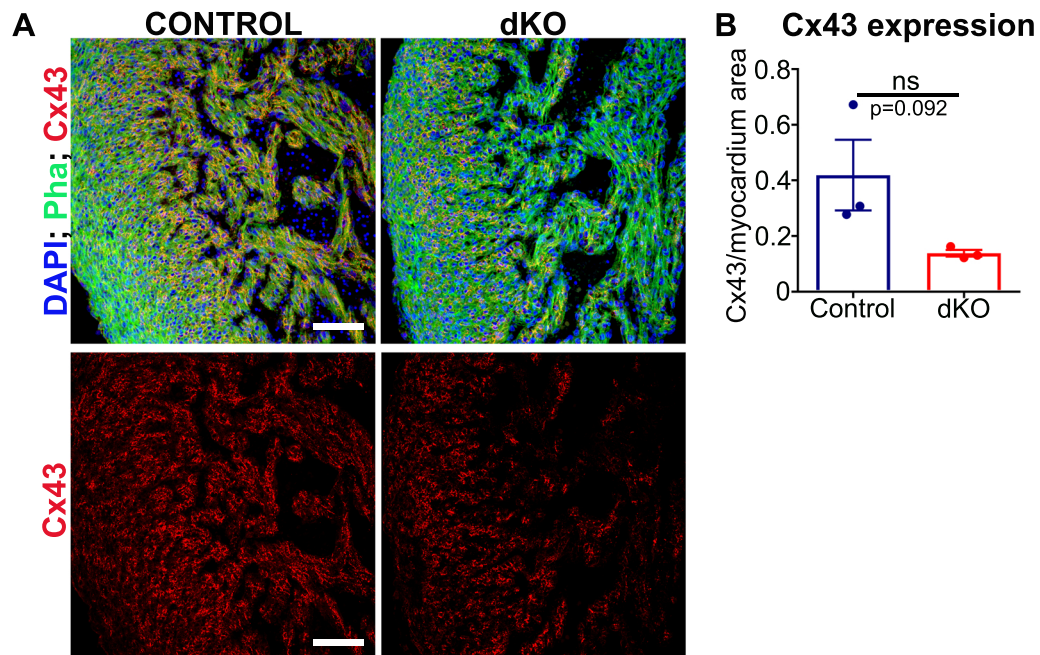


**Figure 26. dKO hearts present reduced Cx43 expression.** (A). Confocal images of ventricular myocardium stained for Cx43 in red and phalloidin in green. Low panels show red channel of the image above. Scale bar: 100µm. (B). Graph showing the quantification of Cx43 expression per myocardium area (pixel<sup>2</sup>). Datapoints represent the mean of 3 sections per heart.

We hypothesize that downregulation of *Meis1* and *Meis2* in developing cardiomyocytes leads to misregulation of calcium signaling and downregulation of Cx43, which contributes to the development of lethal cardiac arrhythmias by the end of gestation.

### Meis function in adult heart homeostasis

To further explore the function of Meis in CMs we developed an inducible mouse model using  $\alpha$ -MHC-MerCreMer<sup>tg/wt</sup>, that allowed us to study Meis role in adult CMs. This Cre driver is also specific for CMs but recombination will only be induced in the presence of tamoxifen (Tx) (Fig. 27A). Oral-gavage Tx was administered at 1mg/day for five consecutive days in mice around ten weeks of age (Fig. 27B).

### *Meis1* And *Meis2* Double Deletion In Adult CMs Causes Cardiac Hypertrophy And Interstitial Fibrosis

Echocardiography analysis showed increased left ventricular mass and left ventricular posterior wall thickness in *Meis1*<sup>flox/flox</sup>;*Meis2*<sup>flox/flox</sup>; $\alpha$ -MHC-MerCreMer<sup>tg/wt</sup>

(idKO) hearts compared to *Meis1<sup>flox/flox</sup>;Meis2<sup>flox/flox</sup>;α-MHC-MerCreMer<sup>wt/wt</sup>* (Control) (Fig. 27C, D). The change was evident two weeks after Tx induction and was maintained along the time-course of the experiment (Fig. 27D). Nonetheless, left ventricular ejection fraction was conserved between groups, indicating normal systolic function (Fig. 27D). The E/A ratio was preserved, also indicating absence of diastolic dysfunction (Fig. 27D). Twelve weeks after Tx induction, heart weight to tibia length ratio showed a non-significant tendency in idKO hearts to present larger size compared to controls (Fig. 27E, F).

Histological analysis revealed that Meis deletion in adult CMs induced interstitial fibrosis (Fig. 28A). Fibrosis was present at 4w after tamoxifen induction and maintained without further increase during twelve weeks of follow-up (Fig. 28B). Since it was described that *α-MHC-MerCreMer* may produce cardiac toxicity in the presence of tamoxifen (Koitabashi *et al*, 2009; Bersell *et al*, 2013), we decided to characterize a model of Tx administration to *MerCreMer* carriers of this allele in the absence of Meis floxed alleles. Sirius red staining at four weeks after tamoxifen administration revealed slightly more interstitial collagen deposition in *α-MHC-MerCreMer<sup>tg/wt</sup>* mice (CRE) than in their wild type littermates (WT) (Fig. 29A, B).

The amount of collagen deposition was, however, much below than the observed in idKO hearts and similar to mice used as Control, so we considered unlikely that the toxicity of the *MerCreMer* significantly influences the histological characterization of idKO hearts.

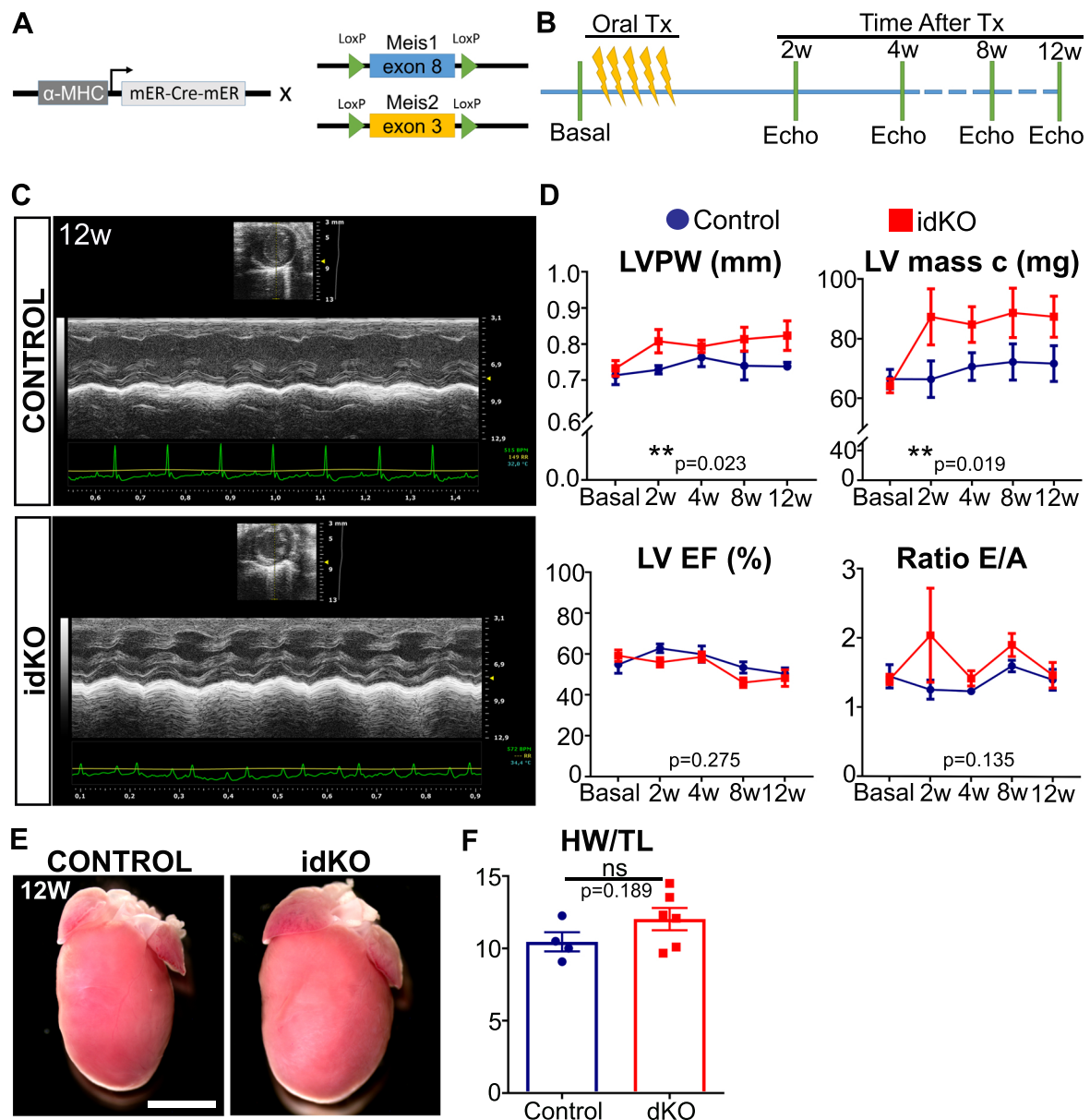


**Figure 27. *Meis1* and *Meis2* inducible deletion in adult hearts leads to mild-hypertrophy.** (A). Mouse model for the simultaneous deletion of *Meis1* and *Meis2* in adult CMs. (B). Schematic representation of analysis timing (“W” is “weeks”) and Tx treatment during the experiment. (C). Echocardiography images of ventricular walls in short axis and M mode 12 weeks after Tx treatment in Control and idKO. Green line shows ECG of the mouse during the study. (D). Graphs summarizing the results obtained after echo analysis regarding left ventricular posterior wall thickness (LVPW), left ventricular mass (LV mass), Left ventricular ejection fraction (LV EF) and ratio E/A (n= 5-10/ group). Adj.P values are obtained with Two-way ANOVA analysis for genotype factor. (E). Whole-mount images of hearts harvested 12 weeks after Tx administration. Scale bar: 5mm. (F). Graph showing ratio between heart weight and tibia length of Control and idKO hearts harvested 12 weeks after Tx.

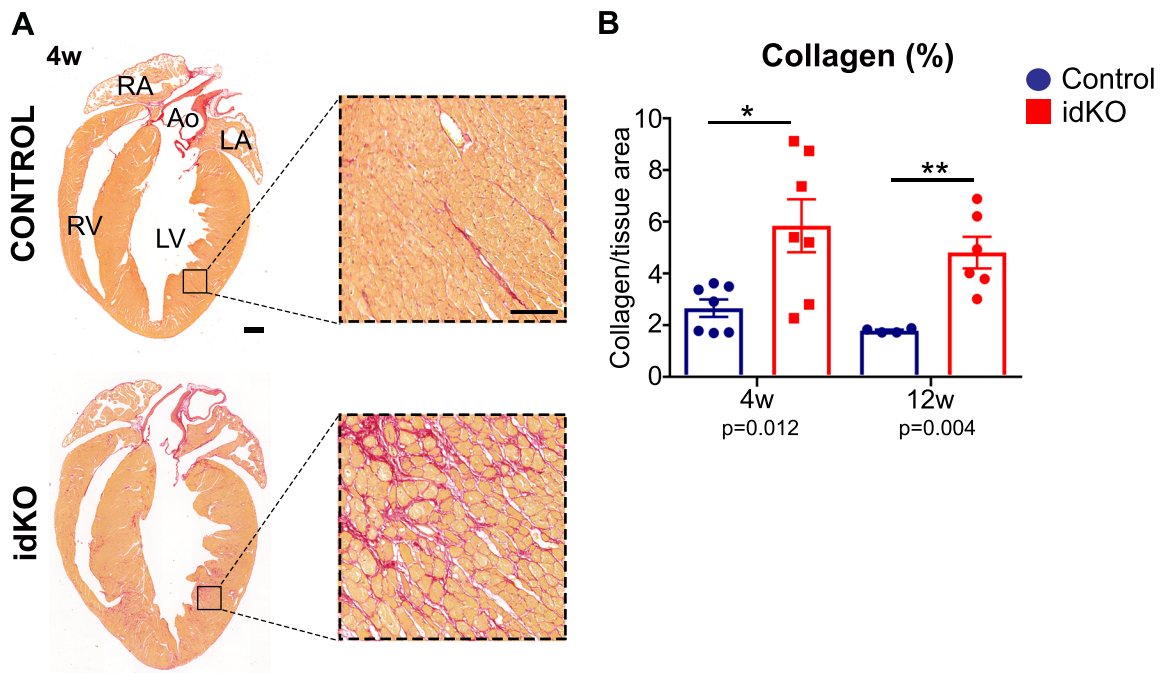


**Figure 28. Meis1 and Meis2 loss of function in adult CMs induces interstitial fibrosis.** (A). Adult heart sections stained with Sirius Red to study collagen deposition. Scale bar: 500  $\mu$ m. Black boxes show magnification of ventricular myocardium. Scale bar: 100 $\mu$ m. (B). Graph indicating the area percentage positive for Sirius Red staining, 4 and 12 weeks after Tx. Datapoints represent the mean of 3 sections per heart (only ventricular part).

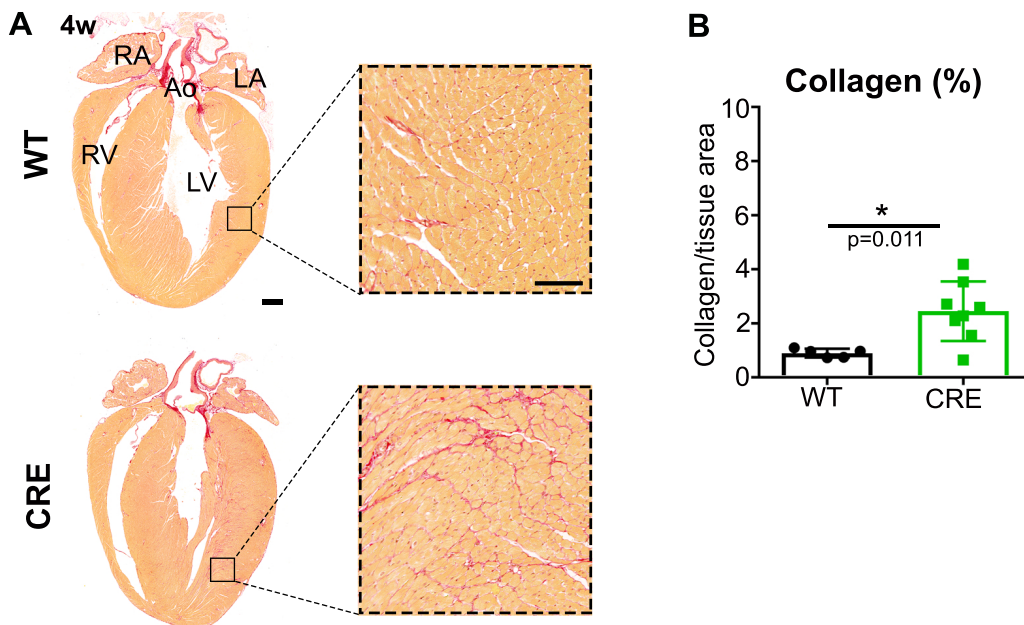


**Figure 29.  $\alpha$ -MHC-MerCreMer carrier mice develop mild interstitial fibrosis .** (A). Adult heart sections stained with Sirius Red to study collagen deposition in  $\alpha$ -MHC-MerCreMer<sup>tg/wt</sup> and their wild type siblings. Scale bar: 500  $\mu$ m. Black boxes show magnification of ventricular myocardium. Scale bar: 100 $\mu$ m. (B). Graph indicating area percentage positive for Sirius Red in each genotype. Datapoints represent the mean of 3 sections per heart (only ventricular part).

### *Loss Of Function Of Meis1 And Meis2 In Adult CMs Leads To Polyploidization Of Mononucleated CMs*

Trying to sort out the origin of mild-hypertrophy in idKO mice, we administered BrdU in the drinking water for three weeks and isolated CMs by Langendorff perfusion, immediately, after BrdU administration ended (Fig. 30A). After they adhere to the culture dish, areas occupied by single cardiomyocytes were measured on CMs populations classified by their nucleation (mononucleated, binucleated and polynucleated). No significant size differences were found between control and idKO cardiomyocytes (Fig. 30B, C).

Then, we evaluated the proliferation status of CMs in both groups. Quantification of BrdU positive CMs revealed a significant increase of BrdU-positive CMs in idKO hearts that was preferential for the mononucleated population (Fig. 30D, E). The percentage of bi and polynucleated CMs that incorporated BrdU in the nuclei were also elevated in idKO hearts, although not significantly (Fig. 30E).

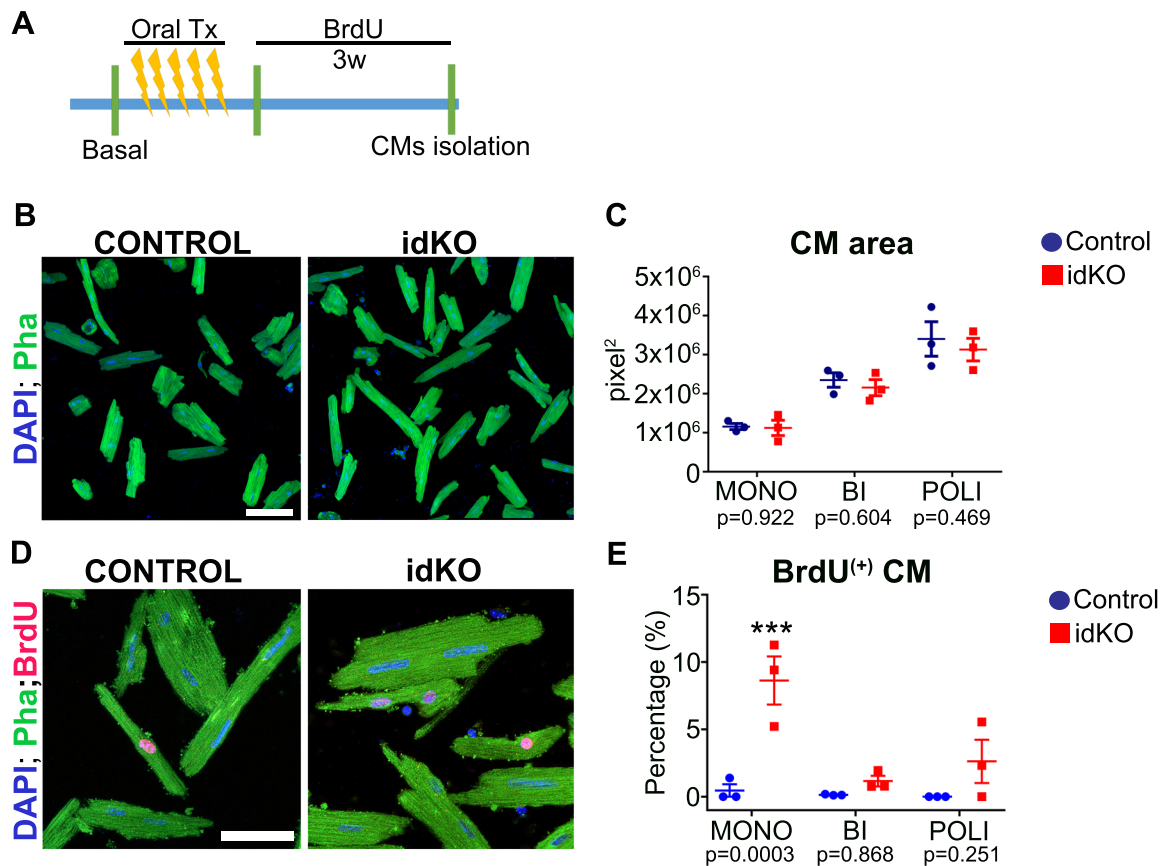


**Figure 30. idKOs show normal CM size and increased BrdU incorporation in mononucleated CMs.** (A). Schematic summary of the experimental design. (B). Confocal images of isolated CMs from Control and idKO hearts. Scale bar 50 $\mu$ m. (C). Quantification of single CM areas, classified by number of nuclei per cell. (D). Confocal images of isolated CMs from Control and idKO hearts showing BrdU incorporation. Scale bar 50 $\mu$ m. (E). Quantification of BrdU<sup>+</sup> CMs classified by number of nuclei per cell. MONO, n $\approx$ 250 cells; BI, n $\approx$ 3000 cells; POLI, n $\approx$ 150 cells.

In order to determine whether this DNA synthesis was linked to proliferation or to endoreplication, we estimated the ploidy of mononucleated CMs by nuclear DAPI intensity, nuclear volume and cell size. We found that the nuclei that had incorporated BrdU exhibited approximately double DAPI intensity and double cell size compared to BrdU-negative cardiomyocytes (Fig. 31A, B, C). However, we were not able to detect differences due to genotype in this parameters. Classification of mononucleated CMs according to their nuclear volume showed roughly two cell populations –likely 2n and 4n– with similar distributions in control and idKO hearts (Fig. 31D, E). These results suggest that the majority of spontaneous BrdU incorporation by mononucleated adult cardiomyocytes is related to polyploidization and not proliferation.

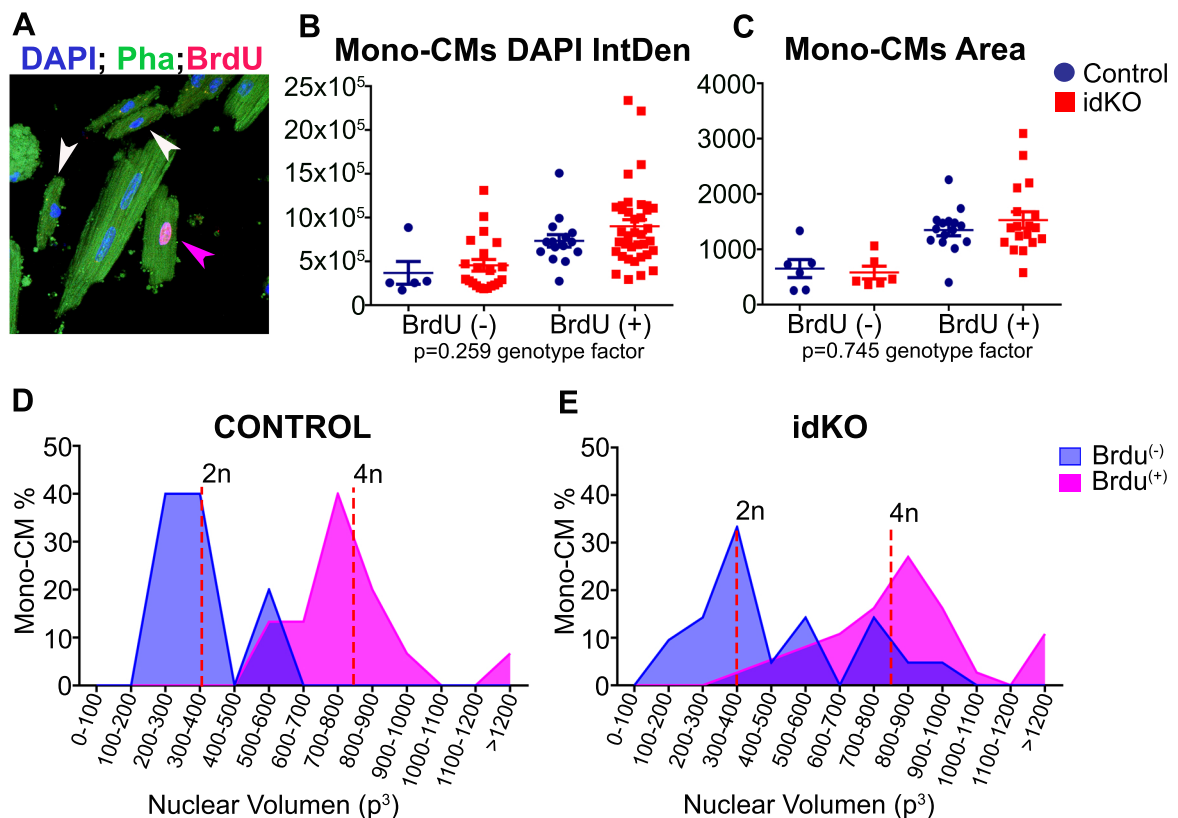


**Figure 31. The majority of BrdU<sup>+</sup> mononucleated CMs undergo DNA endoreplication and not proliferation.** (A). Confocal image of isolated CMs from idKO adult hearts showing differences in mononucleated CM size. Arrowheads point to mononucleated CMs, BrdU<sup>+</sup> CMs in pink and BrdU<sup>-</sup> CMs in white. (B). Quantification of the DAPI intensity of mononucleated CM nuclei segmented from Control and idKO hearts. (C). Graph showing mononucleated CM size depending on BrdU incorporation and genotype. (D-E) Histogram of nuclear volume of BrdU<sup>+</sup> and BrdU<sup>-</sup> mononucleated CMs from Control (n=22) and idKO (n=58) mice.

### Double Inducible Deletion Of *Meis1* And *Meis2* In Adult CMs Causes Slower Ventricular Conduction

Since our previous results showed that *Meis* TFs are preferentially expressed in adult CMs of the conduction system and that are necessary for the establishment of ventricular conduction during development, we decided to perform electrocardiograms in *Meis1* and *Meis2* double specific loss of function in adult CMs.

We followed the same experimental timing as previously mentioned (Fig. 32A), performing ECG at different time points after Tx induction. We found progressive elongation of the QRS complex in the idKO mice (Fig. 32B, C). P, PR and QTc showed no significant differences between genotypes (Fig. 32C). However, QTc which is a

more robust measurement for QT interval, showed and increased in idKO at 2 weeks that seemed to be ameliorated along time (Fig. 32C). Moreover, QRS amplitude significantly dropped in mutant mice at the first point analyzed and the decrease was maintained during the experiment (Fig. 32B, C).

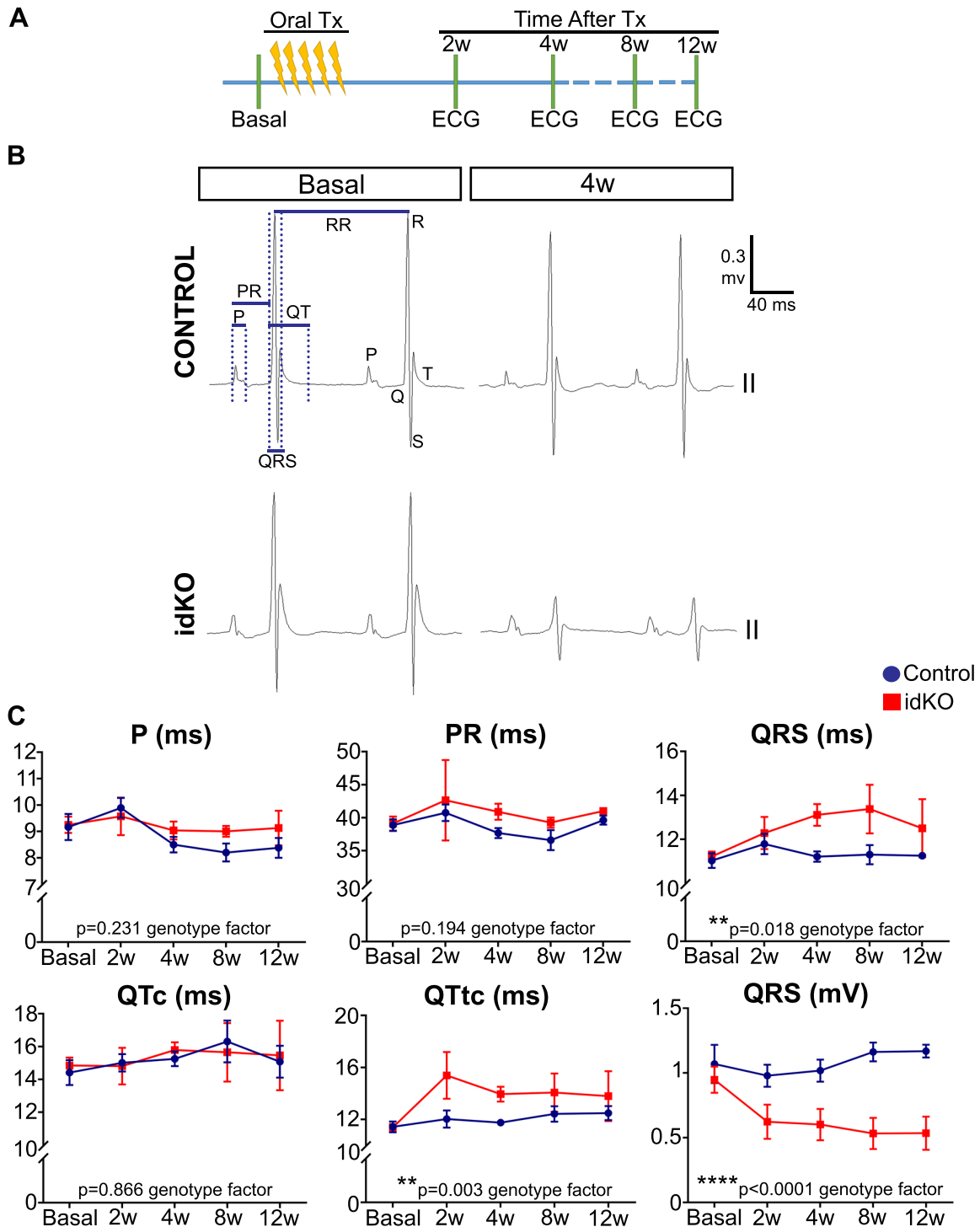


**Figure 32. QRS complex is elongated upon *Meis1* and *Meis2* double deletion in adult CMs.** (A). Representation of experimental design. “W” means weeks (B). Control and idKO ECGs from anesthetized adult mice at basal and 4 weeks experimental points. (C). Graphs indicating measurements of the duration of the different ECG intervals (P, PR, QRS, QTc and QTtc) and QRS amplitude (mV) in controls and idKOs at the indicated experimental time points.

This result suggests that atrial and atrio-ventricular conduction are normal while ventricular conduction is impaired in idKOs mice.

We also checked whether QRS and QTtc intervals were normal in *MerCreMer* carrier animals. Comparing CRE and WT animals we did not detect any significant QRS and QTtc elongation (Fig. 33A, B), supporting the idea that slower ventricular conduction is a consequence of *Meis1* and *Meis2* double inducible deletion in the adult heart. In addition, we measured QRS amplitude, which was significantly decreased in *MerCreMer* carriers after Tx treatment, indicating that Meis loss of function may not be causative of the QRS amplitude drop.

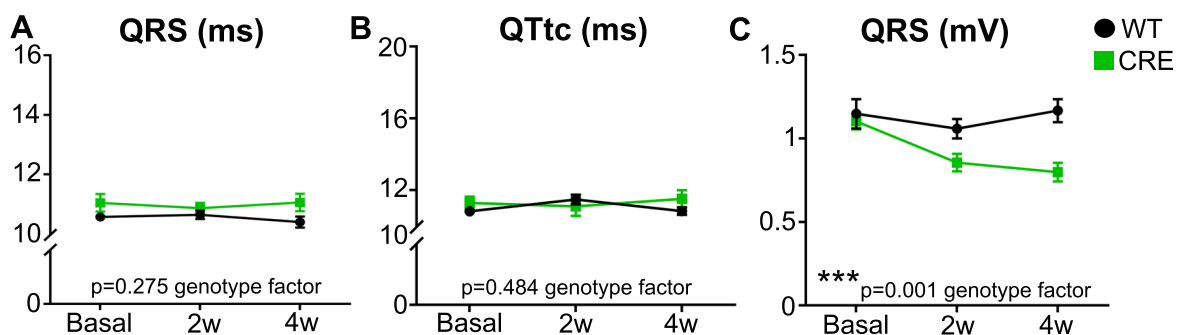


**Figure 33. Measurement of ECG intervals in *MerCreMer* carriers.** Graphs showing comparisons between CRE mice and their WT littermates before and after Tx treatment for QRS length (A), QTc length (B) and QRS amplitude (C).

Altogether, these data demonstrate Meis TFs are necessary for normal adult heart homeostasis and electrical conduction. Moreover, they suggest that Meis could be controlling similar processes in development and adulthood, related to normal ventricular impulse propagation.

## Molecular mechanisms under the control of Meis1 and Meis2 in adult cardiomyocytes

### *Meis1 And Meis2 Regulate Calcium Signaling And Conduction System Markers*

To further explore the function of Meis TFs in adult CMs we aimed to understand the molecular changes that take place upon inducible deletion of *Meis1* and *Meis2*. We performed RNA-seq analysis 2 weeks after Tx administration separately from adult atria and ventricles. 263 DEGs were found in the ventricles, while only two changed in atria (Fig. 34A) (Supp. Table 3, 4). Therefore, we studied the possibility of low efficiency Cre recombination in the atria. Specific quantification of *Meis1* exon 8 and *Meis2* exon 3 in the RNAseq showed efficient deletion of both exons in ventricles, but almost no reduction in atria (Fig. 34B). These findings suggest low efficiency of *MerCreMer* in atria that could explain the absence of changes detected in that region.

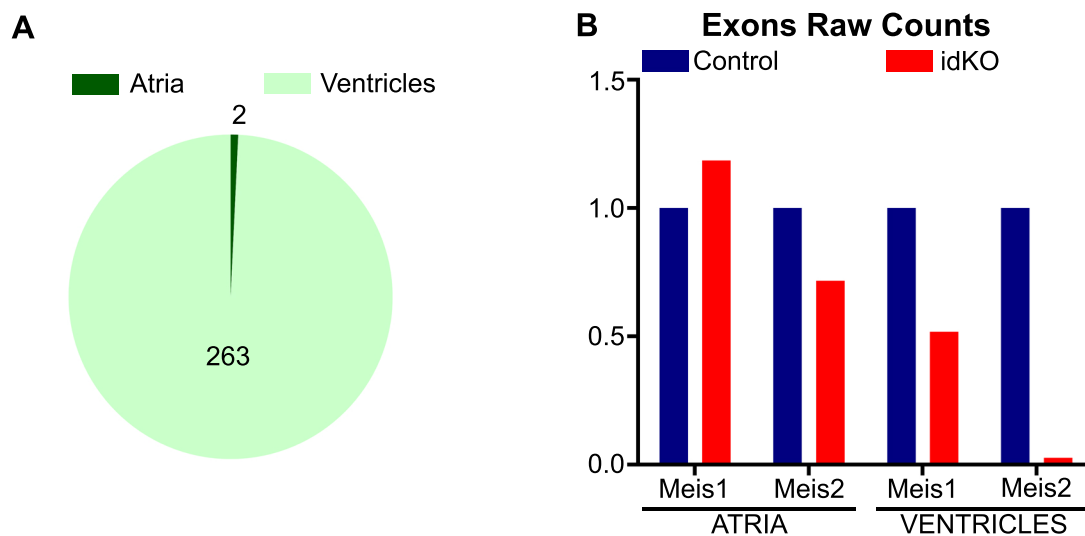
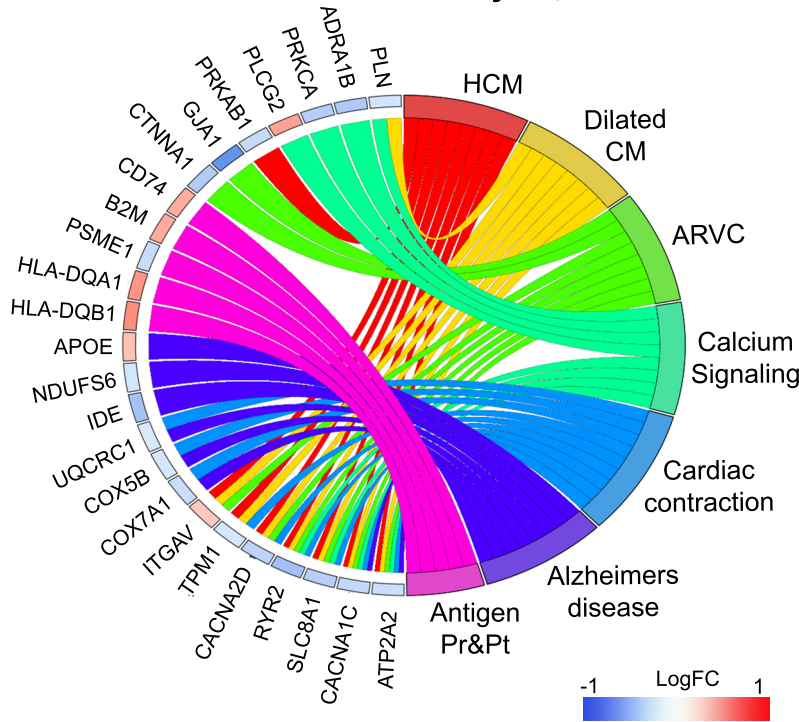


**Figure 34. The  $\alpha$ -MHC-MerCreMer allele does not recombine efficiently in the atria of adults.** (A). Number of DEGs found in atria and ventricles by RNA-seq analysis of Control vs idKO hearts. (B). Quantification of *Meis1* exon8 and *Meis2* exon 3 in RNA-seq from atria and ventricles. (C). Number of statically significant upregulated and downregulated genes in idKO ventricles.

We performed GSEA in the KEGG database and found that DEGs were mainly related to cardiomyopathies and calcium signaling pathway (Fig. 35A). Genes regulating sodium currents in CMs, *Scn5a* and *Scn10a*, were significantly downregulated, suggesting sodium current might be also deficient in idKO mice (Supp. Table 5).

**A Gene set enrichment analysis; KEGG**



**B PKP2 cKO ; M1M2 idKO**

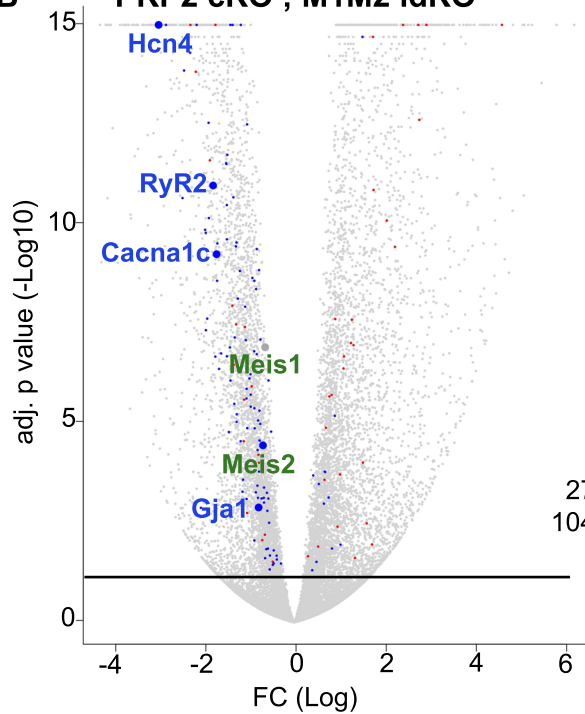


**Figure 35. ARVC and calcium signaling related genes appeared differentially expressed in idKO ventricles. (A).** GOplot summarizing results from GSEA analysis. Genes and fold changes are represented on the left, and on the right, the associated categories to each gene.

(B). Volcano plot representing genes expressed in *Pkp2* cKO model (grey dots) and DEGs in *Meis1* and *Meis2* idKO ventricles (blue dots are downregulated genes and red upregulated). We only considered for this analysis adj. p-value <0.05 (black line) from both models. Numbers in the right are the overlapping genes regarding fold change direction.

Moreover, genes related to Arrhythmogenic Right Ventricular Cardiomyopathy (ARVC) appeared as the most altered gene set. We decided to compare our RNA-seq data with a published RNA-seq from an ARVC mouse model in which *Pkp2* had been conditionally deleted in cardiomyocytes (Cerrone *et al*, 2012). *Pkp2* is a desmosomal protein important for the assembly of CMs. In this model, *Meis1* and *Meis2* appeared significantly downregulated (Fig. 35B green color). Moreover, when we compared the differentially expressed genes in both models we found a correlation between the genes that were changing, especially when focused on the most significantly downregulated ones, such as *Cacna1c* or *RyR2*, essential for calcium signaling (Fig. 35B). *Gja1*, appeared downregulated in both models too. Furthermore, *Hcn4* and *Cntn2*, which are CCS markers, were reduced in idKO ventricles, suggesting a possible affection of the VCS.

Altogether, it is possible that, alterations both in working and conducting myocardium are contributing to QRS elongation in idKO adult hearts.

### *Cx43 Expression Is Significantly Reduced In idKO Ventricular Myocardium*

We then focussed on assessing Cx43 expression because it was reduced in the absence of *Meis1* and *Meis2* in developing CMs, and appeared downregulated in RNA-seq data from adult idKO. IF of Cx43 revealed a significant reduction of the protein in idKO ventricles (Fig. 36A, B). This reduction was already evident 4 weeks after tamoxifen administration. On the contrary, analyzing the atria, the same levels of expression were found between controls and idKO (Fig. 36C, D). These results are consistent with RNA-seq data, since DEGs genes were mainly found in the idKO ventricles.

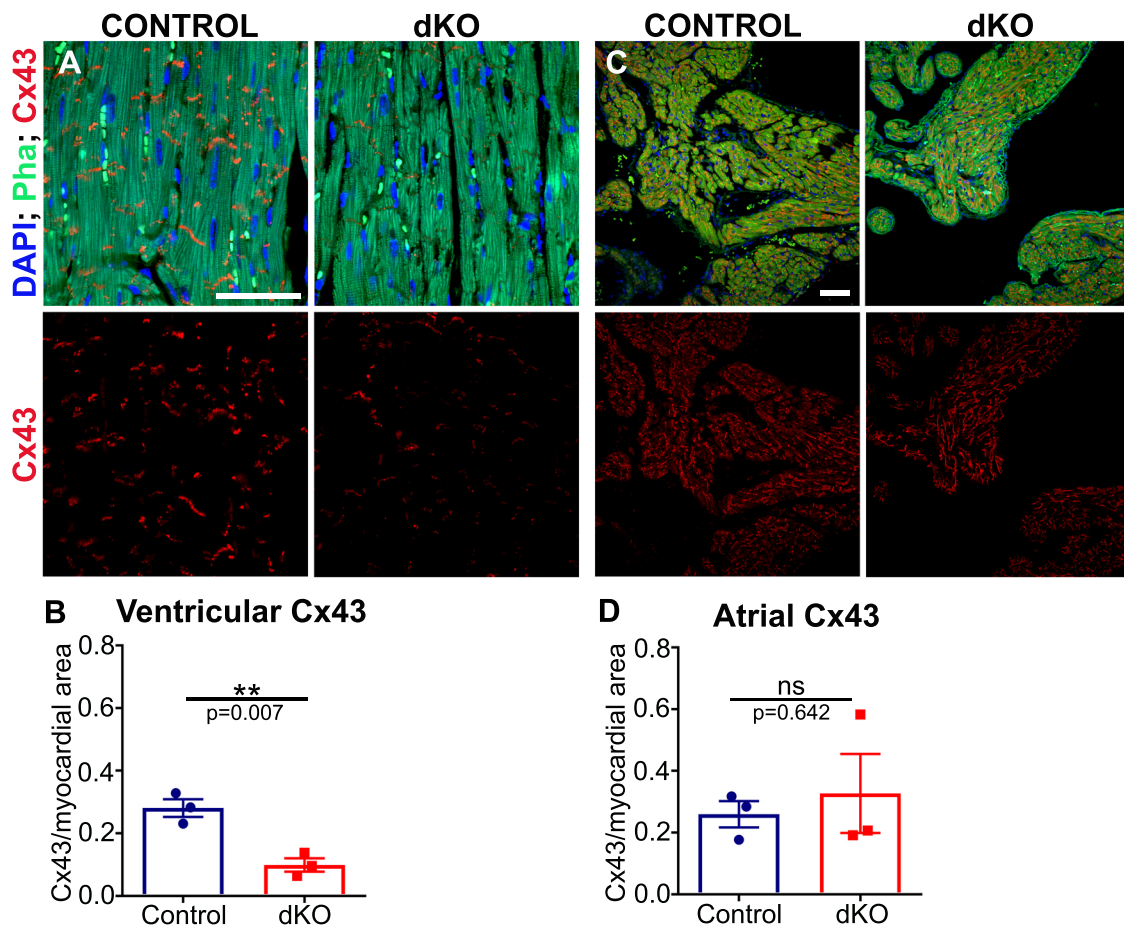


**Figure 36. Cx43 expression is reduced in idKO ventricular myocardium.** (A). Confocal images of Control and idKO ventricular myocardium 4 weeks after Tx, stained for Cx43 (red) and Phalloidin (green). (B). Quantification of Cx43 signal per myocardial area (pixel2) in ventricles. (C). Confocal images showing atria sections with the same staining as in (A). Scale bars in A and C are 50 $\mu$ m. (D). Quantification of Cx43 signal per myocardial area (pixel2) in Atria.

### *Acute Isoproterenol Treatment Does Not Preferentially Induce Arrhythmias in Meis1 and Meis2 idKO*

In the light of these results, we wondered whether idKOs could be more prone to develop arrhythmias under certain conditions. The mouse model for ARVC mentioned above developed arrhythmias after being challenged with the beta adrenergic receptor, isoproterenol (Cerrone *et al*, 2012). Thus, we decided to reproduce the same challenge in idKOs (Fig. 37A). In order to corroborate the treatment was affecting the hearts we measured the RR segment and found a reduction in length irrespective to genotype. Since isoproterenol increases heart rate, the reduction in RR time corroborated the treatment was effective. (Fig. 37B, C). No significant differences between control and

idKO hearts were found either in QRS elongation or any other ECG segments, although idKOs showed normalized QRS length by T2 (Fig. 37D). Sporadic arrhythmias were observed in some mice but were not related to the genotype (Table 1).

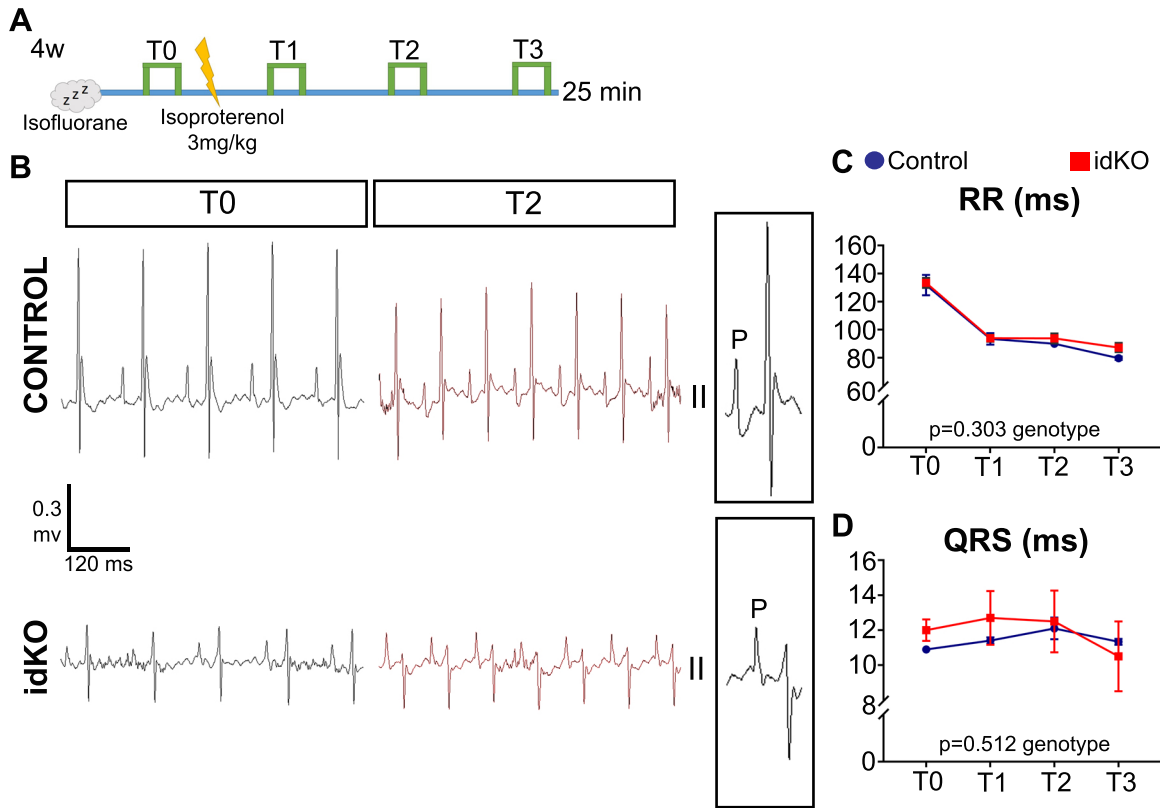


**Figure 37. idKO mice respond similar to Controls after acute isoproterenol treatment.** (A). Schematic representation of ECG recording timing, in anesthetized mice, with isoproterenol induction. T0-T3 represent fragments selected for analysis. (B). Representative ECG fragments of Control and idKO mice before and after isoproterenol injection. Boxes represent magnifications of a representative cardiac cycle. (C-D). Graphs representing RR and QRS length in Control and idKOs at the different time points analyzed.

	Mice with arrhythmic episodes	Total n° of mice
CONTROL	3	5
idKO	2	5

**Table 1. Arrhythmic episodes after isoproterenol injection where not related to genotype.** Table shows the number of mice with sporadic arrhythmic events during ECG recording after acute isoproterenol treatment.

### Putative direct targets of Meis TFs in cardiomyocytes

Taking advantage of all the RNA-seq data collected in this thesis we looked at genes differentially expressed in all the tissues and conditions studied. We found 28 genes that changed expression in developing atria and both developing and adult ventricles (Fig. 38A). The fact that these genes changed expression in different contexts suggests they could represent direct targets of Meis TFs in CMs. Gene ontology analysis for biological processes related 16 of those genes with regulation of transport, secretion, heart development and contraction (Fig. 38B). *Gja1*, *Nppa*, *Wnk1*, *Corin* and *Cacna1c*

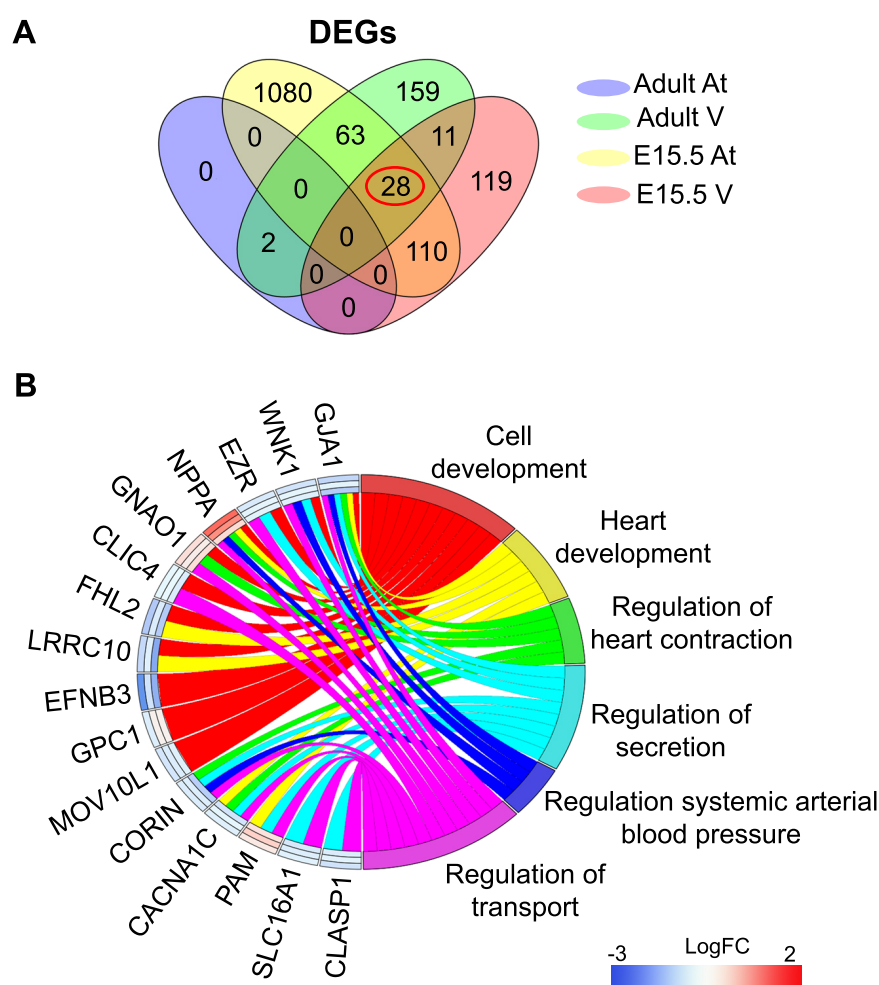


**Figure 38. Analysis of coincident DEGs in the 3 RNA-seq experiments performed reveals putative direct targets of Meis TFs.** (A). Comparison of DEGs found in all RNA-seq studies performed in this project: atria (At) and ventricles (V) from adult and embryonic hearts. (B). GO biological processes enrichment analysis performed with the 28 common DEGs found between adult ventricles and developing atria and ventricles. Fold changes rectangles, from outer to inner, correspond to: Adult ventricle, embryonic ventricle and embryonic atria, respectively.

were implicated in the majority of the processes altered, suggesting they could play a central role in the phenotype (Fig. 38B). On the other hand, *Fhl2*, *Lrrc10* and *Efnb3* appeared as the most downregulated genes (Fig. 38B).

We then decided to look at previous Meis ChIP-seq data from the lab (Longobardi *et al*, 2014; Delgado I *et al*. unpublished) to elucidate whether Meis TFs could bind directly to some of those genes or their previously described regulatory regions (Shen *et al*, 2012). ChIP-seq data from E10.5 embryos and E11.5 embryo trunks, including the heart, revealed putative binding sites of Meis in 5 of the 28 genes and regulatory regions studied: *Cacna1c*, *Clic4* (Chloride intracellular channel), *Gpc1* (Glypican 1), *Pam* (Peptidylglycine- $\alpha$ -amidating-monooxygenase) and *Prps2* (Phosphoribosyl pyrophosphate synthetase 2) (Fig. 39). In addition, we detected putative Meis binding sites in *Scn5a* and *Wnt11* genes, which although not included in the 28 genes commonly changed in all conditions, might also have an important relation with the phenotype describe.

These results suggest that these identified genes could be directly regulated by Meis transcription factors in the context of cardiomyocytes, thereby playing a central role in the development of the phenotypes described in this project.

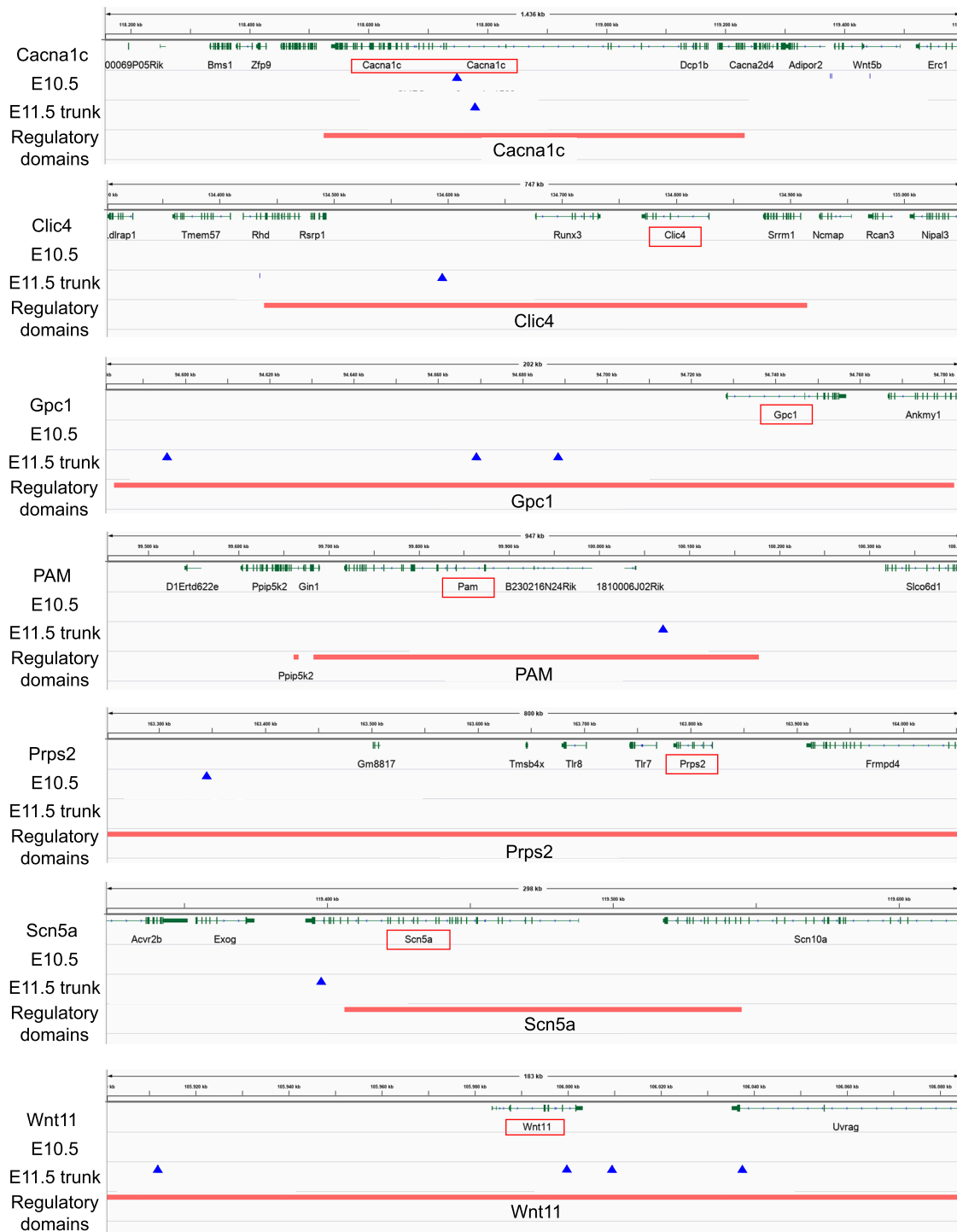


**Figure 39. Putative binding sites of Meis found by ChIP-seq analysis.** Representation of the genes with peaks statically significant in Meis-a ChIP analysis from murine E10.5 embryos and E11.5 trunks. Blue triangles represent the peaks and salmon line the regulatory regions of the genes described in Shen *et al.*, 2012.



# DISCUSSION

*“Sin libertad de pensamiento,  
la libertad de expresión no sirve  
de nada”.*

José Luis Sampedro



In this thesis project we have investigated the role of Meis1 and Meis2 transcription factors in the developing and adult cardiomyocytes. We have found Meis1 and Meis2 co-expression in developing CM is essential for perinatal survival and in adult CMs to maintain a normal tissue homeostasis. Nonetheless, discussion is needed to put in context the value of these results, elucidate possible controversial results and propose future directions suggested by this research.

### Meis expression pattern in the heart

Using mRNA in situ hybridization in wild type mouse embryos, we have described for the first time that *Meis1* and *Meis2* are expressed in SHF progenitors, epicardium and endocardium. Moreover, combining two different approaches, immunofluorescence and a *Meis1-CFP* reporter line, we have been able to describe in detail the expression pattern of Meis1 and Meis2 in the developing myocardium. Previous studies relating Meis1 function with heart development did not analyze protein expression in this organ (Stankunas *et al*, 2008; González-Lázaro *et al*, 2014). In addition, we have identified that Meis2 is expressed in cardiac valves while Meis1 is not. These results are in accordance with previous data published by the group of Dr. Kozmik in 2015, where the Meis2 expression pattern was analyzed in embryos at E13.5 and showed expression in the valves and surrounding cardiomyocytes (Machon *et al*, 2015).

Regarding Meis1 and Meis2 expression in the adult heart, nothing was previously reported. The work of Dr. Sadek, in 2013, studied the expression of Meis1 in the neonatal heart. They proposed that Meis1 is expressed after birth in CMs, but located in the cytoplasm around the nuclei and at P7 Meis1 is translocated to the nucleus (Mahmoud *et al*, 2013). However, in our experiments we always detect Meis signal in the nucleus, both in fetuses and adult hearts.

Our expression studies showed a previously undescribed preferential expression of Meis TFs in the adult CCS. Meis IF and lineage tracing of Meis-expressing cells in adult hearts, showed that the expression of Meis TFs is stronger in CCS CMs than in the working myocardium. This indicates that Meis could play an important role in CCS function or homeostasis, which is in accordance with GWAS studies in different human

cohorts that have associated intronic *Meis1* SNPs with PR interval elongation (Pfeufer *et al*, 2010; Smith *et al*, 2011a; Butler *et al*, 2012b).

### Function of Meis in developing cardiomyocytes

In this study, we have determined that double *Meis1* and *Meis2* deletion in developing CMs leads to perinatal death, probably due to ventricular cardiac arrhythmias. We described morphological alterations in dKO hearts that are not sufficient to explain the lethality of the fetuses, provided the ejection fraction is preserved. However, these results also pointed out to a role of Meis TFs in cardiac morphogenesis and in particular, in atrial and interventricular septum formation. Previous studies on *Meis1*, already described IVS defects upon *Meis1* complete deletion (Stankunas *et al*, 2008; González-Lázaro *et al*, 2014). Nevertheless, in the first study cardiac defects were thought to derive from a possible role of *Meis1* as a partner of *Pbx* in CNC progenitors, but in our model *Meis1* is deleted specifically in CMs and this is sufficient to reproduce the IVS defects.

The atrial finger-like protrusions described in *Meis1* and *Meis2* dKO hearts have never been reported before, suggesting that *Meis1* or *Meis2* loss of function, independently, are not enough to produce this phenotype. We do not know the exact mechanisms underlying this malformation. RNA-seq data allowed us to speculate that extracellular matrix, CM coupling and focal adhesion, might be involved. Plakophilin 2 (*Pkp2*) and Desmocollin 2 (*Dsc2*) are important proteins for desmosome formation and both are downregulated specifically in the developing atria. In addition, *Wnt5a* and *Wnt11*, regulators of planar cell polarity, are significantly downregulated. Thus, we hypothesize that defects in non-canonical Wnt signaling directly regulated by Meis could lead to CM misalignment and failure to form proper intercalated discs, which might contribute to disorganized tissue growth. We plan to study more in detail the atria, regarding relative pectinate muscles volume-to-lumen proportions, orientation of division planes and CM ultrastructure by electron microscopy, in order to unravel the mechanisms of the atrial malformation in *Meis1*, *Meis2* dKOs.

RNA-seq data also revealed alterations of *Gja1* (coding for Cx43 gap junction) in

embryonic atria and ventricles. Important genes for calcium signaling such as *Cacna1c* (coding for Cav1.2), *RyR2* (coding for Ryanodine Receptor 2) and *Atp2a2* (coding for SERCA2), were downregulated upon *Meis1* and *Meis2* double deletion in CMs. A mouse model with a *Cacna1c* mutation leads to lethal arrhythmias at birth (Domes *et al*, 2011) and different studies in mouse models reported that more than 50% reduction in *Gja1* expression can lead to ventricular arrhythmias and sudden death around P21 (Gutstein *et al*, 2001).

All these data, together with the fact that we did not detect an impairment in cardiac function, support our hypothesis on postnatal lethal cardiac arrhythmias occurring in dKO embryos. Moreover, the reduction in Cx43 expression and the slower depolarization rates observed by optical mapping, strongly support this view. Nevertheless, we have not been able to detect cardiac rhythm alterations by non-invasive echocardiography on pregnant females. It was only after surgically exposing the uterus when the alterations appeared. One possibility is that dKO embryos might be more sensitive to temperature changes, so when the temperature drops, the heart rate is slower and cardiac arrhythmias manifest. This might also be the explanation for the low proportion of mutants that show beating after cesarean dissection of fetuses at E16.5 during optical mapping.

An interesting future experiment, would be harvesting fetuses at E18.5 and reanimate them to perform ECG and record the possible arrhythmic events before death. We also plan to better investigate blood flows recorded in embryonic hearts by echocardiography, where we can visualize atrioventricular blocks, changes in SAN rhythm and heart rate variability. Thus, we will have more information about the possible origin of the arrhythmia.

### Function of Meis in adult cardiomyocytes

We showed that *Meis1* and *Meis2* double inducible deletion in adult CMs leads to an increase in ventricular mass and wall thickness with preserved ejection fraction. The mild hypertrophy observed might not be a primary effect of Meis loss of function and it does not progress to heart failure in the temporal window explored in this work.

A possible explanation for the preserved cardiac function is that the increase in cardiac size is not as severe as in other models of hypertrophic cardiomyopathy (Nakamura & Sadoshima, 2018; You *et al*, 2017). Moreover, we were not able to detect significant differences in the size of CMs of idKO hearts. One possibility is that the mild increase in heart size might be mainly due to the interstitial fibrosis observed with preserved number of CMs and contractile function. Nonetheless, it is important to mention that histological images with Sirius Red staining in control and idKO (Fig. 27A) suggested that a local CM hypertrophy, not detected in the global quantifications, could be happening close to the regions with higher increase in collagen deposition. This opens the possibility that there is local CM death leading to fibrosis and hypertrophy of the surrounding CMs for function compensation. If this was the case, the percentage of hypertrophic CMs would be small and upon Langendorff isolation, they would dilute out in the sample so that the differences may not be detectable. We are currently measuring CMs area in sections to address this possibility.

An alternative to this idea would be that mild CM hyperplasia might underlie the increase in cardiac mass. This would be functionally compensatory and fit with the previous reports that link Meis activity and CM exit of the cell cycle (Mahmoud *et al*, 2013, 2014). Therefore, we also explored CM proliferation as another possible factor contributing to the increase of ventricular mass in idKOs. We described here a significant augment of BrdU incorporation in mononucleated CMs of idKOs hearts, however this did not result in actual CM proliferation. Instead, mononucleated CMs became polyploid and increased size. This increase in size of the BrdU+ mononucleated CMs in idKOs likely has a very small contribution to the hypertrophic phenotype, since it represents a very small percentage of the total CM population. These results are apparently contradictory with those reported by the Sadek lab, where Meis1 is proposed as a negative regulator of postnatal CMs proliferation. In fact, after *Meis1* deletion in neonatal CMs, Mahmoud *et al.*, found increased CM proliferation and a higher number of mononucleated CMs by P7. In addition to characterizing proliferation, we have specifically looked for the expression of genes related to cell cycle that were described in the perinatal deletion of *Meis1* by Mahmoud *et al.*, but we did not detect changes in

these factors in the *Meis1* and *Meis2* adult mutants. We think there are two possible explanations for this, either the function of *Meis1* in adult CMs is different to that in perinatal stages, which has not been explored here, or in adult CMs the absence of *Meis* function is not enough to induce the complete cell division process, so it only increases DNA synthesis.

ECG analysis in control and idKOs pointed out possible alterations in conduction velocity upon *Meis1* and *Meis2* deletion in adult CMs. We detected that idKOs have a prolonged QRS complex, which correlates to what we found in dKO fetuses by optical mapping. QRS elongation in humans is a risk factor for ventricular fibrillation (Elhendy *et al*, 2005; Desai *et al*, 2006) but it does not always correspond with a slower ventricular conduction velocity. It has been reported that increased cardiac mass together with normal conduction velocity can also lead to longer QRS complexes (Wiegerinck *et al*, 2006). The most important determinant of ventricular conduction velocity is the sodium current mainly generated by channels encoded by *Scn5a*. RNA-seq data from adult ventricles showed *Scn5a* expression is significantly reduced in idKOs, suggesting that a defective sodium current might underlie the slower ventricular conduction and QRS elongation in our model. It would be very interesting to measure this current by patch-clamp in both CCs and working-myocardium CMs to corroborate these results at the single-cell level.

The reduced Cx43 expression and the interstitial fibrosis might also contribute to QRS elongation. Several mouse models have shown that reduction in Cx43 expression is associated with slower ventricular conduction velocity accompanied by increased incidence of arrhythmias and sudden cardiac death (Gutstein *et al*, 2001; Danik *et al*, 2004; van Rijen *et al*, 2004; Lerner *et al*, 2000). Moreover, rapid Cx43 remodeling or redistribution to the lateral membrane has been found in patients with various cardiac diseases, such as cardiac hypertrophy or dilated cardiomyopathy (Lambiase & Tinker, 2015; Severs *et al*, 2004). Several genes related to these diseases appear altered in idKOs hearts, as the gene set enrichment analysis pointed out, however we did not observe dilation in mutant hearts.

Furthermore, it has been proposed that reduced adhesion between cardiomyocytes might lead to mechanical stress and induce cell death (Moncayo-Arlandi & Brugada, 2017; Basso *et al*, 2009). According to this idea, interstitial fibrosis could be a secondary effect of ID disorganization. Furthermore, *Scn5a* downregulation could be a secondary consequence of Cx43 alteration in the ID (Moncayo-Arlandi & Brugada, 2017). On the other hand, there are evidences of *Scn5a* loss of function in old mice leading to fibrosis and reduced expression of Cx43 (van Veen *et al*, 2005). Thus, determining which is the cause and which the consequence would need further analyses.

As mentioned above, *Meis1* genetic variants have been associated with PR interval elongation in humans (Pfeufer *et al*, 2010; Smith *et al*, 2011b; Butler *et al*, 2012a). However, we did not detect any alterations on this interval upon double inducible deletion of *Meis1* and *Meis2* in CMs. This is likely due to the low efficiency of recombination of  $\alpha$ -MHC-MerCreMer in atria, although the association found in humans does not tell about the type of alteration in *Meis1* function (gain or loss function) that drives the phenotype. Nonetheless, the loss of function of *Meis1* and *Meis2* in adult ventricular CMs also leads to decreased expression of *Hcn4* and *Cntn2*, which are markers of the CCS, and could eventually lead to PR elongation, although we have not detected it. Altogether suggests a specific function of Meis in CCS cardiomyocytes. We consider idKOs might have alterations in the VCS, although we have not been able to find any functional impairment in these cells. We are currently studying the *Cntn2* expression pattern in the Purkinje Fiber network in this model and the consequences of *Meis1* and *Meis2* double specific deletion in CCS, using a *Hcn4-CreERT* knockin line.

The molecular changes found by RNA-seq data in idKO ventricles indicate certain similarities between Meis loss of function and those observed in mouse models of ARVC. A murine model developed by Dr. Delmar (Cerrone *et al*, 2012a) consisting on *Pkp2* (desmosome structural protein) deletion in adult CMs recapitulates some features of human ARVC. In *Pkp2* conditional KO (cKO) mice there is desmosome disorganization that leads to decrease levels of expression of many other proteins important for the intercalated discs, such as Cx43. The pathology starts with interstitial

fibrosis that can affect only the right or both ventricles, and with time evolves to dilated cardiomyopathy, impaired cardiac function and death. Moreover, intracellular calcium homeostasis is affected due to downregulation of key regulatory genes like *RyR2* and *Cacna1c*. Comparing RNA-seq data from *Meis1* and *Meis2* idKO and *Pkp2* cKO, we found that key genes for the ARVC phenotype were commonly affected in both models. Furthermore, PKP2 deletion leads to significant downregulation of *Meis1* and *Meis2* genes. Thus, we propose that Meis TFs could be partly under the control of the regulatory network involved in the ARVC-like phenotype present in *Pkp2* mutant hearts (Cerrone *et al*, 2012a). To further study this possibility, we are currently developing a mouse line with simultaneous *Pkp2* deletion and *Meis2* overexpression in adult CMs. We will determine whether *Meis2* can rescue aspects of the ARVC phenotype in this mouse model.

In humans, ARVC also leads to ventricular arrhythmias and sudden death (Zhao *et al*, 2019). In the murine model of *Pkp2* deletion, arrhythmias only appeared upon acute isoproterenol treatment. However, *Meis1* and *Meis2* idKO mice did not preferentially show arrhythmic episodes after the same treatment. We hypothesized that *Meis1* and *Meis2* inducible deletion in adult CMs recapitulates some features of ARVC but this is not enough to reproduce the complete phenotype found in *Pkp2* cKOs. Actually, in the volcano plot in Fig. 34B, it can be observed that *Pkp2* deletion leads to many more gene expression changes than those observed in Meis mutants.

### Putative direct targets of Meis

In the last part of this thesis project, we examined the putative direct targets of *Meis1* and *Meis2* TFs in cardiomyocytes. Comparing the three RNA-seq performed in developing atria and ventricles and adult ventricles from Control and idKO hearts, we found 28 genes differentially expressed in the three conditions. Gene ontology analysis related 16 of those genes with several biological functions: heart development and contraction, regulation of transport and secretion. Despite the fact that 28 genes are a low input for a gene ontology analysis, the categories found are closely related to the phenotypes described upon Meis loss of function, which suggests this gene list is

relevant to the mechanisms involved in the phenotypic alterations. Furthermore, *Fhl2* and *Lrrc10*, which are strongly downregulated, have been previously described as hypertrophic growth repressor (Okamoto *et al*, 2013) and cardiac excitation-contraction coupling regulator, respectively (Chiamvimonvat & Song, 2018). By contrast, nothing has been reported before about EfnB3 expression or function in the heart, despite of being one of the most downregulated genes in Meis mutants. We are currently working on the expression pattern of this protein.

Analysis of previous Meis ChIP-seq data from the lab, performed in E10.5 embryos and E11.5 embryonic trunk (Longobardi *et al*, 2014; Delgado I *et al*, unpublished), revealed putative Meis binding sites among the genes of interest. As we have explained before, *Cacna1c* could be playing a central role in the development of arrhythmias, together with *Gja1* downregulation. However, our results only detected possible Meis direct regulation in *Cacna1c* and not *Gja1*. *Nppa*, which appears upregulated in all conditions, does not seem to be a direct target of Meis. This result fits with the role of *Nppa* as a general responder to a wide variety of cardiac stresses. Interestingly, we also found *Clic4* and *Gpc1* as potential targets of Meis. *Clic4* is expressed in the sarcoplasmic reticulum and has been proposed to regulate ryanodine-receptors (Ponnalagu *et al*, 2016). *Gpc1* is an extracellular matrix protein whose expression appeared altered in a model of induce arrhythmias in rat (Vakhitova *et al*). *PAM* and *Prps2* also presented putative binding sites for Meis. *PAM* is important for *Nppa* secretion in the atria (Eipper *et al*, 1988; Czyzyk *et al*, 2005) and *Prps2* is implicated in the synthesis of purines and pyrimidines and it has been related to cancer (Mannava *et al*, 2008), but nothing is reported about its function in the heart.

Using the same approach we also identified Meis binding sites in *Scn5a* and *Wnt11* whose downregulation might underlie important features of the Meis mutant phenotypes. Nevertheless, these results are not enough to determine whether Meis is directly regulating those genes or whether is actually binding to some of the genes where we did not detect peaks, and further studies, specific for cardiomyocytes, are needed.

Overall, we propose that *Meis1* and *Meis2* TFs play an important role in the regulation of calcium and sodium transport and gap junction establishment in developing and adult CMs through regulation of *Cacna1c*, *Scn5a* and *Gja1* expression. The downregulation of *Cacna1c* and *Scn5a* upon Meis deletion would impair electrico-mechanical coupling and the intercalated disc structure which could lead to Cx43 downregulation. These defects result in slower ventricular depolarization. Moreover, ID disorganization and CM uncoupling might induce mechanical stress leading to cell death, interstitial fibrosis and mild-hypertrophy, to preserve cardiac function. In the formation of the atria, these alterations in cell-cell coupling, together with misregulation of cell polarity due to decreased expression of *Wnt11* and *Wnt5a*, are probably contributing to the atrial malformations found in dKO embryonic hearts. These alterations lead to an increased susceptibility to suffer arrhythmias in newborns, while in the adult heart it seems that more factors are needed for arrhythmia manifestation.

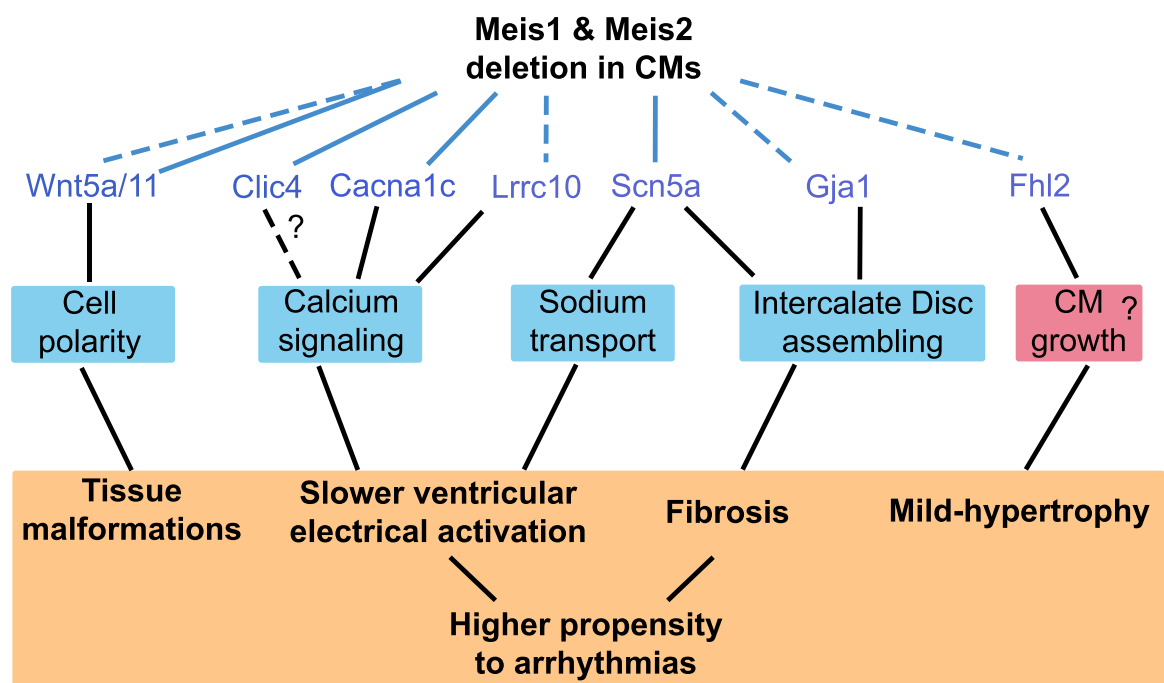


**Figure 40. Summary of defects and gene expression changes found in CMs lacking *Meis1* and *Meis2*.** In blue are represented genes and processes which are impaired upon Meis loss of function in CMs and in red, processes that increase. Blue lines link to potential direct targets of Meis and dashed lines to targets with no evidence of direct regulation. The orange box includes the defects found in mutant hearts.





# CONCLUSIONS

*"The more I learn, the more I  
realize how much I don't know".*  
Albert Einstein



- 1) *Meis1* and *Meis2* transcription factors are expressed in developing and adult cardiomyocytes and are necessary for perinatal survival and adult heart homeostasis.
- 2) The simultaneous deletion of *Meis1* and *Meis2* in developing cardiomyocytes leads to cardiac malformations in atria and ventricles and slower ventricular conduction velocity.
- 3) Fetuses with *Meis1* and *Meis2* cardiomyocyte-specific loss of function show higher frequency of stress-induced arrhythmias than Control littermates.
- 4) Deletion of *Meis1* and *Meis2* in adult cardiomyocytes produces interstitial fibrosis and QRS enlargement, suggesting a slower propagation of the electrical impulse in ventricles.
- 5) *Meis1* and *Meis2* deletion in adult cardiomyocytes stimulates endoreplicative DNA synthesis preferentially in mononucleated cells but does not stimulate cardiomyocyte proliferation.
- 6) The expression of genes encoding calcium signaling factors, sodium channels and Gap-junction proteins are regulated by *Meis1* and *Meis2* transcription factors in cardiomyocytes.
- 7) *Cacna1c*, *Scn5a*, *Clic4*, *Gpc1*, *Wnt11*, *PAM* and *Prps2* are identified as putative direct targets of *Meis1* and *Meis2* in developing and adult cardiomyocytes, helping to understand the phenotypes described in this project.



- 1) Los factores de transcripción *Meis1* y *Meis2* se expresan en cardiomiocitos durante el desarrollo embrionario y en el corazón adulto y son necesarios para la supervivencia de los fetos al nacer y para mantener la homeostasis del corazón adulto.
- 2) La delección simultánea de *Meis1* y *Meis2* en cardiomiocitos durante el desarrollo cardiaco conlleva la aparición de malformaciones en las aurículas y los ventrículos, además de ralentizar la velocidad de conducción en los ventrículos.
- 3) Los fetos con falta de función de *Meis1* y *Meis2* en cardiomiocitos presentan una mayor frecuencia de arritmias cuando se exponen a situaciones de estrés.
- 4) La doble delección de *Meis1* y *Meis2* en cardiomiocitos adultos produce fibrosis intersticial y un alargamiento del complejo QRS, lo que sugiere que la propagación del impulso eléctrico es más lenta.
- 5) La falta de función de *Meis1* y *Meis2* en cardiomiocitos incrementa la proporción de endoreplicación de ADN preferencialmente en células mononucleadas, pero no incrementa la proliferación de los cardiomiocitos.
- 6) Genes que codifican factores implicados en la señalización del calcio en cardiomiocitos, en el establecimiento de las uniones GAP y el transporte del sodio, están regulados por los factores de transcripción *Meis1* y *Meis2*.
- 7) *Cacna1c*, *Scn5a*, *Clic4*, *Gpc1*, *Wnt11*, *PAM* y *Prps2* se identifican como posibles dianas directas de *Meis1* y *Meis2* en cardiomiocitos, lo que ayudaría a explicar gran parte de los fenotipos descritos.





# BIBLIOGRAPHY

*“El fascismo se cura leyendo y  
el racismo se cura viajando”.*  
Miguel de Unamuno



- Aanhaanen WTJ, Mommersteeg MTM, Norden J, Wakker V, de Gier-de Vries C, Anderson RH, Kispert A, Moorman AFM & Christoffels VM (2010) Developmental Origin, Growth, and Three-Dimensional Architecture of the Atrioventricular Conduction Axis of the Mouse Heart. *Circ. Res.* **107**: 728–736
- Agah R, Frenkel P a, French B a, Michael LH, Overbeek P a & Schneider MD (1997) Gene Recombination in Postmitotic Cells. *J. Clin. Invest.* **100**: 169–179
- Andersson KB, Birkeland JAK, Finsen AV, Louch WE, Sjaastad I, Wang Y, Chen J, Molkenkin JD, Chien KR, Sejersted OM & Christensen G (2009) Moderate heart dysfunction in mice with inducible cardiomyocyte-specific excision of the *Serca2* gene. *J. Mol. Cell. Cardiol.* **47**: 180–187
- Andersson T, Magnuson A, Bryngelsson I-L, Frøbert O, Henriksson KM, Edvardsson N & Poçi D (2013) All-cause mortality in 272 186 patients hospitalized with incident atrial fibrillation 1995–2008: a Swedish nationwide long-term case–control study. *Eur. Heart J.* **34**: 1061–1067
- Azcoitia V, Aracil M, Martínez-A C & Torres M (2005) The homeodomain protein Meis1 is essential for definitive hematopoiesis and vascular patterning in the mouse embryo. *Dev. Biol.* **280**: 307–320
- Bassat E, Mutlak YE, Genzelinakh A, Shadrin IY, Baruch Umansky K, Yifa O, Kain D, Rajchman D, Leach J, Riabov Bassat D, Udi Y, Sarig R, Sagi I, Martin JF, Bursac N, Cohen S & Tzahor E (2017) The extracellular matrix protein agrin promotes heart regeneration in mice. *Nature* **547**: 179–184
- Basso C, Corrado D, Marcus FI, Nava A & Thiene G (2009) Arrhythmogenic right ventricular cardiomyopathy. *Lancet* **373**: 1289–1300
- Benes J, Ammirabile G, Sankova B, Campione M, Krejci E, Kvasilova A & Sedmera D (2014) The role of connexin40 in developing atrial conduction. *FEBS Lett.* **588**: 1465–1469
- Bergmann O, Zdunek S, Felker A, Salehpour M, Alkass K, Bernard S, Sjöström SL, Szewczykowska M, Jackowska T, dos Remedios C, Malm T, Andrä M, Jashari R, Nyengaard JR, Possnert G, Jovinge S, Druid H & Frisén J (2015) Dynamics of Cell Generation and Turnover in the Human Heart. *Cell* **161**: 1566–1575
- Bersell K, Choudhury S, Mollova M, Polizzotti BD, Ganapathy B, Walsh S, Wadugu B, Arab S & Kuhn B (2013) Moderate and high amounts of tamoxifen in MHC-MerCreMer mice induce a DNA damage response, leading to heart failure and death. *Dis. Model. Mech.* **6**: 1459–1469

- Blausen BE, Johannes RS & Hutchins GM (1990) Computer-based reconstructions of the cardiac ventricles of human embryos. *Am. J. Cardiovasc. Pathol.* **3**: 37–43
- Bondue A & Blanpain C (2010) Mesp1: a key regulator of cardiovascular lineage commitment. *Circ. Res.* **107**: 1414–27
- Boukens BJ, Rivaud MR, Rentschler S & Coronel R (2014) Misinterpretation of the mouse ECG: ‘musing the waves of *Mus musculus*’. *J. Physiol.* **592**: 4613–26
- Brown CB & Baldwin HS (2006) Neural Crest Contribution to the Cardiovascular System. In *Neural Crest Induction and Differentiation* pp 134–154. Boston, MA: Springer US
- Bruneau BG (2008) The developmental genetics of congenital heart disease. *Nature* **451**: 943–948
- Butler AM, Yin X, Evans DS, Nalls M a., Smith EN, Tanaka T, Li G, Buxbaum SG, Whitsel E a., Alonso A, Arking DE, Benjamin EJ, Berenson GS, Bis JC, Chen W, Deo R, Ellinor PT, Heckbert SR, Heiss G, Hsueh WC, et al (2012) Novel loci associated with PR interval in a genome-wide association study of 10 African American cohorts. *Circ. Cardiovasc. Genet.* **5**: 639–646
- Cai C-L, Liang X, Shi Y, Chu P-H, Pfaff SL, Chen J & Evans S (2003) *Isl1* identifies a cardiac progenitor population that proliferates prior to differentiation and contributes a majority of cells to the heart. *Dev. Cell* **5**: 877–89
- Cecconi F, Proetzel G, Alvarez-Bolado G, Jay D & Gruss P (1997) Expression of *Meis2*, a *Knotted*-related murine homeobox gene, indicates a role in the differentiation of the forebrain and the somitic mesoderm. *Dev. Dyn.* **210**: 184–190
- Cerrone M, Noorman M, Lin X, Chkourko H, Liang F-X, van der Nagel R, Hund T, Birchmeier W, Mohler P, van Veen TA, van Rijen H V. & Delmar M (2012) Sodium current deficit and arrhythmogenesis in a murine model of plakophilin-2 haploinsufficiency. *Cardiovasc. Res.* **95**: 460–468
- Chalice CE & Virágh S (1980) Origin and early differentiation of the sinus node in the mouse embryo heart. *Adv. Myocardiol.* **1**: 267–77
- Chiamvimonvat N & Song L (2018) *LRRC10* (Leucine-Rich Repeat Containing Protein 10) and *REEP5* (Receptor Accessory Protein 5) as Novel Regulators of Cardiac Excitation-Contraction Coupling Structure and Function. *J. Am. Heart Assoc.* **7**:
- Christoffels VM, Habets PEMH, Franco D, Campione M, de Jong F, Lamers WH, Bao Z-Z, Palmer S, Biben C, Harvey RP & Moorman AFM (2000) Chamber Formation and Morphogenesis in the Developing Mammalian Heart. *Dev. Biol.* **223**: 266–278

- Christoffels VM, Mommersteeg MTM, Trowe MO, Prall OWJ, De Gier-De Vries C, Soufan AT, Bussen M, Schuster-Gossler K, Harvey RP, Moorman a. FM & Kispert A (2006) Formation of the venous pole of the heart from an Nkx2-5-negative precursor population requires Tbx18. *Circ. Res.* **98**: 1555–1563
- Christoffels VM & Moorman AFM (2009) Development of the cardiac conduction system: why are some regions of the heart more arrhythmogenic than others? *Circ. Arrhythm. Electrophysiol.* **2**: 195–207
- Clauss S, Bleyer C, Schüttler D, Tomsits P, Renner S, Klymiuk N, Wakili R, Massberg S, Wolf E & Kääh S (2019) Animal models of arrhythmia: classic electrophysiology to genetically modified large animals. *Nat. Rev. Cardiol.*
- Cole-Jeffrey CT, Terada R, Neth MR, Wessels A & Kasahara H (2012) Progressive Anatomical Closure of Foramen Ovale in Normal Neonatal Mouse Hearts. *Anat. Rec. Adv. Integr. Anat. Evol. Biol.* **295**: 764–768
- Coppen SR, Severs NJ & Gourdie RG (1999) Connexin45 expression delineates an extended conduction system in the embryonic and mature rodent heart. *Dev. Genet.* **24**: 82–90
- Czyzyk TA, Ning Y, Hsu M-S, Peng B, Mains RE, Eipper BA & Pintar JE (2005) Deletion of peptide amidation enzymatic activity leads to edema and embryonic lethality in the mouse. *Dev. Biol.* **287**: 301–313
- D’Uva G, Aharonov A, Lauriola M, Kain D, Yahalom-Ronen Y, Carvalho S, Weisinger K, Bassat E, Rajchman D, Yifa O, Lysenko M, Konfino T, Hegesh J, Brenner O, Neeman M, Yarden Y, Leor J, Sarig R, Harvey RP & Tzahor E (2015) ERBB2 triggers mammalian heart regeneration by promoting cardiomyocyte dedifferentiation and proliferation. *Nat. Cell Biol.* **17**: 627–38
- Danik SB, Liu F, Zhang J, Suk HJ, Morley GE, Fishman GI & Gutstein DE (2004) Modulation of Cardiac Gap Junction Expression and Arrhythmic Susceptibility. *Circ. Res.* **95**: 1035–1041
- Davis LM, Kanter HL, Beyer EC & Saffitz JE (1994) Distinct gap junction protein phenotypes in cardiac tissues with disparate conduction properties. *J. Am. Coll. Cardiol.* **24**: 1124–32
- Desai AD, Yaw TS, Yamazaki T, Kaykha A, Chun S & Froelicher VF (2006) Prognostic Significance of Quantitative QRS Duration. *Am. J. Med.* **119**: 600–606
- Dhar Malhotra J, Chen C, Rivolta I, Abriel H, Malhotra R, Mattei LN, Brosius FC, Kass RS & Isom LL (2001) Characterization of sodium channel alpha- and beta-subunits

in rat and mouse cardiac myocytes. *Circulation* **103**: 1303–10

Domes K, Ding J, Lemke T, Blaich A, Rg J, Wegener W, Brandmayr J, Moosmang S & Hofmann F (2011) Truncation of Murine Ca v 1.2 at Asp-1904 Results in Heart Failure after Birth. *J. Biol. Chem.* **286**: 33863–33871

van Eif VWW, Devalla HD, Boink GJJ & Christoffels VM (2018) Transcriptional regulation of the cardiac conduction system. *Nat. Rev. Cardiol.* **15**: 617–630

Eipper BA, May V & Braas KM (1988) Membrane-associated peptidylglycine alpha-amidating monooxygenase in the heart. *J. Biol. Chem.* **263**: 8371–9

Elhendy A, Hammill SC, Mahoney DW & Pellikka PA (2005) Relation of QRS Duration on the Surface 12-Lead Electrocardiogram With Mortality in Patients With Known or Suspected Coronary Artery Disease. *Am. J. Cardiol.* **96**: 1082–1088

Engel FB, Schebesta M, Duong MT, Lu G, Ren S, Madwed JB, Jiang H, Wang Y & Keating MT (2005) p38 MAP kinase inhibition enables proliferation of adult mammalian cardiomyocytes. *Genes Dev.* **19**: 1175–87

Estigoy CB, Pontén F, Odeberg J, Herbert B, Guilhaus M, Charleston M, Ho JW, Cameron D & dos Remedios CG (2009) Intercalated discs: multiple proteins perform multiple functions in non-failing and failing human hearts. *Biophys. Rev.* **1**: 43–49

Evans SM, Yelon D, Conlon FL & Kirby ML (2010) Myocardial Lineage Development. *Circ. Res.* **107**: 1428–1444

Fahed AC, Gelb BD, Seidman JG & Seidman CE (2013) Genetics of Congenital Heart Disease. *Circ. Res.* **112**: 707–720

Fearnley CJ, Llewelyn Roderick H & Bootman MD (2011) Calcium signaling in cardiac myocytes. *Cold Spring Harb. Perspect. Biol.* **3**:

Fye WB (1994) A history of the origin, evolution, and impact of electrocardiography. *Am. J. Cardiol.* **73**: 937–49

Gabisonia K, Prosdocimo G, Aquaro GD, Carlucci L, Zentilin L, Secco I, Ali H, Braga L, Gorgodze N, Bernini F, Burchielli S, Collesi C, Zandonà L, Sinagra G, Piacenti M, Zacchigna S, Bussani R, Recchia FA & Giacca M (2019) MicroRNA therapy stimulates uncontrolled cardiac repair after myocardial infarction in pigs. *Nature* **569**: 418–422

Gard JJ, Yamada K, Green KG, Eloff BC, Rosenbaum DS, Wang X, Robbins J, Schuessler RB, Yamada KA & Saffitz JE (2005) Remodeling of gap junctions and

- slow conduction in a mouse model of desmin-related cardiomyopathy. *Cardiovasc. Res.* **67**: 539–47
- Giliberti A, Currò A, Papa FT, Frullanti E, Ariani F, Coriolani G, Grosso S, Renieri A & Mari F (2019) MEIS2 gene is responsible for intellectual disability, cardiac defects and a distinct facial phenotype. *Eur. J. Med. Genet.*
- von Gise A, Lin Z, Schlegelmilch K, Honor LB, Pan GM, Buck JN, Ma Q, Ishiwata T, Zhou B, Camargo FD & Pu WT (2012) YAP1, the nuclear target of Hippo signaling, stimulates heart growth through cardiomyocyte proliferation but not hypertrophy. *Proc. Natl. Acad. Sci.* **109**: 2394–2399
- Goldbarg AN, Hellerstein HK, Bruell JH & Daroczy AF (1968) Electrocardiogram of the Normal Mouse, *Mus Musculus: General Considerations and Genetic Aspects.* *Cardiovasc. Res.* **2**: 93–99
- González-Lázaro M, Roselló-Díez A, Delgado I, Carramolino L, Sanguino MA, Giovinazzo G & Torres M (2014) Two new targeted alleles for the comprehensive analysis of Meis1 functions in the mouse. *Genesis* **52**: 967–975
- Gordan R, Gwathmey JK & Xie L-H (2015) Autonomic and endocrine control of cardiovascular function. *World J. Cardiol.* **7**: 204–14
- Gutstein DE, Morley GE, Tamaddon H, Vaidya D, Schneider MD, Chen J, Chien KR, Stuhlmann H & Fishman GI (2001) Conduction slowing and sudden arrhythmic death in mice with cardiac-restricted inactivation of connexin43. *Circ. Res.* **88**: 333–9
- Heallen T, Zhang M, Wang J, Bonilla-Claudio M, Klysik E, Johnson RL & Martin JF (2011) Hippo Pathway Inhibits Wnt Signaling to Restrain Cardiomyocyte Proliferation and Heart Size. *Science (80-. ).* **332**: 458–461
- Hisa T, Spence SE, Rachel R a, Fujita M, Nakamura T, Ward JM, Devor-Henneman DE, Saiki Y, Kutsuna H, Tessarollo L, Jenkins N a & Copeland NG (2004) Hematopoietic, angiogenic and eye defects in Meis1 mutant animals. *EMBO J.* **23**: 450–459
- Ivanovitch K, Temiño S & Torres M (2017) Live imaging of heart tube development in mouse reveals alternating phases of cardiac differentiation and morphogenesis. *Elife* **6**:
- Jansen JA, van Veen TAB, de Bakker JMT & van Rijen HVM (2010) Cardiac connexins and impulse propagation. *J. Mol. Cell. Cardiol.* **48**: 76–82
- Jiang X, Rowitch DH, Soriano P, McMahon AP & Sucov HM (2000) Fate of the mammalian cardiac neural crest. *Development* **127**: 1607–16

- Kelly RG (2012) The Second Heart Field. *Current topics in developmental biology* pp 33–65.
- Kelly RG, Brown NA & Buckingham ME (2001) The arterial pole of the mouse heart forms from Fgf10-expressing cells in pharyngeal mesoderm. *Dev. Cell* **1**: 435–40
- Kelly RG, Buckingham ME & Moorman AF (2014) Heart Fields and Cardiac Morphogenesis. *Cold Spring Harb. Perspect. Med.* **4**: a015750–a015750
- Keyte AL, Alonzo-Johnsen M & Hutson MR (2014) Evolutionary and developmental origins of the cardiac neural crest: Building a divided outflow tract. *Birth Defects Res. Part C Embryo Today Rev.* **102**: 309–323
- Kimura W, Muralidhar S, Canseco DC, Puente B, Zhang CC, Xiao F, Abderrahman YH & Sadek HA (2014) Redox Signaling in Cardiac Renewal. *Antioxid. Redox Signal.* **21**: 1660–1673
- Koitabashi N, Bedja D, Zaiman AL, Pinto YM, Zhang M, Gabrielson KL, Takimoto E & Kass DA (2009) Avoidance of Transient Cardiomyopathy in Cardiomyocyte-Targeted Tamoxifen-Induced MerCreMer Gene Deletion Models. *Circ. Res.* **105**: 12–15
- Krainock M, Toubat O, Danopoulos S, Beckham A, Warburton D & Kim R (2016) Epicardial Epithelial-to-Mesenchymal Transition in Heart Development and Disease. *J. Clin. Med.* **5**:
- Kreuzberg MM, Liebermann M, Segschneider S, Dobrowolski R, Dobrzynski H, Kaba R, Rowlinson G, Dupont E, Severs NJ & Willecke K (2009) Human connexin31.9, unlike its orthologous protein connexin30.2 in the mouse, is not detectable in the human cardiac conduction system. *J. Mol. Cell. Cardiol.* **46**: 553–559
- Kreuzberg MM, Söhl G, Kim J-S, Verselis VK, Willecke K & Bukauskas FF (2005) Functional Properties of Mouse Connexin30.2 Expressed in the Conduction System of the Heart. *Circ. Res.* **96**: 1169–1177
- Lambiase PD & Tinker A (2015) Connexins in the heart. *Cell Tissue Res.* **360**: 675–684
- Lawson KA, Meneses JJ & Pedersen RA (1991) Clonal analysis of epiblast fate during germ layer formation in the mouse embryo. *Development* **113**: 891–911
- Lee K-F, Simon H, Chen H, Bates B, Hung M-C & Hauser C (1995) Requirement for neuregulin receptor erbB2 in neural and cardiac development. *Nature* **378**: 394–398
- Lerner DL, Yamada KA, Schuessler RB & Saffitz JE (2000) Accelerated onset and

- increased incidence of ventricular arrhythmias induced by ischemia in Cx43-deficient mice. *Circulation* **101**: 547–52
- Li F, Wang X, Capasso JM & Gerdes AM (1996) Rapid Transition of Cardiac Myocytes from Hyperplasia to Hypertrophy During Postnatal Development. *J. Mol. Cell. Cardiol.* **28**: 1737–1746
- Longobardi E, Penkov D, Mateos D, De Florian G, Torres M & Blasi F (2014) Biochemistry of the tale transcription factors PREP, MEIS, and PBX in vertebrates. *Dev. Dyn.* **243**: 59–75
- Louw JJ, Corveleyn A, Jia Y, Hens G, Gewillig M & Devriendt K (2015) MEIS2 involvement in cardiac development, cleft palate, and intellectual disability. *Am. J. Med. Genet. Part A* **167**: 1142–1146
- Machon O, Masek J, Machonova O, Krauss S & Kozmik Z (2015) Meis2 is essential for cranial and cardiac neural crest development. *BMC Dev. Biol.* **15**: 40
- Madisen L, Zwingman TA, Sunkin SM, Oh SW, Zariwala HA, Gu H, Ng LL, Palmiter RD, Hawrylycz MJ, Jones AR, Lein ES & Zeng H (2010) A robust and high-throughput Cre reporting and characterization system for the whole mouse brain. *Nat. Neurosci.* **13**: 133–140
- Mahmoud AI, Canseco D, Xiao F & Sadek H a. (2014) Cardiomyocyte cell cycle: Meising something? *Cell Cycle* **13**: 1057–1058
- Mahmoud AI, Kocabas F, Muralidhar S a, Kimura W, Koura AS, Thet S, Porrello ER & Sadek H a (2013) Meis1 regulates postnatal cardiomyocyte cell cycle arrest. *Nature* **497**: 249–53
- Mann RS & Affolter M (1998) Hox proteins meet more partners. *Curr. Opin. Genet. Dev.* **8**: 423–9
- Mannava S, Grachtchouk V, Wheeler LJ, Im M, Zhuang D, Slavina EG, Mathews CK, Shewach DS & Nikiforov MA (2008) Direct role of nucleotide metabolism in C-MYC-dependent proliferation of melanoma cells. *Cell Cycle* **7**: 2392–2400
- Martin-Puig S, Wang Z & Chien KR (2008) Lives of a heart cell: tracing the origins of cardiac progenitors. *Cell Stem Cell* **2**: 320–31
- Mercader N (2005) Proximodistal identity during vertebrate limb regeneration is regulated by Meis homeodomain proteins. *Development* **132**: 4131–4142
- Mercader N, Leonardo E, Azpiazu N, Serrano a, Morata G, Martínez C & Torres M (1999) Conserved regulation of proximodistal limb axis development by Meis1/

Hth. *Nature* **402**: 425–429

Miquerol L, Beyer S & Kelly RG (2011) Establishment of the mouse ventricular conduction system. *Cardiovasc. Res.* **91**: 232–42

Miquerol L, Moreno-Rascon N, Beyer S, Dupays L, Meilhac SM, Buckingham ME, Franco D & Kelly RG (2010) Biphasic Development of the Mammalian Ventricular Conduction System. *Circ. Res.* **107**: 153–161

Mitchell GF, Jeron A & Koren G (1998) Measurement of heart rate and Q-T interval in the conscious mouse. *Am. J. Physiol.* **274**: H747-51

Mjaatvedt CH, Nakaoka T, Moreno-Rodriguez R, Norris RA, Kern MJ, Eisenberg CA, Turner D & Markwald RR (2001) The outflow tract of the heart is recruited from a novel heart-forming field. *Dev. Biol.* **238**: 97–109

Mohan R, Boukens BJ, Christoffels VM, Mohan R, Boukens BJ & Christoffels VM (2017) Lineages of the Cardiac Conduction System. *J. Cardiovasc. Dev. Dis.* **4**: 5

Mollova M, Bersell K, Walsh S, Savla J, Das LT, Park S-Y, Silberstein LE, dos Remedios CG, Graham D, Colan S & Kühn B (2013) Cardiomyocyte proliferation contributes to heart growth in young humans. *Proc. Natl. Acad. Sci.* **110**: 1446–1451

Mommersteeg MTM, Hoogaars WMH & Prall OWJ Molecular Pathway for the Localized Formation of the Sinoatrial Node. *Circ. Res.* **16**: 354-62.

Moncayo-Arlandi J & Brugada R (2017) Unmasking the molecular link between arrhythmogenic cardiomyopathy and Brugada syndrome. *Nat. Rev. Cardiol.* **14**: 744–756

Moskow JJ, Bullrich F, Huebner K, Daar IO & Buchberg AM (1995) Meis1, a PBX1-related homeobox gene involved in myeloid leukemia in BXH-2 mice. *Mol. Cell. Biol.* **15**: 5434–43

Munshi NV (2012) Gene regulatory networks in cardiac conduction system development. *Circ. Res.* **110**: 1525–37

Munshi N V, McAnally J, Bezprozvannaya S, Berry JM, Richardson JA, Hill JA & Olson EN (2009) Cx30.2 enhancer analysis identifies Gata4 as a novel regulator of atrioventricular delay. *Development* **136**: 2665–74

Myers DC & Fishman GI (2003) Molecular and functional maturation of the murine cardiac conduction system. *Trends Cardiovasc. Med.* **13**: 289–95

Nakamura M & Sadoshima J (2018) Mechanisms of physiological and pathological cardiac hypertrophy. *Nat. Rev. Cardiol.* **15**: 387–407

- Nakamura T, Colbert MC & Robbins J (2006) Neural Crest Cells Retain Multipotential Characteristics in the Developing Valves and Label the Cardiac Conduction System. *Circ. Res.* **98**: 1547–1554
- Nakamura T, Jenkins NA & Copeland NG (1996) Identification of a new family of Pbx-related homeobox genes. *Oncogene* **13**: 2235–42
- Nerbonne JM & Kass RS (2005) Molecular Physiology of Cardiac Repolarization. *Physiol. Rev.* **85**: 1205–1253
- Nielsen MS, Axelsen LN, Sorgen PL, Verma V, Delmar M & Holstein-Rathlou N-H (2012) Gap junctions. *Compr. Physiol.* **2**: 1981–2035
- Obame FN, Plin-Mercier C, Assaly R, Zini R, Dubois-Randé JL, Berdeaux A & Morin D (2008) Cardioprotective effect of morphine and a blocker of glycogen synthase kinase 3 beta, SB216763 [3-(2,4-dichlorophenyl)-4(1-methyl-1H-indol-3-yl)-1H-pyrrole-2,5-dione], via inhibition of the mitochondrial permeability transition pore. *J. Pharmacol. Exp. Ther.* **326**: 252–8
- Okamoto R, Li Y, Noma K, Hiroi Y, Liu P-Y, Taniguchi M, Ito M & Liao JK (2013) FHL2 prevents cardiac hypertrophy in mice with cardiac-specific deletion of ROCK2. *FASEB J.* **27**: 1439–1449
- Ollion J, Cochenec J, Loll F, Escudé C & Boudier T (2013) TANGO: a generic tool for high-throughput 3D image analysis for studying nuclear organization. *Bioinformatics* **29**: 1840–1841
- Oulad-Abdelghani M, Chazaud C, Bouillet P, Sapin V, Chambon P & Dollé P (1997) Meis2, a novel mouse Pbx-related homeobox gene induced by retinoic acid during differentiation of P19 embryonal carcinoma cells. *Dev. Dyn.* **210**: 173–83
- Parker SE, Mai CT, Canfield MA, Rickard R, Wang Y, Meyer RE, Anderson P, Mason CA, Collins JS, Kirby RS, Correa A & National Birth Defects Prevention Network (2010) Updated national birth prevalence estimates for selected birth defects in the United States, 2004-2006. *Birth Defects Res. Part A Clin. Mol. Teratol.* **88**: 1008–1016
- Pfeufer A, van Noord C, Marciante KD, Arking DE, Larson MG, Smith AV, Tarasov K V, Müller M, Sotoodehnia N, Sinner MF, Verwoert GC, Li M, Kao WHL, Köttgen A, Coresh J, Bis JC, Psaty BM, Rice K, Rotter JI, Rivadeneira F, et al (2010) Genome-wide association study of PR interval. *Nat. Genet.* **42**: 153–159
- Ponnalagu D, Rao SG, Farber J, Xin W, Hussain AT, Shah K, Tanda S, Berryman MA, Edwards JC & Singh H (2016) Data supporting characterization of CLIC1, CLIC4,

CLIC5 and DmCLIC antibodies and localization of CLICs in endoplasmic reticulum of cardiomyocytes. *Data Br.* **7**: 1038–1044

Porrello ER, Mahmoud AI, Simpson E, Hill J a, Richardson J a, Olson EN & Sadek H a (2011) Transient regenerative potential of the neonatal mouse heart. *Science* **331**: 1078–1080

Puente BN, Kimura W, Muralidhar SA, Moon J, Amatruda JF, Phelps KL, Grinsfelder D, Rothermel BA, Chen R, Garcia JA, Santos CX, Thet S, Mori E, Kinter MT, Rindler PM, Zacchigna S, Mukherjee S, Chen DJ, Mahmoud AI, Giacca M, et al (2014) The Oxygen-Rich Postnatal Environment Induces Cardiomyocyte Cell-Cycle Arrest through DNA Damage Response. *Cell* **157**: 565–579

Quaife-Ryan GA, Sim CB, Ziemann M, Kaspi A, Rafahi H, Ramialison M, El-Osta A, Hudson JE & Porrello ER (2017) Multicellular Transcriptional Analysis of Mammalian Heart Regeneration. *Circulation* **136**: 1123–1139

van Rijen HVM, Eckardt D, Degen J, Theis M, Ott T, Willecke K, Jongsma HJ, Opthof T & de Bakker JMT (2004) Slow conduction and enhanced anisotropy increase the propensity for ventricular tachyarrhythmias in adult mice with induced deletion of connexin43. *Circulation* **109**: 1048–55

Ryoo HD, Marty T, Casares F, Affolter M & Mann RS (1999) Regulation of Hox target genes by a DNA bound Homothorax/Hox/Extradenticle complex. *Development* **126**: 5137–48

Saga Y, Kitajima S & Miyagawa-Tomita S (2000) Mesp1 expression is the earliest sign of cardiovascular development. *Trends Cardiovasc. Med.* **10**: 345–52

Saga Y, Miyagawa-Tomita S, Takagi A, Kitajima S, Miyazaki J i & Inoue T (1999) MesP1 is expressed in the heart precursor cells and required for the formation of a single heart tube. *Development* **126**: 3437–47

Sedmera D, Pexieder T, Vuillemin M, Thompson RP & Anderson RH (2000) Developmental patterning of the myocardium. *Anat. Rec.* **258**: 319–37

Sedmera D, Reckova M, DeAlmeida A, Coppen SR, Kubalak SW, Gourdie RG & Thompson RP (2003) Spatiotemporal pattern of commitment to slowed proliferation in the embryonic mouse heart indicates progressive differentiation of the cardiac conduction system. *Anat. Rec.* **274A**: 773–777

Severs NJ, Dupont E, Coppen SR, Halliday D, Inett E, Baylis D & Rothery S (2004) Remodelling of gap junctions and connexin expression in heart disease. *Biochim. Biophys. Acta - Biomembr.* **1662**: 138–148

- SHANNON TR & BERS DM (2004) Integrated Ca<sup>2+</sup> Management in Cardiac Myocytes. *Ann. N. Y. Acad. Sci.* **1015**: 28–38
- Shen Y, Yue F, McCleary DF, Ye Z, Edsall L, Kuan S, Wagner U, Dixon J, Lee L, Lobanenkov V. & Ren B (2012) A map of the cis-regulatory sequences in the mouse genome. *Nature* **488**: 116–120
- Simsek T, Kocabas F, Zheng J, Deberardinis RJ, Ahmed I, Olson EN, Schneider JW, Zhang CC & Hesham A (2014) Reflects Their Location in a Hypoxic Niche. **7**: 380–390
- Singh R, Hoogaars WM, Barnett P, Grieskamp T, Rana MS, Buermans H, Farin HF, Petry M, Heallen T, Martin JF, Moorman AFM, 't Hoen PAC, Kispert A & Christoffels VM (2012) Tbx2 and Tbx3 induce atrioventricular myocardial development and endocardial cushion formation. *Cell. Mol. Life Sci.* **69**: 1377–89
- Smith JG, Magnani JW, Palmer C, Meng Y a., Soliman EZ, Musani SK, Kerr KF, Schnabel RB, Lubitz S a., Sotoodehnia N, Redline S, Pfeufer A, Müller M, Evans DS, Nalls M a., Liu Y, Newman AB, Zonderman AB, Evans MK, Deo R, et al (2011) Genome-wide association studies of the PR interval in African Americans. *PLoS Genet.* **7**:
- Sohal DS, Nghiem M, Crackower MA, Witt SA, Kimball TR, Tymitz KM, Penninger JM & Molkenstein JD (2001) Temporally regulated and tissue-specific gene manipulations in the adult and embryonic heart using a tamoxifen-inducible Cre protein. *Circ. Res.* **89**: 20–5
- Soonpaa MH, Kim KK, Pajak L, Franklin M & Field LJ (1996) Cardiomyocyte DNA synthesis and binucleation during murine development. *Am. J. Physiol. Circ. Physiol.* **271**: H2183–H2189
- Später D, Abramczuk MK, Buac K, Zangi L, Stachel MW, Clarke J, Sahara M, Ludwig A & Chien KR (2013) A HCN4+ cardiomyogenic progenitor derived from the first heart field and human pluripotent stem cells. *Nat. Cell Biol.* **15**: 1098–106
- Spieler D, Kaffe M, Knauf F, Bessa J, Tena JJ, Giesert F, Schormair B, Tilch E, Lee H, Horsch M, Czamara D, Karbalai N, Toerne C Von, Waldenberger M, Gieger C, Lichtner P, Claussnitzer M, Naumann R, Müller-Myhsok B, Torres M, et al (2014) Restless Legs Syndrome-Associated intronic common variant in Meis1 alters enhancer function in the developing telencephalon. *Genome Res.* **24**: 592–603
- Stankunas K, Shang C, Twu KY, Kao SC, Jenkins N a., Copeland NG, Sanyal M, Selleri L, Cleary ML & Chang CP (2008) Pbx/Meis deficiencies demonstrate multigenetic

origins of congenital heart disease. *Circ. Res.* **103**: 702–709

Staudt DW, Liu J, Thorn KS, Stuurman N, Liebling M & Stainier DYR (2014) High-resolution imaging of cardiomyocyte behavior reveals two distinct steps in ventricular trabeculation. *Development* **141**: 585–593

Susaki EA, Tainaka K, Perrin D, Yukinaga H, Kuno A & Ueda HR (2015) Advanced CUBIC protocols for whole-brain and whole-body clearing and imaging. *Nat. Protoc.* **10**: 1709–1727

Tam PP & Behringer RR (1997) Mouse gastrulation: the formation of a mammalian body plan. *Mech. Dev.* **68**: 3–25

Tzahor E & Poss KD (2017) Cardiac regeneration strategies: Staying young at heart. *Science* **356**: 1035–1039

Unnisa Z, Clark JP, Roychoudhury J, Thomas E, Tessarollo L, Copeland NG, Jenkins NA, Grimes HL & Kumar AR (2012) Meis1 preserves hematopoietic stem cells in mice by limiting oxidative stress. *Blood* **120**: 4973–4981

Vakhitova I V, Antipina EI, Yamidanov RS, Khisamutdinova RI, Zarudiĭ FS, Baschenko NZ, Dokichev VA, Tomilov I V & Nefedov OM. Animal in vivo model of arrhythmia for genes target identification for 5-amino-exo-3-azatricyclo [5.2.1.0(2,6)]decan-4-one. *Bioorg. Khim.* **37**: 821–9

van Veen TAB, Stein M, Royer A, Le Quang K, Charpentier F, Colledge WH, Huang CL-H, Wilders R, Grace AA, Escande D, de Bakker JMT & van Rijen HVM (2005) Impaired Impulse Propagation in *Scn5a* -Knockout Mice. *Circulation* **112**: 1927–1935

Verheije R, Kupchik GS, Isidor B, Kroes HY, Lynch SA, Hawkes L, Hempel M, Gelb BD, Ghoumid J, D'Amours G, Chandler K, Dubourg C, Loddo S, Tümer Z, Shaw-Smith C, Nizon M, Shevell M, Van Hoof E, Anyane-Yeboah K, Cerbone G, et al (2019) Heterozygous loss-of-function variants of MEIS2 cause a triad of palatal defects, congenital heart defects, and intellectual disability. *Eur. J. Hum. Genet.* **27**: 278–290

Vincent SD & Buckingham ME (2010) How to Make a Heart. *Curr Top Dev Biol.* **90**:1–41.

Virágh S CC (1977) The development of the conduction system in the mouse embryo heart. II. Histogenesis of the atrioventricular node and bundle. *Dev Biol*: 397–411

Viragh S & Challice CE (1981) The origin of the epicardium and the embryonic myocardial circulation in the mouse. *Anat. Rec.* **201**: 157–168

- Waldo KL, Kumiski DH, Wallis KT, Stadt HA, Hutson MR, Platt DH & Kirby ML (2001) Conotruncal myocardium arises from a secondary heart field. *Development* **128**: 3179–88
- Walsh S, Pontén A, Fleischmann BK & Jovinge S (2010) Cardiomyocyte cell cycle control and growth estimation in vivo—an analysis based on cardiomyocyte nuclei. *Cardiovasc. Res.* **86**: 365–373
- Watanabe Y & Buckingham M (2010) The formation of the embryonic mouse heart. *Ann. N. Y. Acad. Sci.* **1188**: 15–24
- Van Weerd JH & Christoffels VM (2016) The formation and function of the cardiac conduction system. *Dev.* **15;142**: 197–210
- Wessels A & Pérez-Pomares JM (2004) The epicardium and epicardially derived cells (EPDCs) as cardiac stem cells. *Anat. Rec. Part A Discov. Mol. Cell. Evol. Biol.* **276A**: 43–57
- Wessels A & Sedmera D (2003) Developmental anatomy of the heart: a tale of mice and man. *Physiol. Genomics* **15**: 165–176
- Wiegerinck RF, Verkerk AO, Belterman CN, van Veen TAB, Baartscheer A, Opthof T, Wilders R, de Bakker JMT & Coronel R (2006) Larger Cell Size in Rabbits With Heart Failure Increases Myocardial Conduction Velocity and QRS Duration. *Circulation* **113**: 806–813
- Wiese C, Grieskamp T, Airik R, Mommersteeg MTM, Gardiwal A, de Gier-de Vries C, Schuster-Gossler K, Moorman AFM, Kispert A & Christoffels VM (2009) Formation of the Sinus Node Head and Differentiation of Sinus Node Myocardium Are Independently Regulated by Tbx18 and Tbx3. *Circ. Res.* **104**: 388–397
- Wong P, Iwasaki M, Somervaille TCP, So CWE & Cleary ML (2007) Meis1 is an essential and rate-limiting regulator of MLL leukemia stem cell potential. *Genes Dev.* **21**: 2762–2774
- Wu M, Smith CL, Hall JA, Lee I, Luby-Phelps K & Tallquist MD (2010) Epicardial spindle orientation controls cell entry into the myocardium. *Dev. Cell* **19**: 114
- You J, Wu J, Zhang Q, Ye Y, Wang S, Huang J, Liu H, Wang X, Zhang W, Bu L, Li J, Lin L, Ge J & Zou Y (2017) Differential cardiac hypertrophy and signaling pathways in pressure versus volume overload. *Am. J. Physiol. Circ. Physiol.* **314**: 552–562
- Zaffran S, Kelly RG, Meilhac SM, Buckingham ME & Brown NA (2004) Right ventricular myocardium derives from the anterior heart field. *Circ. Res.* **95**: 261–8

Zha Y, Xia Y, Ding J, Choi J-H, Yang L, Dong Z, Yan C, Huang S & Ding H-F (2014) MEIS2 is essential for neuroblastoma cell survival and proliferation by transcriptional control of M-phase progression. *Cell Death Dis.* **5**: e1417

Zhao G, Qiu Y, Zhang HM & Yang D (2019) Intercalated discs: cellular adhesion and signaling in heart health and diseases. *Heart Fail. Rev.* **24**: 115–132

Zoni-Berisso M, Lercari F, Carazza T & Domenicucci S (2014) Epidemiology of atrial fibrillation: European perspective. *Clin. Epidemiol.* **6**: 213





## **DIGITAL CONTENT**

- Doctoral thesis in PDF
- Summary & Resumen in PDF
- Supplementary table 1: DEGs obtained from E15.5 ventricles RNA-seq.
- Supplementary table 2: DEGs obtained from E15.5 atria RNA-seq.
- Supplementary table 3: DEGs obtained from adult atria RNA-seq.
- Supplementary table 4: DEGs obtained from adult ventricles RNA-seq.
- Supplementary table 5: Gene Ontology analysis with overlapping genes.
- Supplementary table 6: Gene set enrichment analysis in KEGG database with DEGs from adult ventricles.
- Supplementary table 7: Gene set enrichment analysis in KEGG database with DEGs from E15.5 ventricles.
- Supplementary table 8: Gene set enrichment analysis in KEGG database with DEGs from E15.5 atria.
- Article publish in *Development*: “Myc is dispensable for cardiomyocyte development but rescues Mycn-deficient hearts through functional replacement and cell competition”. I was working on this project during the first two years of my thesis at the same time we were generating the mouse models for the study of Meis function.



# ANEXO I



## RESEARCH REPORT

# *Myc* is dispensable for cardiomyocyte development but rescues *Mycn*-deficient hearts through functional replacement and cell competition

Noelia Muñoz-Martín<sup>1</sup>, Rocío Sierra<sup>1</sup>, Thomas Schimmang<sup>2</sup>, Cristina Villa del Campo<sup>1,\*</sup> and Miguel Torres<sup>1,\*</sup>

## ABSTRACT

*Myc* is considered an essential transcription factor for heart development, but cardiac defects have only been studied in global *Myc* loss-of-function models. Here, we eliminated *Myc* by recombining a *Myc* floxed allele with the *Nkx2.5Cre* driver. We observed no anatomical, cellular or functional alterations in either fetuses or adult cardiac *Myc*-deficient mice. We re-examined *Myc* expression during development and found no expression in developing cardiomyocytes. In contrast, we confirmed that *Mycn* is essential for cardiomyocyte proliferation and cardiogenesis. Mosaic *Myc* overexpression in a *Mycn*-deficient background shows that *Myc* can replace *Mycn* function, recovering heart development. We further show that this recovery involves the elimination of *Mycn*-deficient cells by cell competition. Our results indicate that *Myc* is dispensable in cardiomyocytes both during cardiogenesis and for adult heart homeostasis, and that *Mycn* is exclusively responsible for cardiomyocyte proliferation during heart development. Nonetheless, our results show that *Myc* can functionally replace *Mycn*. We also show that cardiomyocytes compete according to their combined *Myc* and *Mycn* levels and that cell competition eliminates flawed cardiomyocytes, suggesting its relevance as a quality control mechanism in cardiac development.

**KEY WORDS:** Heart development, Transcription factor, Proliferation, Apoptosis, Cell competition, Mouse

## INTRODUCTION

*Myc* transcription factors promote cell growth and division, being essential for proliferation in healthy tissues and tumours. *Myc* proteins belong to the basic helix-loop-helix-domain family and exert their functions mainly by regulating transcription. There are three members of the *Myc* family of transcription factors in mammals: *Myc*, *Mycn* and *Mycl*. All three transcripts show spatially restricted patterns during post-implantation embryonic development (Zimmerman et al., 1986). Deregulation of these genes has been linked with tumour formation and cell growth.

*Myc* expression is required for normal embryonic development in mammals, displaying widespread expression from early stages of development, and becoming regionally restricted starting at embryonic day (E) 7.5. Global *Myc* knockout embryos die between E9.5 and E10.5, showing defects in heart, pericardium and neural

tube, and delay or failure of embryo turning (Davis et al., 1993). Strong *Myc* overexpression in transgenic mice enhances myocyte proliferation during heart development, promoting cardiac hyperplasia, which suggested the idea of an essential role of *Myc* in cardiomyocyte growth and proliferation during development (Jackson et al., 1990). In contrast, strong *Myc* overexpression during postnatal life leads to premature cardiomyocyte hypertrophy (Machida et al., 1997; Xiao et al., 2001) and heart-specific deletion of *Myc* prevents hypertrophic growth in response to hemodynamic, pharmacological (Zhong et al., 2006) and cold-induced (Bello Roufai et al., 2007) hypertrophy. *Myc* mRNA levels in whole hearts decrease in correlation with the transition from hyperplastic to hypertrophic growth (Schneider et al., 1986) and *Myc* is not expressed in adult cardiomyocytes under normal conditions but becomes strongly activated following hypertrophic stimuli (Izumo et al., 1988; Pollack et al., 1994), which suggests that the physiological function of *Myc* in postnatal cardiomyocytes is restricted to the hypertrophic response to a challenge. In agreement with this idea, *Myc* deletion in cardiomyocytes of unchallenged adult mouse hearts does not lead to cardiac function alterations (Zhong et al., 2006).


Further experiments in a model of moderate overexpression of *Myc* produced a very different set of results. Mild *Myc* overexpression in a cellular mosaic fashion does not produce overt phenotypical alterations during embryonic development or adult life, but induces the phenomenon of cell competition, by which cells with enhanced anabolism eliminate and replace neighbours without altering tissue homeostasis (Claveria et al., 2013; Claveria and Torres, 2016). In cardiac-specific models of *Myc* mosaic overexpression at moderate levels, *Myc*-enhanced cardiomyocytes trigger the elimination of neighbouring wild-type cardiomyocytes both during development and in the adult heart (Villa del Campo et al., 2014, 2016).

The changes induced by moderate *Myc* overexpression in cardiomyocytes remain within homeostatic limits both during development and in the adult heart (Villa del Campo et al., 2014). Notably, in these experiments, *Myc*-enhanced adult hearts are not prone to hypertrophy but display a mild hyperplastic phenotype (Villa del Campo et al., 2014). The contrast of these results with those obtained by strong overexpression of *Myc* in transgenic mice (Machida et al., 1997; Xiao et al., 2001) suggests that the effects of *Myc* overexpression depend on the levels induced.

Although the results obtained in overexpression experiments suggest a role for *Myc* during cardiomyocyte development, there are no studies reporting developmental cardiac-specific deletion of *Myc*. Furthermore, the conditional deletion of *Myc* in the blood/endothelial lineage produces heart defects similar to those observed in complete *Myc* elimination (He et al., 2008), raising the possibility that the cardiac defects observed in the global mutant do not result from a primary function in cardiomyocytes. In contrast, *Mycn* is essential for cardiomyocyte development in conditional deletion

<sup>1</sup>Cardiovascular Development Program, Centro Nacional de Investigaciones Cardiovasculares, CNIC, 28029 Madrid, Spain. <sup>2</sup>Instituto de Biología y Genética Molecular, Universidad de Valladolid y Consejo Superior de Investigaciones Científicas, 47003, Valladolid, Spain.

\*Authors for correspondence (mtorres@cnic.es; cristina.villa@cnic.es)

 M.T., 0000-0003-0906-4767

models (Harmelink et al., 2013) whereas *Mycl* expression and mutant phenotypes do not affect the heart (Hatton et al., 1996). *Myc* and *Mycn* show high sequence and structure homology and this translates into a highly conserved function, as exemplified by full rescue by *Mycn* of the *Myc* global knockout in a knock-in replacement mouse model (Malynn et al., 2000).

*Mycn* global mutants die *in utero* between E10.5 and E11.5, displaying smaller size and hypoplastic heart (Charron et al., 1992; Moens et al., 1993; Sawai et al., 1993; Stanton et al., 1992), a phenotype that is reproduced in a cardiomyocyte-specific deletion of *Mycn* using a *cTnT-Cre* driver (Harmelink et al., 2013). *Mycn* is required for ventricular wall morphogenesis through its role in regulating compact layer cardiomyocyte growth, proliferation and maturation. The defects in heart growth were attributed exclusively to the reduction in proliferation and not to increased cell death (Harmelink et al., 2013).

Here, we studied the role of *Myc* during heart development, the ability of *Myc* to rescue *Mycn* deficiency during cardiogenesis and the involvement of cell competition and cardiomyocyte replacement in this rescue. We report the absence of *Myc* expression or function in developing cardiomyocytes and the ability of *Myc*-expressing cardiomyocyte populations to repopulate *Mycn*-deficient hearts and rescue *Mycn* function. Our results indicate that *Mycn* is essential for cardiomyocyte development, but *Myc* is not involved in this process. Nonetheless, *Myc* is able to mimic *Mycn* function, rescue *Mycn*-deficient cells and promote the elimination of *Mycn*-deficient cells to restore a viable heart.

## RESULTS AND DISCUSSION

### *Myc* is dispensable for heart development and adult heart homeostasis

To study the role of *Myc* during heart development, we conditionally deleted *Myc* in mice using the *Nkx2.5-Cre* strain, which drives widespread Cre-mediated recombination in cardiac precursors from around E8.0 (Stanley et al., 2002). *Nkx2.5-Cre*-mediated recombination is complete in cardiomyocytes and affects a large part of endocardial (Stanley et al., 2002) and epicardial (Zhou et al., 2008) precursors. Embryos resulting from elimination of *Myc* function in cardiac progenitors (cKO-*Myc*) (*Myc<sup>fllox/fllox</sup>; Nkx2.5-Cre<sup>tg/+</sup>*) were viable and did not display any phenotypic abnormality (Fig. 1A). cKO-*Myc* mice reached adulthood in the expected proportions (Table S1) and presented normal cardiac morphology (Fig. 1A).

Measurements of heart weight revealed no significant differences in size between cKO-*Myc* homozygous, heterozygous and wild-type hearts (Fig. 1B). The density of cardiomyocyte nuclei was similar between cKO-*Myc* homozygous, heterozygous and wild-type hearts (Fig. 1C,D), indicating no alterations in cardiomyocyte size or number.

To assess the function of cKO-*Myc* hearts, we performed echocardiographic assays on 10-week-old adult mice. No significant differences were found between groups in ejection fraction and fractional shortening parameters, indicating that the function of cKO-*Myc* hearts is not affected by the loss of *Myc* (Fig. 1E). Overall, cKO-*Myc* hearts display normal morphology and function and, therefore, our data indicate that *Myc* function in the *Nkx2.5-Cre<sup>+</sup>* lineages is dispensable for heart formation and adult heart homeostasis.

### *Myc* is not expressed in developing cardiomyocytes

The results obtained could be explained by lack of *Myc* function during cardiomyocyte development or by compensation of a

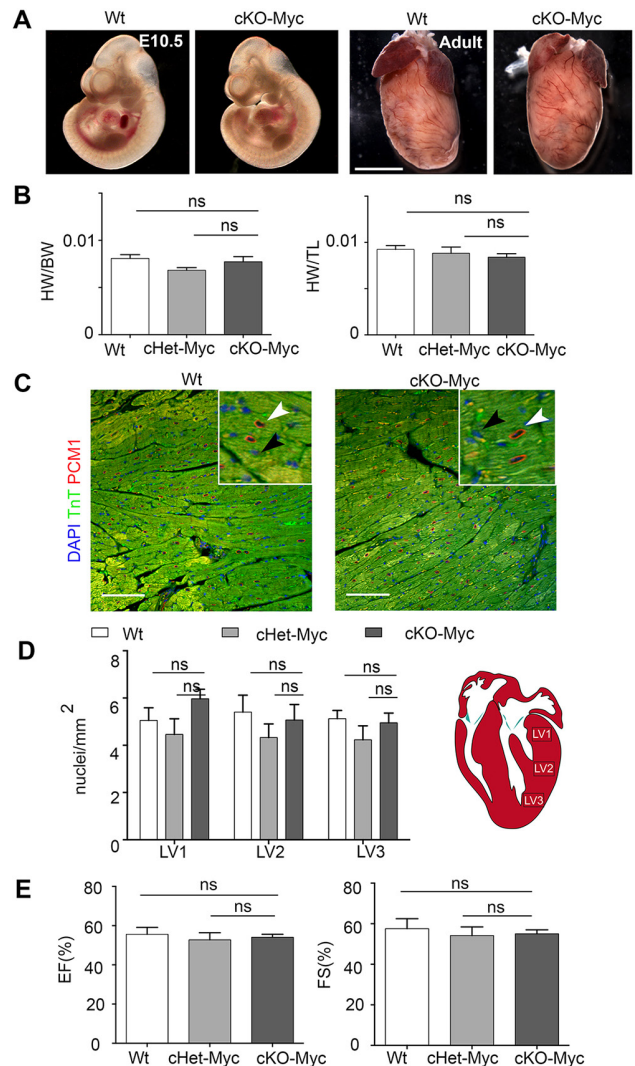


**Fig. 1. *Myc* deletion in the *Nkx2.5* lineage.** (A) Left: Whole-mount E10.5 wild-type (Wt) and *Mycn<sup>fllox/fllox</sup>; Nkx2.5-Cre<sup>tg/+</sup>* (cKO-*Myc*) embryos. Right: Whole-mount Wt and cKO-*Myc* adult hearts. (B) Heart/body weight (HW/BW) and heart weight/tibia length (HW/TL) ratios in 10-week-old animals. (C) Confocal images from sections of adult hearts stained with anti-PCM1 (red) and anti-TnT (green). Insets show magnification of cardiomyocyte (white arrow) and non-cardiomyocyte (black arrow) nuclei in heart sections, as detected with PCM-1 antibody. (D) Quantification of cardiomyocyte nuclei per area in three different regions of the left ventricle. Location of the regions within the left ventricle is identified in the schematic as LV1, LV2 and LV3. (E) Ejection fraction (EF) and fractional shortening (FS) measured by echocardiography in adult mice. Data in C,E,F are mean±s.e.m.; ns, not significant ( $P>0.05$ ).  $n=3-8$  mice/condition. Scale bars: 500  $\mu$ m (A); 100  $\mu$ m (C).

putative *Myc* function by *Mycn*. *Myc* RNA expression has been reported by northern blot in mid-gestation samples from whole myocardium (Jackson et al., 1990; Schneider et al., 1986) and *Myc* protein expression has been reported by western blot from whole adult myocardium (Zhong et al., 2006). Here, we performed *in situ* hybridization (ISH) to determine which cells express *Myc* during myocardial development. In agreement with previous reports (Uslu et al., 2014), *Myc* mRNA was expressed at E9.5 in the neural tube, branchial arches, cephalic regions and other non-cardiac tissues (Fig. 2A). At this stage, *Myc* mRNA was not detected in the heart tube, but within the cardiogenic region, expression was seen in the

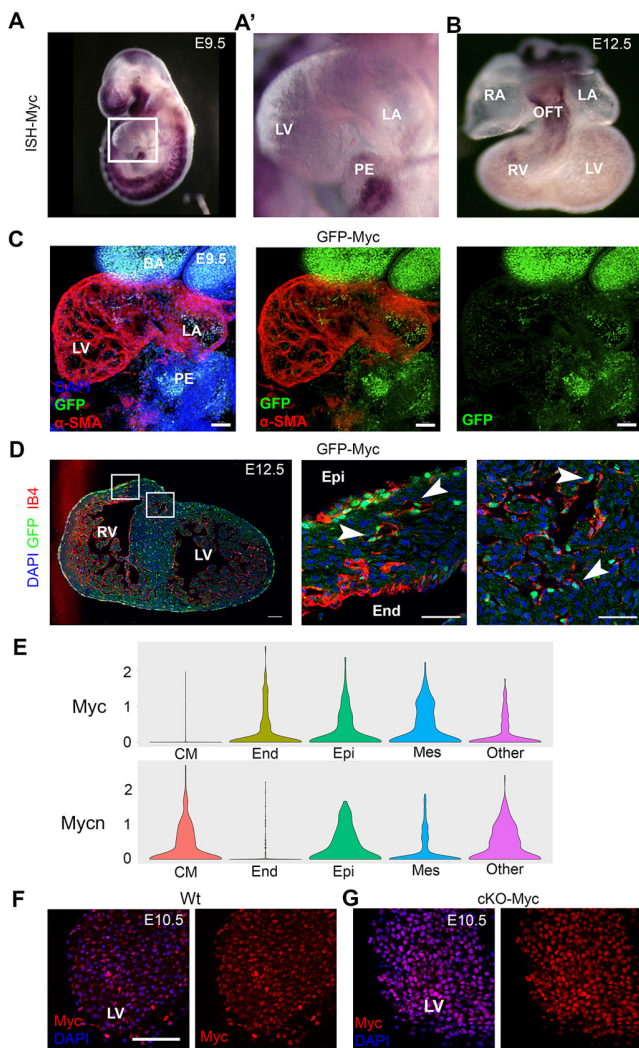


**Fig. 2. Myc is not detected in cardiomyocytes during heart development.** (A,A') Whole-mount *Myc* ISH of an E9.5 wild-type embryo, with detail of the heart in A' (magnification of the boxed area in A). (B) Whole-mount *Myc* ISH of an E12.5 wild-type embryonic heart. (C) Confocal section of a whole-mount E9.5 *GFP-Myc* embryo showing *GFP-Myc* expression and  $\alpha$ -SMA immunostaining. (D) Confocal section of an E12.5 *GFP-Myc* heart showing *GFP-Myc* expression and isolectin GS-IB4 (IB4) as an endothelial marker. Middle and right panels show magnification of the boxed areas of the left panel. Arrowheads point to endothelial cells expressing *GFP-Myc*. (E) Violin plots showing *Myc* and *Mycn* mRNA expression in different cardiac cell types at E10.5. The data are a re-analysis of original data by Li et al., 2016. Violin plots show relative cell abundance (x-axis) versus log<sub>2</sub> of normalized reads (y-axis) for *Myc* or *Mycn* mRNAs. (F,G) Confocal sections of whole E10.5 wild-type (Wt; F) and cKO-*Myc* (G) hearts showing staining for DAPI and *Myc*. BA, branchial arches; CM, cardiomyocytes; End, endocardium (endocardium/endothelium in E); Epi, epicardium; LA, left atria; LV, left ventricle; Mes, mesenchymal cells; OFT, outflow tract; PE, proepicardium; RA, right atria; RV, right ventricle. Scale bars: 70  $\mu$ m (C); 100  $\mu$ m (D, left); 50  $\mu$ m (D, middle and right, and F,G).

proepicardium (Fig. 2A'). Analysis at later stages showed weak *Myc* mRNA detection in the distal outflow tract (OFT) and subepicardium at E12.5 (Fig. 2B). To confirm *Myc* expression in the developing heart, we took advantage of a *GFP-Myc* knock-in reporter line in which endogenous *Myc* protein expression is reported by green fluorescent protein (GFP) fused to the endogenous *Myc* mRNA open reading frame (Huang et al., 2008).

In agreement with our ISH results, *GFP-Myc* expression at E9.5 was strongly detected in the branchial arches and in the proepicardium (Fig. 2C). In the heart tube, no *GFP-Myc* expression was detected in the myocardium, whereas the endocardium displayed a positive signal. Sectioning of *GFP-Myc* E12.5 hearts showed no *GFP-Myc* expression in cardiomyocytes. It was detected in endothelial cells within the myocardium and subepicardium, with endocardial expression mostly absent (Fig. 2D). In addition, we analysed previous data of single cell RNA-seq from developing mouse hearts at stage E10.5 (Li et al., 2016). *Myc* and *Mycn* mRNAs show complementary patterns in the endothelial and cardiomyocyte populations of E10.5 hearts. *Myc* mRNA is strongly present in endothelial cells, but it is not detected in cardiomyocytes, whereas *Mycn* mRNA shows the opposite expression pattern (Fig. 2E). In addition, the mRNAs of both genes are detected in epicardial, mesenchymal and other mixed cell populations (Fig. 2E).

These results contradict our previous characterization of *Myc* protein distribution using an anti-*Myc* antibody in immunofluorescence, in which a clear signal was detected in cardiomyocytes at E10.5 (Villa del Campo et al., 2014). To resolve this contradiction, we repeated the immunofluorescence comparing wild-type and cKO-*Myc* hearts at E10.5 (Fig. 2F,G). Detection of *Myc* expression in wild-type embryos clearly identified a nuclear signal in cardiomyocytes (Fig. 2F). This signal remained unchanged in cKO-*Myc* hearts (Fig. 2G). This result contrasts with the observation that this antibody has been validated for endogenous *Myc* detection in the E6.5 mouse epiblast (Claveria et al., 2013). Although the most plausible explanation for this result is cross-reaction with *Mycn*, which is expressed in developing cardiomyocytes but not in the E6.5 epiblast (Harmelink et al., 2013; Moens et al., 1993), in *Mycn<sup>fllox/fllox</sup>;Nkx2.5-Cre<sup>tg/WT</sup>* embryos, the signal persisted (Fig. S1), indicating non-specificity of unknown origin.

We conclude that *Myc* does not play a role in cardiomyocyte development because it is not expressed in this lineage and, thus, it does not act redundantly with *Mycn*.

### Forced *Myc* expression in a mosaic fashion is sufficient to rescue cKO-*Mycn* cardiac defects

A relevant question is whether the different effects reported for *Myc* overexpression in cardiomyocytes result from *Myc* mimicking *Mycn* function. As mentioned above, *Mycn* can replace *Myc* functions when knocked in to the *Myc* locus (Malynn et al., 2000). Here, we investigated whether *Myc* could replace *Mycn* function in the developing heart. To test this, we used *Myc* overexpression from the Cre-inducible *Rosa26R-iMOS* mosaic system (Claveria et al., 2013). The *iMOS<sup>TMyc</sup>* allele allows the induction of mild overexpression of *Myc* in a cellular mosaic fashion (Claveria et al., 2013) (Fig. S2A). In this mosaic model, 75% of recombined cells overexpress *Myc* and are reported by EYFP expression, whereas 25% of recombined cells do not overexpress *Myc* and are reported by ECFP expression (Fig. S2). *Mycn<sup>fllox/fllox</sup>;Nkx2.5-Cre<sup>tg/+</sup>* embryos in which *Mycn* has been conditionally deleted in heart precursors (cKO-*Mycn*) are not viable past E10.5-E11.5 (Fig. 3A, middle), in accordance with the phenotype previously reported for *Mycn* deletion in cardiomyocytes (Harmelink et al., 2013). In contrast, cardiac *Mycn*-deficient littermates in which the *iMOS<sup>TMyc</sup>* mosaic has been activated (*Mycn<sup>fllox/fllox</sup>;iMOS<sup>TMyc/+</sup>;Nkx2.5-Cre<sup>tg/+</sup>*) were viable and indistinguishable from *iMOS<sup>TMyc</sup>* activation on wild-type (*Mycn<sup>+/+</sup>;iMOS<sup>TMyc/+</sup>;Nkx2.5-Cre<sup>tg/+</sup>*) or *Mycn*-heterozygous (*Mycn<sup>fllox/+</sup>;iMOS<sup>TMyc/+</sup>;Nkx2.5-Cre<sup>tg/+</sup>*) backgrounds (Fig. 3A, right); both genotypes being phenotypically normal (Villa del Campo et al., 2014; this study). Histological

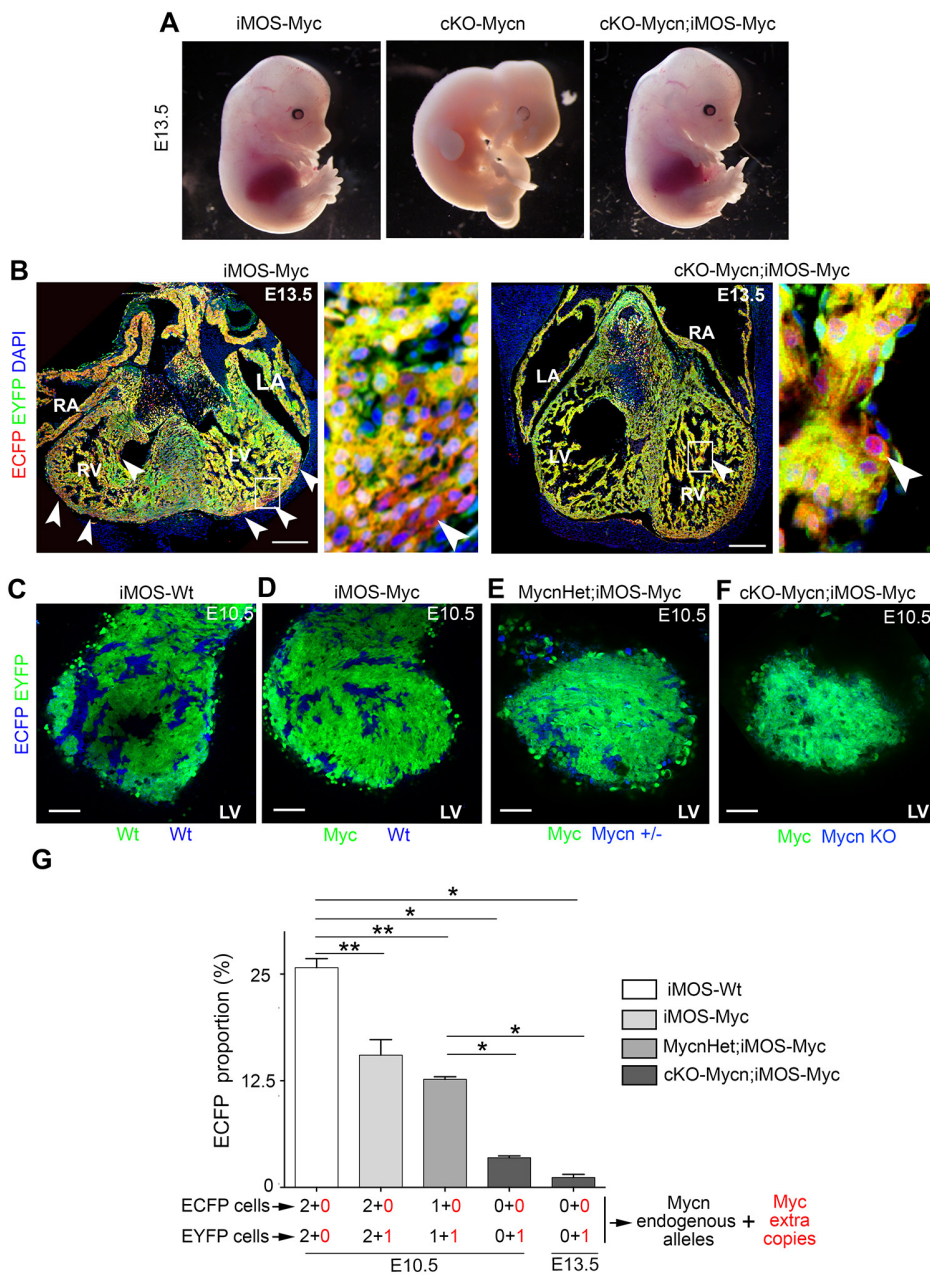


**Fig. 3. Myc mosaic overexpression rescues cardiac Mycn deficiency.**

(A) Whole-mounts of E13.5 embryos of the following genotypes: *Mycn*<sup>+/+</sup>; *iMOS*<sup>T1Myc/+</sup>; *Nkx2.5-Cre*<sup>tg/+</sup> (iMOS-Myc; left), *Mycn*<sup>fllox/fllox</sup>; *Nkx2.5-Cre*<sup>tg/+</sup> (cKO-Mycn; middle) and *Mycn*<sup>+/+</sup>; *iMOS*<sup>T1Myc/+</sup>; *Nkx2.5-Cre*<sup>tg/+</sup> (cKO-Mycn;iMOS-Myc; right). (B) Confocal section of E13.5 iMOS-Myc and cKO-Mycn hearts, showing EYFP-Myc (yellow) and ECFP-WT (red) cell populations. Arrowheads point to ECFP-positive cells, also displayed in the magnification of boxed areas.

(C-F) Confocal sections of E10.5 iMOS-Wt (*Mycn*<sup>+/+</sup>; *iMOS*<sup>WT/+</sup>; *Nkx2.5-Cre*<sup>tg/+</sup>; C), iMOS-Myc (D), *Mycn*Het;iMOS-Myc (*Mycn*<sup>fllox/+</sup>; *iMOS*<sup>T1Myc/+</sup>; *Nkx2.5-Cre*<sup>tg/+</sup>; E) and cKO-Mycn;iMOS-Myc (F) whole-mount hearts showing endogenous fluorescence from the EYFP (green) and ECFP (blue) cell populations. (G) Percentage of ECFP cells in hearts of iMOS-WT and iMOS-Myc mosaics in the three different *Mycn* backgrounds. The number of *Myc* and *Mycn* combined alleles in each cell population of the different mosaics is shown below the graph. LA, left atria; LV, left ventricle; RA, right atria; RV, right ventricle. *n*=3 cKO-Mycn, *n*=3 iMOS-Myc in *Mycn* heterozygous or wild-type backgrounds. Data in G are mean±s.e.m.; \**P*<0.05; \*\**P*<0.01. Scale bars: 100 μm.

analysis and study of the contribution of the cells recombined by *Nkx2.5-Cre* at E13.5 showed normal contribution of cardiac progenitors to the heart and no morphological alterations were observed in *iMOS*<sup>T1Myc</sup>-rescued *Mycn*-deficient hearts compared with *iMOS*<sup>T1Myc</sup> hearts (Fig. 3B). These results indicate that mosaic overexpression of *Myc*, driven by the endogenous *Rosa26* promoter, is enough to functionally replace the loss of *Mycn* expression during heart development.

#### Cell competition contributes to the rescue of *Mycn*-deficient hearts by stimulating the replacement of deficient cells

The complete phenotypic rescue of cKO-Mycn hearts suggested that, in addition to cell-autonomous replacement of *Mycn* function by *Myc*, some non-cell-autonomous mechanism would operate to either eliminate or rescue the 25% of cells that do not activate *Myc*. To understand which of these mechanisms is at work, we determined

the proportion of ECFP and EYFP cardiomyocyte populations in different genetic configurations. Control *iMOS*<sup>WT</sup> mosaics expressing only the fluorescent proteins over a wild-type background produce a 25-75% distribution of ECFP and EYFP cardiomyocytes when activated by the *Nkx2.5-Cre* driver (*iMOS*<sup>WT/+</sup>; *Nkx2.5-Cre*<sup>tg/+</sup>) (Fig. 3C,G; Fig. S2). The same experiment performed with the *iMOS*<sup>T1Myc</sup> mosaic reduces the wild-type (ECFP) cell population that does not overexpress *Myc* to 15% from the original 25% (Fig. 3D,G), as a result of cell competition (Fig. 3G) (Villa del Campo et al., 2014). When the *iMOS*<sup>T1Myc</sup> mosaic was induced over a cardiac *Mycn*-heterozygous background (*Mycn*<sup>fllox/+</sup>; *iMOS*<sup>T1Myc/+</sup>; *Nkx2.5-Cre*<sup>tg/+</sup>), the proportion of *Mycn*<sup>+/-</sup> (ECFP) cardiomyocytes observed in E10.5 hearts was about 12.5% (Fig. 3E,G) whereas when the *iMOS*<sup>T1Myc</sup> mosaic was induced over a cardiac *Mycn* homozygous deletion (*Mycn*<sup>fllox/fllox</sup>; *iMOS*<sup>T1Myc/+</sup>; *Nkx2.5-Cre*<sup>tg/+</sup>), the proportion of *Mycn*-KO (ECFP) cells dropped to 3.7% at E10.5 and to 1% at

E13.5 (Fig. 3B,F,G). These results suggest not only the cell-autonomous replacement of *Mycn* by *Myc*, but also that a replacement of *Mycn*-KO cardiomyocytes by *Myc*-overexpressing cardiomyocytes contributes to the rescue of cardiac *Mycn* deficiency.

We next explored the possibility that the elimination of this cell population takes place by cell competition. Elimination of *Mycn*-KO cardiomyocytes when confronted with *Myc*-overexpressing cardiomyocytes was much more efficient than elimination of wild-type or *Mycn*-heterozygous cells, which would fit a scenario in which both *Myc* and *Mycn* act additively to determine cardiomyocyte competition ability. An alternative view would be that *Mycn*-KO cells are not actively eliminated but just diluted out because of their limited ability to proliferate (Fig. 4A,B). To discriminate between these possibilities, we determined the frequency of apoptosis in *Mycn*-KO cardiomyocytes both when in a homotypic environment in *Mycn<sup>fllox/fllox</sup>;Nkx2.5-Cre<sup>tg/+</sup>* hearts, and when confronted with a *Myc*-overexpressing cardiomyocyte population in *Mycn<sup>fllox/fllox</sup>;iMOS<sup>TIMyc/+</sup>;Nkx2.5-Cre<sup>tg/+</sup>* hearts. We found that the apoptotic rate in *Mycn*-KO cardiomyocytes is very low and similar to that found

in wild-type hearts (Fig. 4C,D), which agrees with previous reports (Harmelink et al., 2013). In contrast, *Mycn*-KO cardiomyocytes exposed in mosaic hearts to *Myc*-overexpressing cardiomyocytes, display a strong increase in the frequency of apoptosis (Fig. 4E,F). These results indicate that confrontation with *Myc*-overexpressing rescued cells produces a strong selective apoptotic elimination of *Mycn*-KO cells, which are otherwise viable in a homotypic environment.

Taken together, our results show that *Myc* is not required for heart development in the *Nkx2.5-Cre<sup>+</sup>* lineage and is not detectably expressed in developing cardiomyocytes. Although this excludes a function of *Myc* in cardiomyocytes, the study is not conclusive regarding *Myc* functions in endothelial or epicardial lineages that are not completely affected by *Nkx2.5-Cre* recombination. In the context of previous evidence from endogenous *Myc* expression and function analyses in the adult heart (Jackson et al., 1990; Schneider et al., 1986; Zhong et al., 2006), it is concluded that *Myc* expression and its role in heart physiology are restricted to stress responses during adult life, whereas *Mycn* fully assumes the constitutive roles of the family during

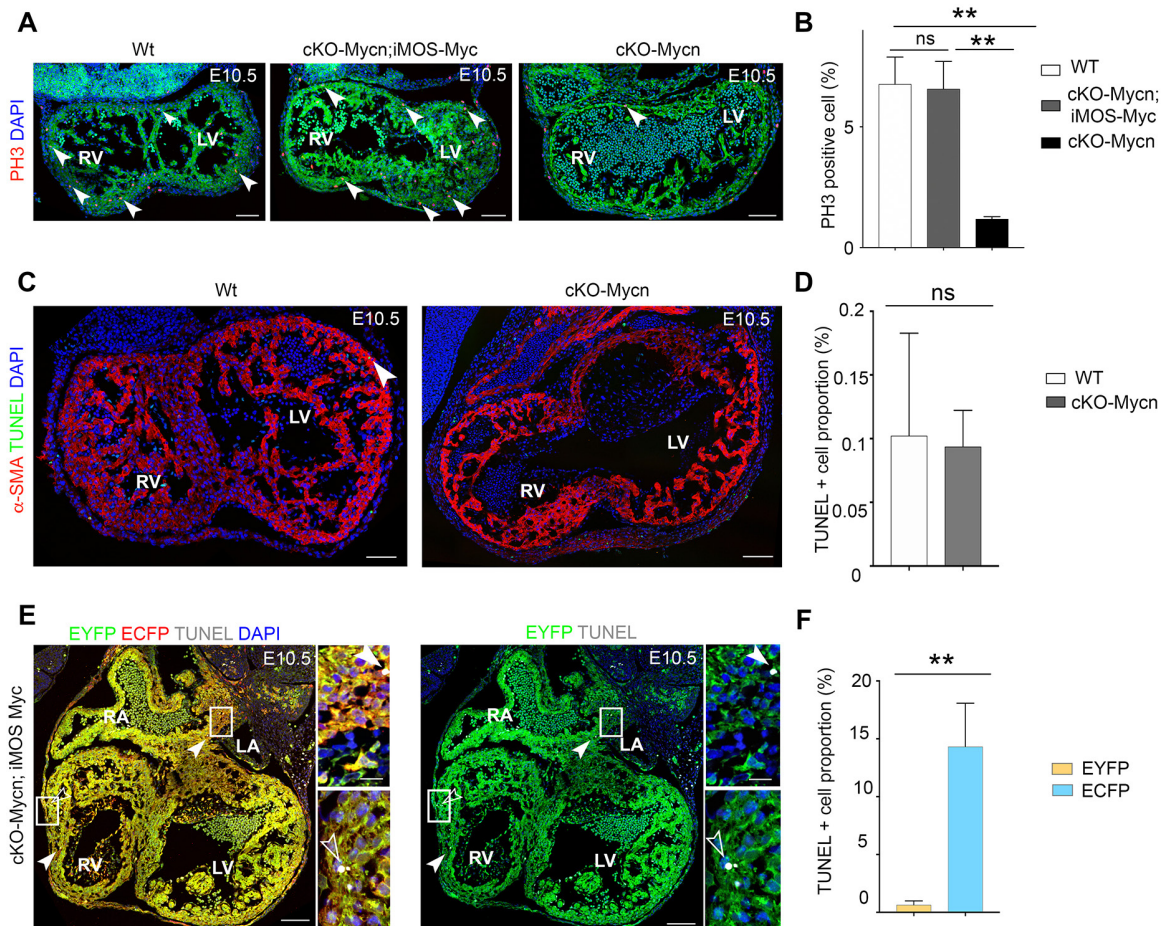


**Fig. 4. *Mycn*-deficient cardiomyocytes are eliminated by apoptosis when confronted with *Myc*-overexpressing neighbours.** (A) Confocal sections of wild-type (Wt), cKO-Mycn;iMOS-Myc and cKO-Mycn E10.5 hearts (from left to right) showing PH3 staining in red. Arrowheads point to PH3-positive cardiomyocytes. (B) Percentage of PH3-positive cardiomyocytes at E10.5 from the different groups in A. (C) Confocal sections of Wt and cKO-Mycn E10.5 hearts stained by TUNEL and  $\alpha$ -SMA immunolabelling. Arrowhead points to TUNEL-positive cardiomyocytes. (D) Percentage of TUNEL-positive cardiomyocytes from the hearts in C. (E) Confocal sections of cKO-Mycn;iMOS-Myc hearts at E10.5 showing EYFP and ECFP populations in the myocardium. Filled arrowheads and top insets (magnifications of the boxed areas) show TUNEL<sup>+</sup> ECFP<sup>+</sup> cells. Empty arrowheads and bottom insets show TUNEL<sup>+</sup> EYFP<sup>+</sup> cells. (F) Percentage of EYFP- and ECFP-positive cardiomyocytes also positive for TUNEL staining in E10.5 cKO-Mycn;iMOS-Myc hearts. LA, left atria; LV, left ventricle; RA, right atria; RV, right ventricle.  $n=3$  cKO-Mycn;iMOS-Myc,  $n=4$  cKO-Mycn,  $n=3$  iMOS-Myc. Data in B,D,F are mean $\pm$ s.e.m.; \* $P<0.05$ ; \*\* $P<0.01$ ; ns, not significant Scale bars: 100  $\mu$ m (A,C,E, main panels); 20  $\mu$ m (insets in E).

cardiogenesis. In addition, we show that Myc can replace Mycn functionally during cardiomyocyte development and that cell competition contributes to rescuing heart function by stimulating the elimination of defective cells. This demonstration adds to previous evidence indicating that the developing heart can adapt to the progressive loss of up to 50% of its cardiomyocyte population by compensatory proliferation of the healthy population (Drenckhahn et al., 2008). In contrast to this previously reported model, in which the unhealthy cardiomyocyte population is not eliminated by cell death but just diluted out (Drenckhahn et al., 2008), in the model presented here the unhealthy cell population is not prone to cell death when in isolation but undergoes massive cell death when confronted with a Myc-rescued cardiomyocyte population. These results suggest an endogenous role for cell competition in the correction of contingent defects that may appear in cardiomyocytes during development.

## MATERIALS AND METHODS

### Mouse strains

*iMOS* mouse lines have been previously described (Claveria et al., 2013). Homozygous *iMOS* females were mated with males carrying *Nkx2.5-Cre* (Stanley et al., 2002) to generate embryos. The *Mycn* floxed allele has been previously described (Knoepfler et al., 2002), as has been the Myc-GFP reporter (Huang et al., 2008). Mice were genotyped by PCR. All animal procedures were conducted in accordance with applicable institutional guidelines.

### ISH

Whole-mount ISH was performed on E9.5 embryos and E12.5 hearts as described previously, using a Myc probe (Claveria et al., 2013)

### Confocal microscopy

Histological sections and whole-mount embryos were imaged with a Nikon A1R confocal microscope using 405, 458, 488, 568 and 633 nm wavelengths and 20×/0.75 dry and 40/1.30 oil objectives. Cardiomyocyte nuclei were counted using the ImageJ (NIH; <http://rsb.info.nih.gov/ij>) cell counter. To estimate cardiomyocyte size, the number of nuclei was divided by the myocardial area calculated using ImageJ threshold detection. Areas occupied by EYFP and ECFP cells and EYFP and ECFP cell number were quantified using ImageJ threshold detection and particle analysis tools. ECFP was scored either by direct detection of ECFP or by subtracting the EYFP<sup>+</sup> area from the anti-GFP<sup>+</sup> area, when immunostaining was performed.

### Measurements in adults

After sacrifice, mice were weighed and hearts were extracted and rinsed in PBS. Hearts were weighed and tibia length of the posterior left leg was measured with a caliper.

### Immunofluorescence

Embryos were fixed overnight at 4°C in 2% paraformaldehyde (PFA) in PBS and whole-mount stained or embedded in gelatin and cryosectioned. Embryonic hearts were fixed in 2% PFA overnight at 4°C and stained as whole-mounts. Adult hearts were perfused and fixed in 2% PFA in PBS 24 h at 4°C and paraffin-embedded for sectioning. Primary antibodies used were PCMI (1:100; Sigma, HPA023370),  $\alpha$ -SMA (1:500; Sigma, C-6198), Myc (1:300; Millipore, D84C12), goat anti GFP antibody (1:100; Aacris, R1091P), c-TnT (1:200; Thermo Scientific, Ms-295-P0), IB4-647 (1:500; Thermo Scientific, I32450). Immunofluorescence was performed following standard procedures. Briefly, cryosections were permeabilized with PBT (PBS with 0.5% Triton X-100) and blocked with 10% goat serum, except for anti-GFP, for which 10% donkey serum was used. Primary antibodies were incubated at 4°C overnight and secondaries for 1 h at room temperature. Secondary antibodies used were donkey anti-goat 488 (Invitrogen, A11055), goat anti-rabbit 594 (Invitrogen, A11012), goat anti-mouse 488 (Invitrogen, A11029), goat anti-mouse 594 (Invitrogen, A11005), donkey anti-goat 647 (Invitrogen, A21447), Streptavidin-647 (Invitrogen, A32728). Sections were mounted using Vectashield (Vector Laboratories, H-1000). Terminal deoxynucleotidyl

transferase dUTP nick end labelling (TUNEL) was performed on heart sections using terminal deoxynucleotidyl transferase (TdT) and biotin-16-2-deoxyuridine-5-triphosphate (1:500; Biotin-16-dUTP) (both from Roche), and developed with 647-conjugated streptavidin (1:500; Jackson ImmunoResearch). E9.5 embryos were cleared before whole-mount confocal acquisition using ethyl cinnamate as described by Klingberg et al. (2017).

### Echocardiography study

Transthoracic echocardiography was performed blind by an expert operator using a high-frequency ultrasound system (Vevo 2100, Visualsonics, Canada) with a 40-MHz linear probe on a heating platform. Mice were lightly anaesthetized with 0.5-2% isoflurane in oxygen, adjusting the isoflurane to maintain heart rate at 450±50 bpm. A base-apex electrocardiogram was continuously monitored. Images were analysed using Vevo 2100 Workstation software. Parasternal standard, 2D and MM, long and short axis views at the level of the papillary muscles (LAX and SAX view, respectively) were acquired.

### Statistical analysis

Expected versus observed frequencies were compared using the  $\chi^2$  method. Adult heart parameters were analysed with unpaired *t*-tests comparing wild type versus Myc-KO and wild type versus heterozygotes separately. Nuclei/myocardium area data were analysed by two-way ANOVA. To compare average percentages of ECFP cells between more than two groups, the Kruskal–Wallis test was used (assuming non-normal distributions). For comparisons of two groups, the Mann–Whitney test was used. All comparisons were made using Prism statistical software.

### Single cell RNA-seq analysis

Single cell transcriptome data were downloaded from Gene Expression Omnibus (GSE76118; Li et al., 2016). Cells were classified into Epicardium, Endocardium, Mesenchymal and Cardiomyocytes, as in Li et al., 2016. *Myc* and *Mycn* mRNA expression was analysed for each population and is represented in violin plots.

### Acknowledgements

We thank members of the Torres group for stimulating discussions and suggestions. We thank members of the microscopy, bioinformatics and histopathology CNIC units, led by Valeria Caiolla, Fátima Sánchez-Cabo and Antonio de Molina-Iracheta, respectively, for excellent support and sample processing. We also thank the CNIC Advanced Imaging Unit and the CNIC Animal Facility personnel for their excellent work and support.

### Competing interests

The authors declare no competing or financial interests.

### Author contributions

Conceptualization: C.V.d.C., M.T.; Methodology: N.M.-M., R.S., C.V.d.C.; Formal analysis: N.M.-M., C.V.d.C.; Investigation: N.M.-M., C.V.d.C.; Resources: T.S.; Writing - original draft: N.M.-M., C.V.d.C., M.T.; Writing - review & editing: T.S., C.V.d.C., M.T.; Supervision: M.T.; Funding acquisition: M.T.

### Funding

This work is supported by a grant from the Fondation Leducq [‘Redox Regulation of Cardiomyocyte Renewal’ 17CVD04] and by grants from the Ministerio de Ciencia, Innovación y Universidades [BFU2015-71519-P and RD16/0011/0019 (ISCIII)]. N.M.-M. was supported by a pre-doctoral contract from ‘la Caixa’ Foundation [LACAIXA-SO14]. The CNIC is supported by the Ministerio de Ciencia, Innovación y Universidades and the Pro CNIC Foundation, and is a Severo Ochoa Center of Excellence (SEV-2015-0505).

### Supplementary information

Supplementary information available online at <http://dev.biologists.org/lookup/doi/10.1242/dev.170753.supplemental>

### References

- Bello Roufai, M., Li, H. and Sun, Z. (2007). Heart-specific inhibition of protooncogene c-myc attenuates cold-induced cardiac hypertrophy. *Gene Ther.* **14**, 1406-1416.
- Charron, J., Malynn, B. A., Fisher, P., Stewart, V., Jeannotte, L., Goff, S. P., Robertson, E. J. and Alt, F. W. (1992). Embryonic lethality in mice homozygous for a targeted disruption of the N-myc gene. *Genes Dev.* **6**, 2248-2257.

- Claveria, C. and Torres, M.** (2016). Cell competition: mechanisms and physiological roles. *Annu. Rev. Cell Dev. Biol.* **32**, 411-439.
- Claveria, C., Giovino, G., Sierra, R. and Torres, M.** (2013). Myc-driven endogenous cell competition in the early mammalian embryo. *Nature* **500**, 39-44.
- Davis, A. C., Wims, M., Spotts, G. D., Hann, S. R. and Bradley, A.** (1993). A null c-myc mutation causes lethality before 10.5 days of gestation in homozygotes and reduced fertility in heterozygous female mice. *Genes Dev.* **7**, 671-682.
- Drenckhahn, J. D., Schwarz, Q. P., Gray, S., Laskowski, A., Kiriazis, H., Ming, Z., Harvey, R. P., Du, X.-J., Thorburn, D. R. and Cox, T. C.** (2008). Compensatory growth of healthy cardiac cells in the presence of diseased cells restores tissue homeostasis during heart development. *Dev. Cell* **15**, 521-533.
- Harmelink, C., Peng, Y., DeBenedittis, P., Chen, H., Shou, W. and Jiao, K.** (2013). Myocardial Mycn is essential for mouse ventricular wall morphogenesis. *Dev. Biol.* **373**, 53-63.
- Hatton, K. S., Mahon, K., Chin, L., Chiu, F. C., Lee, H. W., Peng, D., Morgenbesser, S. D., Horner, J. and DePinho, R. A.** (1996). Expression and activity of L-Myc in normal mouse development. *Mol. Cell. Biol.* **16**, 1794-1804.
- He, C., Hu, H., Braren, R., Fong, S.-Y., Trumpp, A., Carlson, T. R. and Wang, R. A.** (2008). c-myc in the hematopoietic lineage is crucial for its angiogenic function in the mouse embryo. *Development* **135**, 2467-2477.
- Huang, C.-Y., Bredemeyer, A. L., Walker, L. M., Bassing, C. H. and Sleckman, B. P.** (2008). Dynamic regulation of c-Myc proto-oncogene expression during lymphocyte development revealed by a GFP-c-Myc knock-in mouse. *Eur. J. Immunol.* **38**, 342-349.
- Izumo, S., Nadal-Ginard, B. and Mahdavi, V.** (1988). Protooncogene induction and reprogramming of cardiac gene expression produced by pressure overload. *Proc. Natl. Acad. Sci. USA* **85**, 339-343.
- Jackson, T., Allard, M. F., Sreenan, C. M., Doss, L. K., Bishop, S. P. and Swain, J. L.** (1990). The c-myc proto-oncogene regulates cardiac development in transgenic mice. *Mol. Cell. Biol.* **10**, 3709-3716.
- Klingberg, A., Hasenberg, A., Ludwig-Portugall, I., Medyukhina, A., Männ, L., Brenzel, A., Engel, D. R., Figge, M. T., Kurts, C. and Gunzer, M.** (2017). Fully automated evaluation of total glomerular number and capillary tuft size in nephritic kidneys using lightsheet microscopy. *J. Am. Soc. Nephrol.* **28**, 452-459.
- Knoepfler, P. S., Cheng, P. F. and Eisenman, R. N.** (2002). N-myc is essential during neurogenesis for the rapid expansion of progenitor cell populations and the inhibition of neuronal differentiation. *Genes Dev.* **16**, 2699-2712.
- Li, G., Xu, A., Sim, S., Priest, J. R., Tian, X., Khan, T., Quertermous, T., Zhou, B., Tsao, P. S., Quake, S. R. et al.** (2016). Transcriptomic profiling maps anatomically patterned subpopulations among single embryonic cardiac cells. *Dev. Cell* **39**, 491-507.
- Machida, N., Brissie, N., Sreenan, C. and Bishop, S. P.** (1997). Inhibition of cardiac myocyte division in c-myc transgenic mice. *J. Mol. Cell. Cardiol.* **29**, 1895-1902.
- Malynn, B. A., de Alboran, I. M., O'Hagan, R. C., Bronson, R., Davidson, L., DePinho, R. A. and Alt, F. W.** (2000). N-myc can functionally replace c-myc in murine development, cellular growth, and differentiation. *Genes Dev.* **14**, 1390-1399.
- Moens, C. B., Stanton, B. R., Parada, L. F. and Rossant, J.** (1993). Defects in heart and lung development in compound heterozygotes for two different targeted mutations at the N-myc locus. *Development* **119**, 485-499.
- Pollack, P. S., Houser, S. R., Budjak, R. and Goldman, B.** (1994). c-myc gene expression is localized to the myocyte following hemodynamic overload in vivo. *J. Cell. Biochem.* **54**, 78-84.
- Sawai, S., Shimono, A., Wakamatsu, Y., Palmes, C., Hanaoka, K. and Kondoh, H.** (1993). Defects of embryonic organogenesis resulting from targeted disruption of the N-myc gene in the mouse. *Development* **117**, 1445-1455.
- Schneider, M. D., Payne, P. A., Ueno, H., Perryman, M. B. and Roberts, R.** (1986). Dissociated expression of c-myc and a fos-related competence gene during cardiac myogenesis. *Mol. Cell. Biol.* **6**, 4140-4143.
- Stanley, E. G., Biben, C., Elefanti, A., Barnett, L., Koentgen, F., Robb, L. and Harvey, R. P.** (2002). Efficient Cre-mediated deletion in cardiac progenitor cells conferred by a 3'UTR-ires-Cre allele of the homeobox gene Nkx2-5. *Int. J. Dev. Biol.* **46**, 431-439.
- Stanton, B. R., Perkins, A. S., Tessarollo, L., Sassoon, D. A. and Parada, L. F.** (1992). Loss of N-myc function results in embryonic lethality and failure of the epithelial component of the embryo to develop. *Genes Dev.* **6**, 2235-2247.
- Uslu, V. V., Petretich, M., Ruf, S., Langenfeld, K., Fonseca, N. A., Marioni, J. C. and Spitz, F.** (2014). Long-range enhancers regulating Myc expression are required for normal facial morphogenesis. *Nat. Genet.* **46**, 753-758.
- Villa del Campo, C., Claveria, C., Sierra, R. and Torres, M.** (2014). Cell competition promotes phenotypically silent cardiomyocyte replacement in the mammalian heart. *Cell Reports* **8**, 1741-1751.
- Villa Del Campo, C., Lioux, G., Carmona, R., Sierra, R., Muñoz-Chápuli, R., Claveria, C. and Torres, M.** (2016). Myc overexpression enhances of epicardial contribution to the developing heart and promotes extensive expansion of the cardiomyocyte population. *Sci. Rep.* **6**, 35366.
- Xiao, G., Mao, S., Baumgarten, G., Serrano, J., Jordan, M. C., Roos, K. P., Fishbein, M. C. and MacLellan, W. R.** (2001). Inducible activation of c-myc in adult myocardium in vivo provokes cardiac myocyte hypertrophy and reactivation of DNA synthesis. *Circ. Res.* **89**, 1122-1129.
- Zhong, W., Mao, S., Tobis, S., Angelis, E., Jordan, M. C., Roos, K. P., Fishbein, M. C., de Alborán, I. M. and MacLellan, W. R.** (2006). Hypertrophic growth in cardiac myocytes is mediated by Myc through a Cyclin D2-dependent pathway. *EMBO J.* **25**, 3869-3879.
- Zhou, B., von Gise, A., Ma, Q., Rivera-Feliciano, J. and Pu, W. T.** (2008). Nkx2-5 and Isl1-expressing cardiac progenitors contribute to proepicardium. *Biochem. Biophys. Res. Commun.* **375**, 450-453.
- Zimmerman, K. A., Yancopoulos, G. D., Collum, R. G., Smith, R. K., Kohl, N. E., Denis, K. A., Nau, M. M., Witte, O. N., Toran-Allerand, D., Gee, C. E. et al.** (1986). Differential expression of myc family genes during murine development. *Nature* **319**, 780-783.

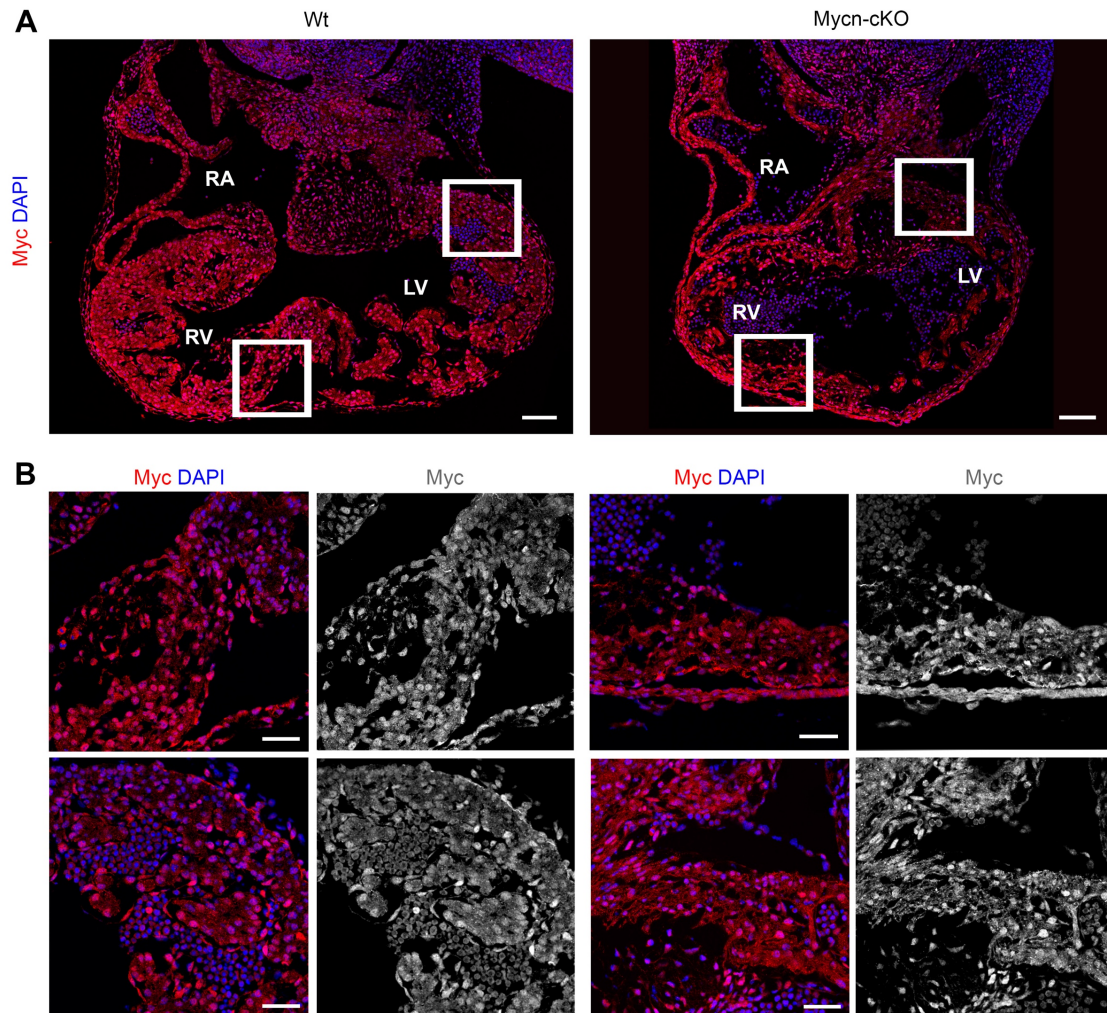


**Figure S1. Myc antibody staining in *Mycn*-deficient hearts.** **A.** Confocal images showing Myc antibody staining in sections of a E10.5 WT heart (left) and *Mycn*-cKO (right). **B.** Magnification of boxed areas in A. WT heart is shown on left panels and *Mycn*-cKO on right panels. Greyscale images of antibody staining are shown in both cases. Bar 100  $\mu\text{m}$  in A and 50  $\mu\text{m}$  in B. LV: Left ventricle, RV: Right ventricle, RA: Right atria, LA: Left atria,

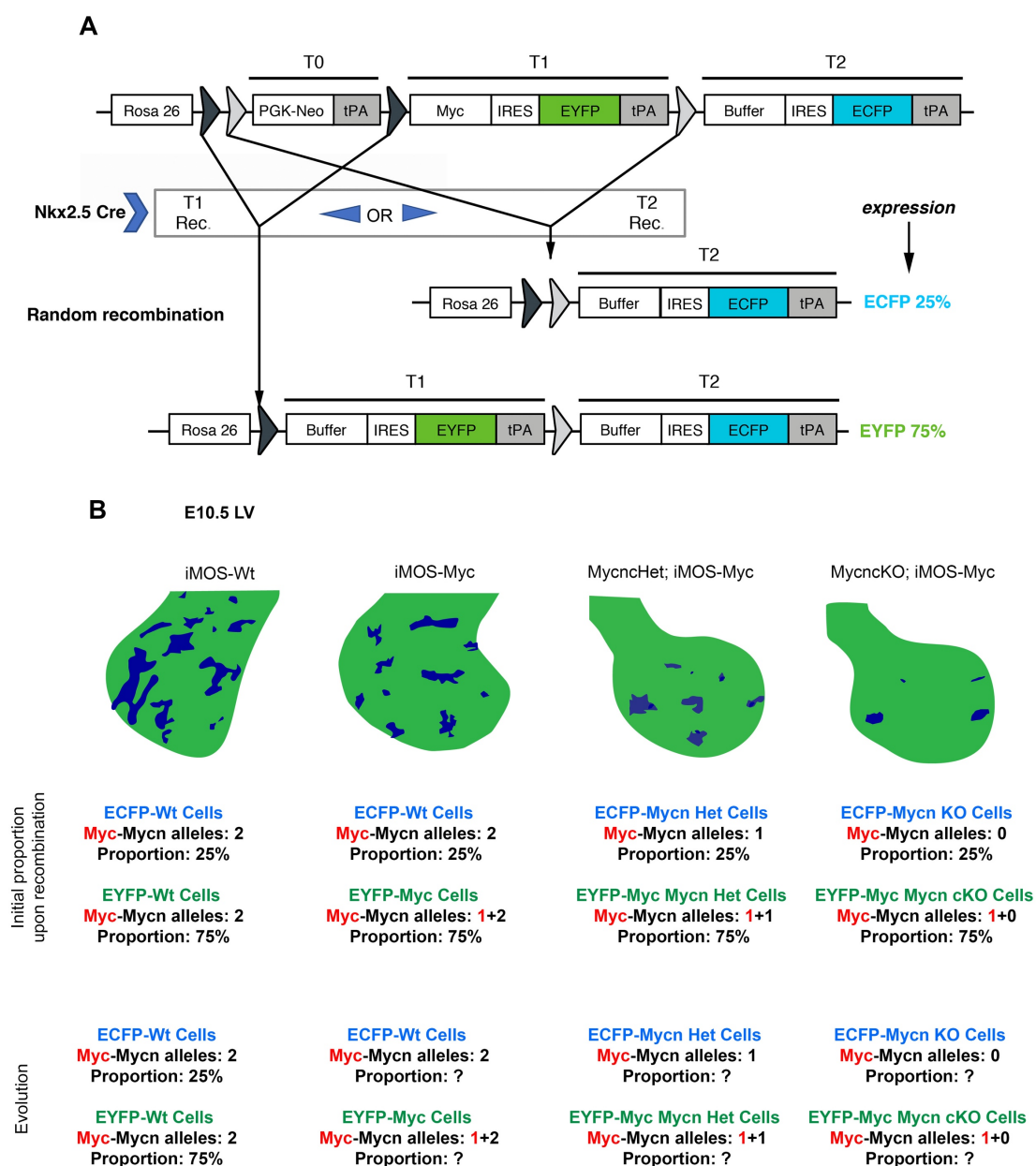


**Figure S2. Summary of the iMOS-mosaic system and the different genetic combinations used in this work. A.** Schematic of the  $iMOS^{T1-Myc}$  allele. The system consists of three cassettes knocked-in to the *Rosa26* locus that can be excised by Cre recombination at random due to two pairs of LoxP sites. When the T0 cassette is excised, T1 is expressed and the cell and its progeny will be labelled in EYFP and overexpress Myc (EYFP-Myc). When T2 recombination takes place both T0 and T1 are excised leading to the expression of T2 (ECFP-WT) in the resulting cell and its progeny. Due to the distances between the lox sites and the Cre efficiency, the proportions of each cell type upon recombination is 75:25 (EYFP:ECFP), as determined experimentally in several tissues. Upon Cre-recombinase exposure, the system thus generates two labelled cell populations at random but reproducible frequencies. **B.** Schematics of E10.5

LV showing the two labelled cell populations in iMOS-WT, iMOS-Myc, MycnHet;iMOS-Myc and MycncKO;iMOS-Myc embryos. Below the images, the proportions and corresponding allele ratio for Myc and Mycn of each cell type is shown. At initial timepoints the relative proportion of EYFP and ECFP proportions is 75:25. In iMOS-Wt this is maintained because no cell population has a competitive advantage over the other. When an imbalance in Myc and Mycn alleles between neighbouring cells is implemented due to the iMOS system and the conditional deletion of Mycn, these proportions vary with developmental progression. Green and blue colours represent the EYFP and ECFP cell populations, respectively.

**Table S1. Observed and expected frequencies of adult mice of the different genotypes**

<b>Genotype</b>	<b>Adult mice</b>	<b>Observed frequency</b>	<b>Expected frequency</b>
WT	20	0.266	0.25
cHet-Myc	38	0.506	0.50
cKO-Myc	18	0.240	0.25





# ACKNOWLEDGMENTS

No podría comenzar este apartado de otra manera que no fuera agradeciendo a Miguel por haberme dado la oportunidad de empezar este proyecto. Siempre has tenido la puerta del despacho abierta para resolver mis dudas y dar interpretación a los resultados más inesperados. Nos enseñas a superarnos, a tener pensamiento crítico, a trabajar de forma independiente y, en definitiva, a crecer como científicos. Crees en nosotros y en nuestras posibilidades, mucho más que nosotros mismos, y estoy convencida de que esa, es una de las claves para que un grupo funcione bien.

I also wanted to thank Dr. Sedmera and his group for their warm welcome during my stay in Prague. It was a really nice experience.

Tampoco podría olvidarme de Silvia, quién me guio en mi primera etapa en el CNIC. Estoy enormemente agradecida por haberme seleccionado como estudiante CICERONE y haberme enseñado tanto durante el Máster. Recuerdo con mucho cariño esos primeros meses, que además me allanaron un poco el camino de inicio en la tesis. Durante ese tiempo, tres personitas maravillosas me acompañaron cada día, y me enseñaron todo lo que sabían y más. Iván y las Beas, sois geniales, os merecéis lo mejor, siempre tenéis una sonrisa para alegrarle el día a cualquiera que lo necesite. Aunque me cambié al grupo Torres, tanto Silvia, como vosotros, seguisteis ahí de forma muy cercana. Gracias.

Agradezco a todas las personas que han pasado por el grupo de Miguel, y que de una u otra manera han contribuido a mi experiencia en él. Todos ellos han sido y son la pieza fundamental de mi día a día en el laboratorio. Entre los antiguos miembros, destacar a Laura Carramolino por empezar todo esto, aunque coincidiéramos poco tiempo. Kenzo, for being such a funny guy, y Cova por su espíritu de “runner”.

Vane, eres una “crack”, eficiente y constante, nos ayudas cuando te lo pedimos y cuando no, también. Rocío y Susana, sois junto a Vane, los tres pilares que mantienen el grupo. Cada una tan diferente y a la vez tan necesaria ¡Esos cardios no se hubieran

aislado tan bien sin tu ayuda, Rocío! Susana, siempre alerta, controlando los cruces y las peticiones para que no haya fallos. Además, las tres siempre tenéis palabras de ánimo en esos momentos de saturación. Cris, mi compañera de paper, y esa persona que puede resolver dudas de competición, corazón y lo que haga falta. Irene, y sus valiosas patitas, siempre dando alegría en el bench. Lorena, el claro ejemplo de la eficiencia, no dejo de asombrarme con tu forma de trabajar, de mayor quiero ser como tú ;). Isaac, me encanta tener la suerte de trabajar en un grupo con personas que ven el mundo de forma diferente, es decir, como un ingeniero, jejeje.

José, eres esa persona que cuando menos te lo esperas, te dice cualquier tontería y te alegra el día. Nos conocimos antes de saber que seríamos compañeros de grupo, pero eso fue precisamente lo que más nos unió. El almeriense más guapo de la tercera norte y mi confesor en ocasiones. Queda pendiente que me lleves a tu palacete de Aguadulce. Ester !! No se puede ser más buena. Cuando llegaste al labo hice lo que pude para enseñarte lo poco que había aprendido. En muy poco tiempo te hiciste totalmente independiente y ahora soy yo la que te pide consejos. Además, siempre te preocupas de que estemos bien y de ayudarnos. Miquel, sin duda una de esas personas que destaca, estoy segura de que llegarás donde te propongas. Por otro lado, mi consejero en finanzas y alguien con quien debatir sobre la vida en general. Llega el turno de Morena, el último fichaje, pero que también promete. Me ha encantado compartir este tiempo contigo y muchas gracias por los ánimos en estos últimos meses. Consuelo, estar separadas por varias plantas dificulta un poco conocernos más, aún así siempre vienes sonriente a las reuniones y te preocupas por nosotros. No tengo dudas de que aportas y aportarás grandes cosas al grupo. Tere! Aunque pertenezcas al grupo de Silvia, tantas comidas juntas te hacen ser parte también de los Torres. Gracias por los ánimos en la recta final.

Diréis ¿falta gente? Quedan esas tres personas que más que compañeras, son amigas, Ghislaine, Sandra y Lin. Cada una diferente e imprescindible, todas inteligentes. Ghislaine tiene la locura y la pasión, es esa amiga que se deja llevar, que entrega todo sin esperar nada a cambio. Sandra es la calma (la locura la tiene,

pero la oculta), mi compañera de aventuras, el apoyo incondicional (y la que me pela las mandarinas). Lin, la transparencia y la que se lanza a la piscina pase lo que pase (y la de la risa contagiosa). Las tres me habéis dado tanto que no se puede resumir aquí. Habéis estado en lo bueno, lo genial, lo regular, los tropezones, las caídas, las estampidas, las risas, los llantos...la vida.

En general, me siento muy afortunada de haber vivido estos años en el CNIC, es un sitio tan abierto, que permite la conexión con muchas más personas, a parte del propio laboratorio. David Filgueiras ha sido uno de los grandes apoyos, aportando su experiencia en electrofisiología. Todo el grupo de Enrique Lara y de José Luis de la Pompa, con los que he compartido ratones, reactivos, protocolos, dudas... Todos los grupos del CNIC, especialmente la 3N, han contribuido a mi crecimiento personal y científico.

Tanto ha sido así, que es inevitable llevarse alguna amistad de esos grupos. Briane, thanks for being always there for a hug, and for having those nice baby hands. Espero que vivamos alguna aventura más después de todo esto. Otras ya no están en el CNIC, pero siguen presentes, como Marina, Melisa, Raquel...

De igual o mayor importancia han sido las unidades técnicas del CNIC, resolviendo cualquier duda que me pudiera surgir y ayudando en todo lo posible. En especial, Microscopía, Imagen, Bioinformática e Histología. Vero, en microscopía, siempre dispuesta a crear "Macros" que nos ahorren un poquito de tiempo. Las chicas de imagen, imprescindibles para mí, que me han acompañado durante largas horas de trabajo. María Villalba, tan eficiente e inteligente, una gran trabajadora, junto a Ana, Lorena y Eva. Tres compañeras con gran motivación por su trabajo y que con su simpatía han hecho que los días de ECOS fueran mucho mejores. Manuel y Felipe, que desde Bioinformática y con gran amabilidad han atendido todas mis peticiones. Carlos, en tu caso, tengo que agradecer tus consejos sobre estadística y todos los momentos de risas que me has dado en tus visitas a la 3N (a tope).

En el caso de Histología, la historia es un poco diferente, no solo me han enseñado

y ayudado, sino que en la última etapa se han convertido en amigos (o igual para Tania, solo conocidos...?¿), todo el mundo debería comer al menos una vez con ellos, se curan las penas!

Por último, no puedo olvidarme de mi familia, los que están ahí siempre, incluso cuando no están. Mis padres, por transmitirme grandes valores y un amor incondicional. Mi abuela, por ser ejemplo de vitalidad y fuerza. Os quiero.

Pedro, cualquier cosa que escriba se queda corta. Gracias por transformar mi mundo de una forma tan bonita, por querer compartir tanto conmigo y sobre todo, por tu paciencia estos últimos meses.



### **Cover page**

Immunofluorescence in adult mouse auricle of Meis (pink), TnT (green) and DAPI. Confocal image processed with artistic filter in Adobe-Photoshop.

### **Back page**

Wordcloud with heart shape made with the most common words in this thesis.

